Radical Approaches to Syntheses and Mechanisms

Amber Nicole Hancock

Dissertation submitted to the faculty of the Virginia Polytechnic Institute and State University in partial fulfillment of the requirements for the degree of

Doctor of Philosophy
In
Chemistry

James M. Tanko
Louis A. Madsen
Hervé L. Marand
Diego Troya
Timothy E. Long

June 10, 2011
Blacksburg, Virginia USA

Keywords: Kinetics, Mechanism, Deprotonation, Electron Transfer, Radical Cyclization, Homolytic Substitution.

A Radical Approach to Syntheses and Mechanisms

Amber Nicole Hancock

(ABSTRACT)

The critically important nature of radical and radical ion mechanisms in biology and chemistry continues to be recognized as our understanding of these unique transient species grows. The work presented herein demonstrates the versatility of kinetic studies for understanding the elementary chemical reactions of radicals and radical ions. Chapter 2 discusses the use of direct ultrafast kinetics techniques for investigation of crucially important enzymatic systems; while Chapter 3 demonstrates the value of indirect competition kinetics techniques for development of synthetic methodologies for commercially valuable classes of compounds.

The mechanism of decay for aminyl radical cations has received considerable attention because of their suspected role as intermediates in the oxidation of tertiary amines by monoamine oxygenases and the cytochrome P450 family of enzymes. Radical cations are believed to undergo deprotonation as a key step in catalysis. KIE studies performed by previous researchers indicate *N,N*-dimethylaniline radical cations deprotonate in the presence of the bases acetate and pyridine. By studying the electrochemical kinetics of the reaction of para substituted *N,N*-dimethylaniline radical cations with acetate anion, we have produced compelling evidence to the contrary. Rather than deprotonation, acetate reacts with *N,N*-dimethylaniline radical cation by electron transfer, generating the neutral amine and acetoxyl radical. Transport properties of reactants and solvent polarity changes were investigated and confirmed not to influence the electrochemical behavior forming the basis for our mechanistic hypothesis. To reconcile our conclusion with earlier results, KIEs were reinvestigated electrochemically and by nanosecond laser flash photolysis. Rather than a primary isotope effect (associated with C-H bond cleavage), we believe the observed KIEs are secondary. Product studies performed by constant potential coulometry indicate *N,N*-dimethylaniline radical cations are catalytic in carboxylate oxidations. Collectively, our results suggest that aminyl radical cation deprotonations may not be as facile as was previously thought, and that in some cases, may not occur at all.

Interest in design and synthesis of selenium containing heterocycles stems from their ability to function as antioxidants, anti-virals, anti-inflammatories, and immunomodulators. To establish synthetic feasibility of intramolecular homolytic substitution at selenium for preparation of selenocycles, we set out to determine what factors influence cyclization kinetics. A series of photochemically labile Barton and Kim esters have been syntheisized and employed as radical precursors. The effect of leaving radical stability on kinetics has been investigated through determination of rate constants and activation parameters for intramolecular homolytic substitution of the corresponding radicals via competition experiments. Notable leaving group effects on measured kinetic parameters show more facile reactions for radical precursors with more stable leaving radicals. Moreover, cyclizations to form six-membered (as opposed to five-membered) ring systems exhibited order of magnitude decreases in rate constants for a given leaving radical. Our results are congruent with expectations for radical cyclizations trends for the varied experimental parameters and suggest homolytic substitution affords a convenient means for synthesis of selenocycles.

ACKNOWLEDGEMENTS

Foremost, I would like to express my sincerest fondness and gratitude to my advisor, Professor Jim Tanko. You have afforded me every opportunity I have ever asked and more. I assure you that while I can never repay you, I will never forget the things you have done for me. If you start to emit an ethereal glow you will know you have some how managed to grow higher in my regard. I would also like to thank Professor Carl Schiesser for being such a gracious mentor and friend to me during the year I spent with his group. Finally, I could not possibly over emphasize my earnest appreciation for all of the time, patience, critical review, advice and support my committee members: Professor Madsen, Professor Marand, Professor Long and Professor Troya have afforded me in my time here at VT.

A special thanks goes to all of the members of the Tanko and Schiesser groups past and present for being such fantastic friends and coworkers: Jared Spencer, Akiko Nakamura, Shraddha Patil-Patwardhan, Jun Yin, Dr. Liang Chen, Stephanie Zimmeck, Eveline Richert, Justin Curtis, John Ball and Dr. Xiangzhong Li from the Tanko group; and Dr. Maree Staples, Dr Phoebe Macdougall, Dr Michelle Taylor, Dr. Sara Kyne, Dr. Chris Donner, Dr. Sonia Horvat, Dr. Michio Shirai, Nichole Tan, Dr. Corin Storkey, Tu Anh Tran, Caroline Kyi, Lisa Hong and Greg Hamilton of the Schiesser group. I would like to give an extra special thanks for the time and efforts of those who I have worked on projects with Dr. Sofia Lobachevsky, Zhang Zhiyang Secil Tekin and Jenny England. I owe distinctive gratitude Dr. Hayati Celik, you were not only an outstanding mentor in the lab but a sage friend. I would also like to thank my dear friend and supportive colleague, Michelle Grimm. Despite your most ardent objections we have become close (you do hug back and I know you always will). It has been a true pleasure working with both groups(families). Every family has its matriarch; as such, I would like to thank Linda Tanko for keeping the Tanko group so close.

Of insurmountable importance is my dearest friend, Susan Mitroka. We have shared and learned so much from each other and without your friendship I do not know where I would be now. Sometimes I think you know my thoughts and other times I know you do. I owe a huge thanks to my oldest friend Beth Reves for things too many to list. If everyone were as compassionate as you the world would be perfect. I sincerely thank my brother and mother (Vincent and Colleen) for their love. Above all, I'd like to express my sincerest gratitude and adoration to my Wesy. Your love, patience and encouragement have been invaluable. I am so lucky to have you in my life.

“There is nothing you can make that can’t be made,
No one you can save that can’t be saved,
Nothing you can do but you can learn how to be you in time,
It’s easy,
All you need is love.”
-John Lennon

TABLE OF CONTENTS

LIST OF SCHEMES

LIST OF FIGURES

LIST OF TABLES

LIST OF EQUATION

(1.3) 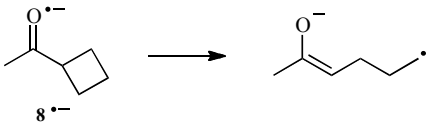 8

8$^{\bullet-}$

(1.4) 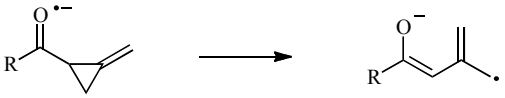 9

9$^{\bullet-}$

R = Ph or c-C_6H_{11}

(1.5) 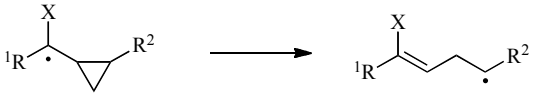 9

R = H, O

(1.6) $$\log(k_o) = \log\left(\frac{k_B T}{h}\right) - \frac{\Delta G_o^{\mp}}{2.303RT}\left(1 + \frac{\Delta G^o}{4\Delta G_o^{\mp}}\right)$$ 13

(1.7) 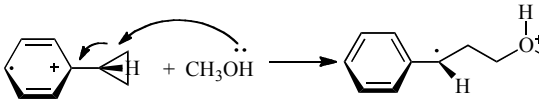 26

(1.8) 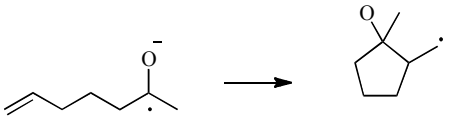 42

(1.9) 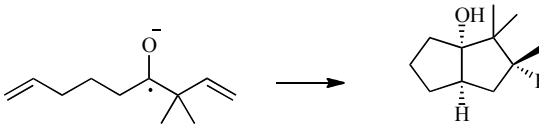 43

20 **21**

(2.1) $$-\frac{d[A]}{dt} = k_{obs}[A]$$ 81

(2.2) $$k_{obs} = k[B]_o$$ 81

(2.3) $$D_x = \frac{D_{analyte} \cdot D_{H_2O(Neat)}}{D_{H_2O(Sample)}}$$ 88

(4.1) $$A \xrightarrow{k} P$$ 153

(4.2) $$-\frac{d[A]}{dt} = k[A]$$ 153

(4.3) $$\ln[A] = -kt + \ln[A]_o$$ 154

(4.4) $A + B \overset{k}{\rightarrow} P$ 154

(4.5) $-\frac{d[A]}{dt} = k[A][B]$ 154

(4.6) $k_{obs} = k[B]_o$ 155

(4. 7) $\frac{\frac{d[RSeH]}{dt}}{\frac{d[Cyc]}{dt}} = \frac{k_T[R'H][RSe\bullet]}{k_{cyc}[RSe\bullet]}$ 157

(4.8) $k_{cyc} = k_T \frac{[R'H][Cyc]}{[RSeH]}$ 157

(4.9) $E = E_o + \frac{RT}{nF}\ln\frac{O}{R}$ 163

(4.10) $\Delta G_o = -nFE_o$ 164

(4.11) $\lambda = \frac{RT}{nF}\left(\frac{k}{\nu}\right)$ 166

(4.12) $\frac{i_{pa}}{i_{pc}} = \left(\frac{k}{F\nu RT}\right)$ 167

(4.13) $E_p - E_{\frac{p}{2}} = \frac{RT}{2nF}\left(\ln(\lambda) - 1.56\right)$ 167

(4.14) $J_i(x,t) = -D_i\frac{\partial C_i(x,t)}{\partial x}$ 170

(4.15) $J_i(x,t) = -D_i\frac{C_i(x+\Delta x,t) - C(x,t)}{\Delta x}$ 171

(4.16) $-\frac{\partial C_i}{\partial t} = D_i\frac{\partial J_i}{\partial x}$ 171

(4.17) $C(x,t+\Delta t) = C(x,t) + \frac{D\Delta t}{\Delta x}[C(x+\Delta x) -2C(x,t) + C(x-\Delta x,t)]$ 171

(4.18) $f(j,k+1) = f(j,k) + \mathbf{D}_M[f(j+1,k) -2f(j,k) + f(j-1,k)]$ 171

(4.19) $D_M = \frac{D\Delta t}{\Delta x^2}$ 171

(4.20) $\mu = \sqrt{\frac{D_a}{k}}$ 173

(4.21) $J \approx 6\sqrt{\frac{D_a}{dx}} + 1$ 174

(4.22) A - e- → A.+ 175

LIST OF ABBREVIATIONS

KIE Kinetic Isotope Effect

HRP Horseradish Peroxidase

P450 Cytochrome P450

GPx Glutathione Peroxidase

MAO Monoamine Oxidase

Nu^- Nucleophile

k Reaction Rate Constant

k_o Ring Opening Rate Constant

HOMO Highest Occupied Molecular Orbital

SET Single Electron Transfer

HAT Hydrogen Atom Transfer

SPLET Sequential Proton Loss Electron Transfer

PCET Proton Coupled Electron Transfer

ETPT Electron Transfer followed by Proton Transfer

SARTAN Selective Angiotensin 2 Receptor Antagonist

S_N2 Bimolecular Nucleophilic Substitution

S_H2 Bimolecular Homolytic Substitution

pK_a Acid Dissociation Constant

ΔG Free Energy

C Celcius

M Moles/liter

S Second

T Temperature

t Time

kcal Kilocalories

mol Moles

ns Nanosecond

nm Nanometer

E_p Peak Potential

$E_{p/2}$ Peak Potential at Half Height

E^o Standard Potential

E_{ox} Oxidation Potential

TIPS Triisopropylsilyl

DCB 1,4-dicyanobenzene

ArOH Phenol

DMSO Dimethylsulfoxide

D_o Diffusion Coefficient

PF_6 Hexafluorophosphate

OAc Acetate

Bn Benzyl

Ph Phenyl

ClO_4 Perchlorate

PTOC Pyridine-2-thione Oxy Carbonyl

THF Tetrahydrofuran

DMP Dimethylpyrrolidinium

DCA Dicyanoanthracene

$PINO^{\cdot}$ *N*-hydroxylphthalimide Radical

$BTNO^{\cdot}$ 1-hydroxyl-benzotriazole Radical

$DPPH^{\cdot}$ Diphenylpicrylhydrazyl Radical

DMA Dimethylaniline

DFT Density Functional Theory

B3LYP Becke/Three-Parameter/Lee-Yang-Parr Exchange-Correlation Functional

UV-vis Ultraviolet Visible Spectroscopy

LFP Laser Flash Photolysis

NMR Nuclear Magnetic Resonance

GC Gas Chromatography

SFC Supercritical Fluid Chromatography

GC-MS Gas Chromatography Mass Spectrometry

LCMS Liquid Chromatography Mass Spectrometry

HPLC High Performance Liquid Chromatography

BE Bulk Electrolysis

CV Cyclic Voltammetry

Contributions:

Chapter 1 is modified from a textbook chapter written by Amber Hancock, dissertation author, and her committee chair and Ph.D. advisor, Prof. Jim Tanko.[1] The intent of this chapter is to convey the utility of mechanistic radical chemistry as well as introducing the recent advances in and purpose of the work discussed in chapters 2 and 3.

ABSTRACT

This Chapter examines similarities between radical and radical ion reactions. Radicals and radical ions have worked their way into almost every facet of mainstream chemistry over the past 60 years. The importance and usefulness now associated with the reactions of radicals is in stark contrast to their prior role as poorly understood scapegoat molecules often blamed for failed reactions. The processes discussed herein demonstrate two critically important concepts to the radical chemist: 1) kinetic studies are an excellent and versatility applicable tool to determine mechanistic data for chemical reactions, and 2) published mechanistic data for more thoroughly studied radical processes have and continue to provide key insight into the factors governing reactivity and mechanism of their charge bearing counterparts.

1.1 Introduction: Radical Cation/Anion and Neutral Radicals a Comparison

Over the past several decades, radicals and radical ions have emerged as an important class of reactive species. Recognition of their role as potential intermediates in numerous organic and bioorganic reactions and development of several new synthetic methods based upon their chemistry has attracted significant attention. This chapter explores parallels between radical and the equivalent radical ion reactions; in

cases where available data facilitates comparison. Generally, it is shown that the results of one class will extrapolate to the other in a useful way. However, as will be seen, the investigator should exercise extreme caution when inferring reactivity trends for a radical ion from a radical. A seemingly subtle molecular change such as introduction of charge can have a profound impact on structure, stability and reactivity of a molecule.

1.2 Cyclopropane Radical Cations and Anions

1.2.1 Cyclopropylcarbinyl → Homoallyl Rearrangements

1.2.1.1 Radical ion probes/clocks based upon the cyclopropylcarbinyl → homoallyl rearrangement

Unimolecular rearrangements based upon cyclopropane chemistry, are useful from a mechanistic perspective (i.e., as mechanistic probes or radical ion clocks). The mechanistic probe approach is essentially an intramolecular trapping experiment. A structural feature (e.g., a cyclopropyl group) is incorporated into a substrate that, in principle, will lead to a rearrangement uniquely ascribed to a radical or radical ion intermediate. Historically, the use of a cyclopropyl group in such an experiment is predicated on the expectation that the relief of ring strain will drive the rearrangement. The prototypical example of such a process, the cyclopropylcarbinyl → homoallyl neutral radical rearrangement **(equation (1.1))** is fast ($k \approx 10^8$ s^{-1}) and essentially irreversible.[2]

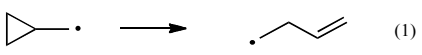
(1) (1.1)

The mechanistic probe approach is founded on two critical assumptions: a) Structurally-rearranged products arise exclusively from the single electron transfer

(SET) pathway, and b) the rearrangement is rapid and (preferably) irreversible. Although the kinetics (and mechanism) of unimolecular rearrangements of neutral radicals have been extensively studied, until recently, very little was actually known regarding analogous rearrangement of radical ions. Frequently it was (and is still) assumed that structural features that lead to facile rearrangement of neutral free radicals would do the same for radical ions.

1.2.1.2 Cyclopropylcarbinyl → Homoallyl type rearrangments of radical anions generated from aromatic ketones

In 1990, we reported our first results pertaining to the chemistry of radical anions generated from substituted phenyl cyclopropyl ketones (**Scheme 1.1**).[3] For R = alkyl or hydrogen, ring opening of $\mathbf{1}^{\bullet-}$ was found to be very slow, and reversible with an equilibrium constant favoring the ring-closed radical anion ($k_o < 10\ s^{-1}$ and $K_{eq} = k_o/k_{-o} = 10^{-8}$ for R = H).[3-4] These results suggested that there were two important considerations in the design of radical ion probes based upon the cyclopropylcarbinyl → homoallyl rearrangement: a) ring strain (the relief of which favors ring opening), and b) resonance energy (which may help or hinder rearrangement, depending on the specific system). Thus for $\mathbf{1}^{\bullet-}$ (R = H or alkyl), ring opening is disfavored (kinetically and thermodynamically) because there is a loss of resonance energy associated with ring opening (the ring-closed radical anion is highly delocalized). Placement of radical stabilizing substituents (R = phenyl or vinyl) on the cyclopropyl group partially compensates for this loss of resonance energy, and ring opening becomes more favorable ($k_o \approx 10^6 - 10^7\ s^{-1}$ for R = $CH{=}CH_2$ or Ph).[5]

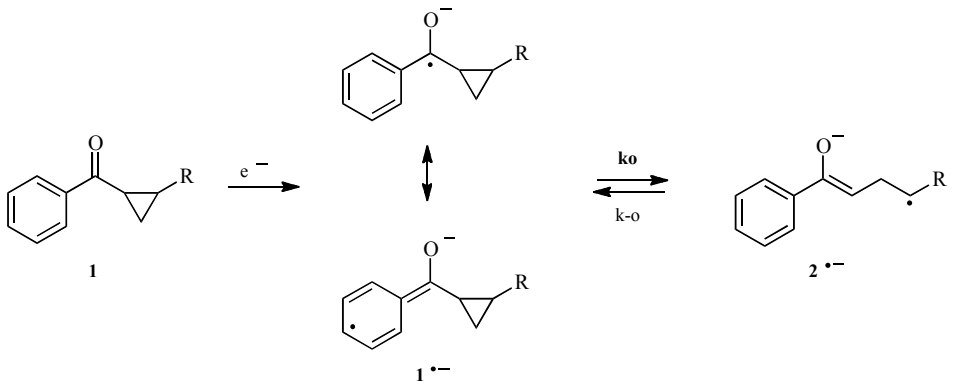

Scheme 1.1 Phenyl cyclopropyl ketones radical anion ring opening. Reproduced by permission of the American Chemical Society .[3]

Based upon this reasoning, spirocyclohexadienones **3** emerged as particularly attractive substrates because ring opening of the corresponding radical ions would be driven by both the relief of cyclopropane ring strain and an increase in resonance energy, because of the formation of an aromatic ring. Both the direct and indirect (mediated) electrochemistry of **3a**-**c** were characterized by rate limiting electron transfer (suggesting a rate constant for ring opening $\geq 10^7$ s^{-1} for their corresponding radical anions). From the indirect electrochemistry, rate constants for electron transfer between **3a**-**c** and a series of aromatic radical anions were measured, and from these results, reduction potentials and reorganization energies were derived using Marcus theory. The value of the symmetry coefficient (α, derived from the direct electrochemistry) and reorganization energy (λ, derived from the Marcus treatment) are consistent with a radical anion which has a discrete lifetime (*i.e.*, electron transfer and ring opening are not concerted).[6]

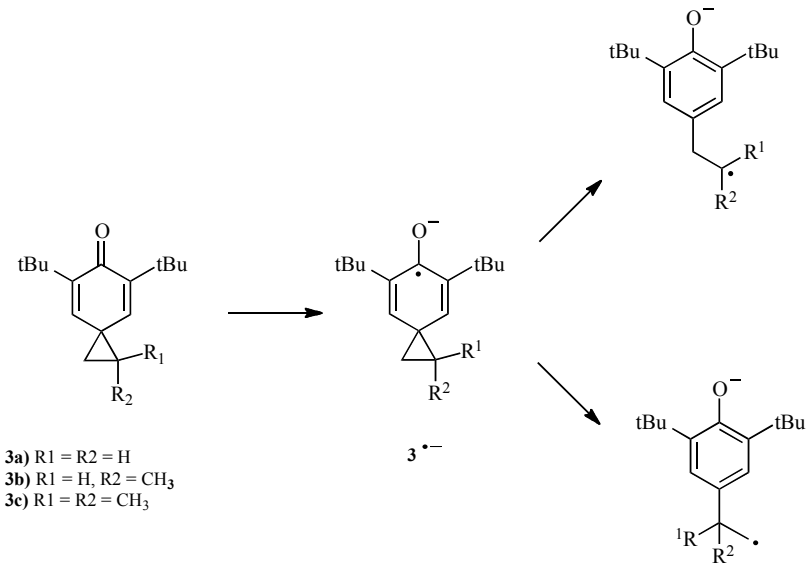

Scheme 1.2 Unsymmetrical radical anions ring opening.

For the unsymmetrical radical anions, ring opening (**Scheme 1.2)** occurs with modest selectivity favoring formation of the more substituted (stable) radical anion (in a 10 : 1 ratio for $\mathbf{3c}^{\bullet-}$ and a 1.2 : 1 ratio for $\mathbf{3b}^{\bullet-}$).[6] The observed regiochemistry for ring opening is very similar to that observed for the 2,2-dimethylcyclopropylcarbinyl and 1-methylcyclopropylcarbinyl neutral free radicals (where the ratios are 6.7 : 1 and 1.2 :1, respectively).[2a] These neutral radicals rearrange with rate constants > 10^8 s^{-1}, and it appears likely that rate constants for ring opening of radical anions $\mathbf{3b}^{\bullet-}$ and $\mathbf{3c}^{\bullet-}$ are of the same order of magnitude. Radical anion $\mathbf{4}^{\bullet-}$ **(equation (1.2)[7] reproduced by permission of** the American Chemical Society**)** was studied by direct electrochemical techniques. Because of extended conjugation in the ring-closed form (compared to spirocyclohexadienones $\mathbf{3}^{\bullet-}$), the rate constant for ring opening of $\mathbf{4}^{\bullet-}$ is sufficiently slow that it can be measured directly by CV. In dimethylformamide (DMF), k_o = 140 s^{-1}.[7]

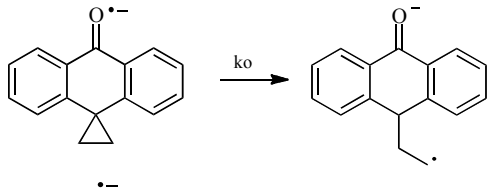

(1.2)

Because of the regiochemistry of radical anion ring opening, spirocyclohexadienone **3c** emerged as a particularly attractive probe for single electron transfer. This probe allows clear experimental distinction between products formed via SET as opposed to a polar pathway (**Scheme 1.3**). Ring opening via a polar pathway (essentially an S_N2 reaction) would result in product(s) where the nucleophile was attached to the least-substituted carbon of the cyclopropyl group **6**; an SET process would yield a product where the nucleophile was attached to the more-substituted carbon **5**. In this manner, it was shown that Grignard (RMgX) and alkyllithium reagents (RLi) react with **3c** mainly via a single electron transfer pathway. The results pertaining to the mechanism for reaction of **3c** with dialkyllithium cuprates (R_2CuLi) were ambiguous, and could be accounted for by either an SET or polar pathway. However, one limitation associated with the use of **3c** was discovered.[8] In protic solvents (PhS^- as nucleophile) reaction of **3c** was found to involve a rare $S_N2(C+)$ mechanism.[9]

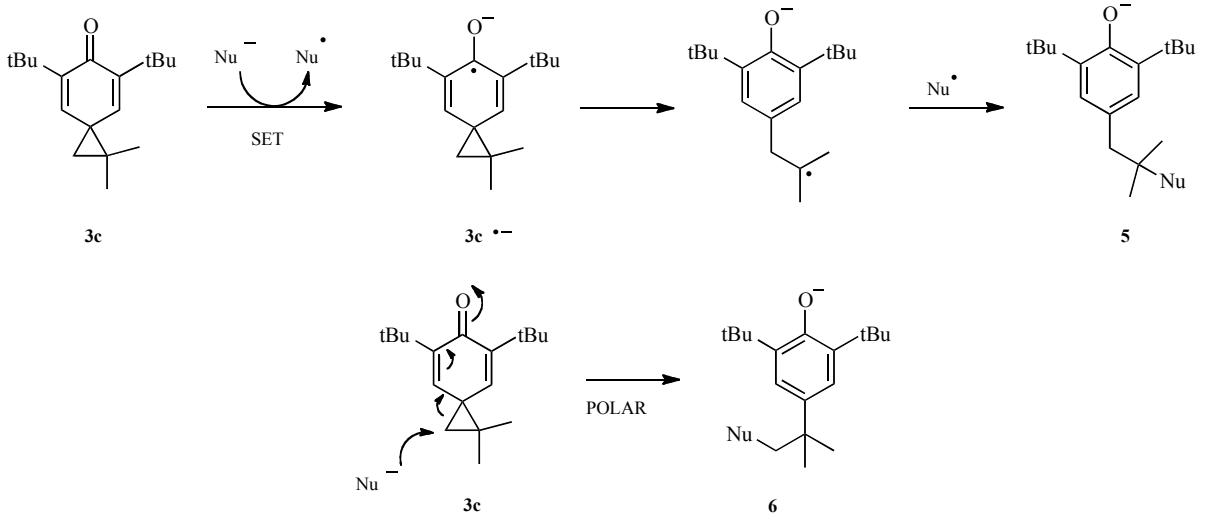

Scheme 1.3. Cyclopropane ring opening via the polar pathway.

1.2.1.3 Cyclopropylcarbinyl → Homoallyl type rearrangements of radical anions generated from aliphatic ketones

Radical anions derived from **7a** and **7b** undergo cyclopropane ring opening, slightly favoring the tertiary distonic radical anion in the case of **7b**$^{\bullet-}$ (**Scheme 1.4**). Electron transfer was found to be the rate limiting step regardless of whether the reduction was carried out directly (CV) or indirectly (homogeneous redox catalysis) suggesting a rate constant for ring opening ≥ 10^7 s^{-1}. (The value of α derived from the direct electrochemistry suggested these radical ions do have a discrete lifetime).[10]

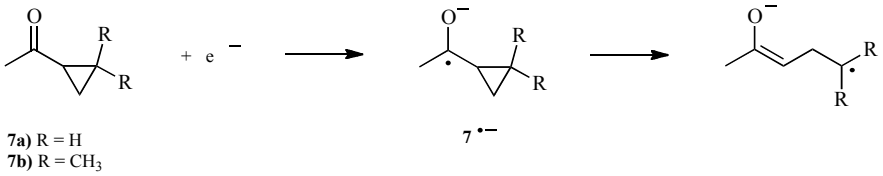

Scheme 1.4 Ketyl radical anions ring opening. Reproduced by permission of the American Chemical Society **.[10]**

Because the kinetics of both the direct and mediated reduction of **7a** and **7b** involves rate limiting electron transfer, the rate constant for ring opening could not be determined. However, it was reasoned that the corresponding cyclobutyl derivative

would undergo ring opening at a significantly lower rate, and that ring opening might be the rate limiting step for this system. In fact, the rate constant for ring opening **(equation (1.3)[7] reproduced by permission of** the American Chemical Society**)** of **8•-** (k = 8 x 10^3 s^{-1}) was found to be similar to that of the cyclobutylcarbinyl (neutral) radical.[10]

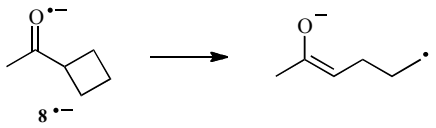

(1.3)

When this cyclobutyl-based rearrangment was used as an intramolecular clock to estimate the rate constant for cyclopropyl ring opening via competition experiments (**Scheme 1.5**), only a cyclopropane ring opened product was detected.[10]

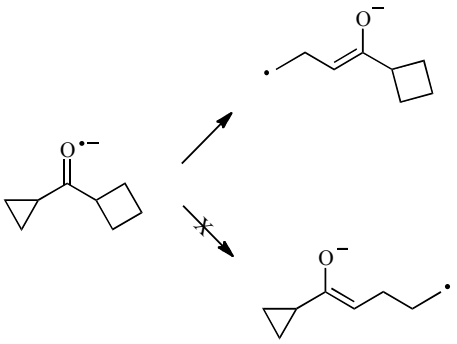

Scheme 1.5. Intramolecular competition between cyclopropane and cyclobutane radical anion ring opening. Reproduced by permission of the American Chemical Society **.[10]**

Compound **$9^{\bullet-}$** undergoes ring opening according to **(equation (1.4)[7] reproduced by permission of** the American Chemical Society**)**. The exocyclic double bond significantly enhances the rate of ring opening (For R = phenyl, an enhancement > 10^3 was estimated).[7] This enhanced rate is likely attributable to the increase in ring strain resulting from the double bond *exo*cyclic to the cyclopropane ring, rather than

resonance stabilization (the rupturing C-C bond is orthogonal to the π-system of the *exo*cyclic double bond).

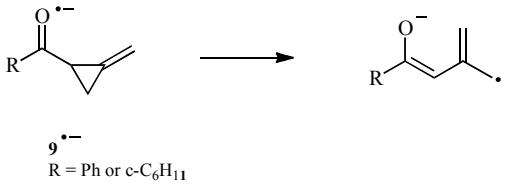

$\mathbf{9}^{\bullet-}$
R = Ph or c-C_6H_{11}

(1.4)

1.2.1.4 Cyclopropylcarbinyl → Homoallyl type rearrangements: structure/reactivity trends

Sufficient data is now available to allow a comparison between cyclopropylcarbinyl → homoallyl-type rearrangements of neutral radicals and radical anions generated from ketones **(equation (1.5)[7] reproduced by permission of** the American Chemical Society**)**. There are certainly similarities: 1) Radical-stabilizing groups at the α-carbon (R^1) decelerate the ring opening process and 2) radical stabilizing substituents on the cyclopropyl group (R^2) accelerate the reaction. For both types of processes, relief of cyclopropyl ring strain is not the sole mitigating factor associated with the rates of these rearrangements. Resonance energy (spin delocalization) in the ring-closed vs. ring-opened form must also be considered.[7]

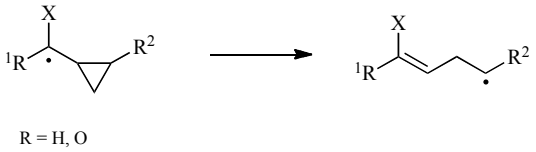

R = H, O

(1.5)

There is an important difference though: For radical anions, charge delocalization is at least as important as, and perhaps more important than, spin delocalization (vide infra). This interplay between charge and spin delocalization in the ring-closed and ring-opened (distonic) radical anions leads to the reactivity order summarized in **Figure 1.1**.[7]

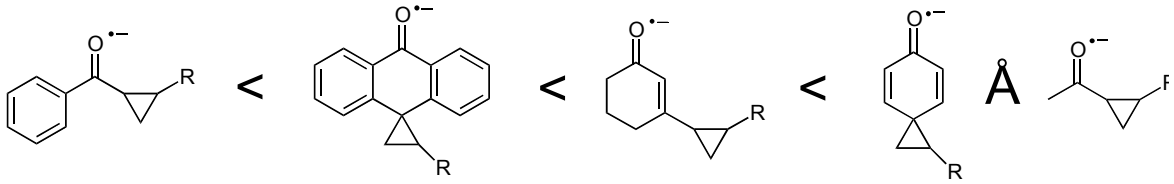

Figure 1.1. Rates of cyclopropylcarbinyl homoallyl type rearrangements of kety radical anions. Reproduced by permission of the American Chemical Society.

For radical anions generated from aromatic ketones (aromatic ketyls), ring opening of the structurally-related neutral (benzylic) radical is much faster. For aliphatic ketones, it is the other way around. Unquestionably, the difference is the ability of the aromatic ring to stabilize the negative charge via resonance (**Scheme 1.6**); (the numbers refer to Mulliken charges calculated by density functional theory.) Clearly, this stabilization of charge is responsible for the low reactivity and thermodynamic stability of the aromatic ketyls.[10]

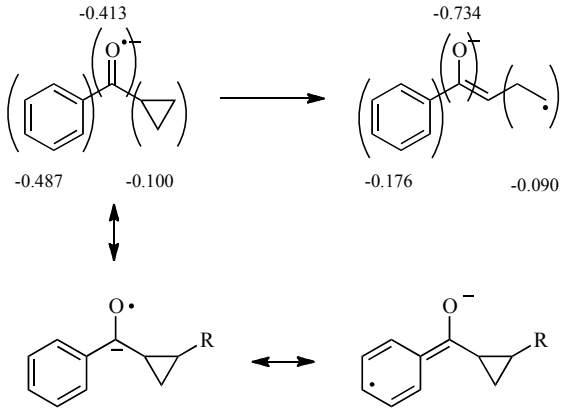

Scheme 1.6. Aromatic ketyl radical anion with calculated Mulliken charges B3LYP/6-31G*.

In contrast, these results show aliphatic ketyls are at least (and likely more) reactive in comparison to alkyl radicals in β-scission-type processes, despite the fact that the former are thermodynamically much more stable (by as much as 27 kcal mol^{-1}). Essentially, the O^- group, being a potent electron donor, is able to stabilize a radical center. The reason that aliphatic ketyls undergo such rapid rearrangement is that the O^-

group also stabilizes the double bond in the ring-opened form, possibly to an even greater extent. (An equivalent, and indistinguishable argument is that the O^- is stabilized by an adjacent radical center in the ring-closed form, and by a double bond in the ring-opened form.) In essence, these systems undergo ring opening at what must be rates comparable to the cyclopropylcarbinyl → homoallyl neutral radical rearrangement because the reactants, products, and transition state are all stabilized by the O^- substituent.

Qualitatively and quantitatively, rate constants (k_o) for ring opening of the radical anions can be rationalized on the basis of the thermodynamic stability of the radical anion (which is related to the formal reduction potential of the ketone), the ability of substituents on the cyclopropyl group to stabilize the radical portion of the distonic radical anion (reflected by the C-C bond strength of the cyclopropane), and the stability of the enolate portion of the distonic radical anion (related to the pK_a of the corresponding ketone). A thermodynamic cycle for estimating the driving force (ΔG^o) for ring opening was developed therefore allowing the nature of the activation/driving force relationship for these rearrangements to be probed. **Figure 1.2** presents a plot of log(k_o) vs. ΔG^o for cyclopropylcarbinyl → homoallyl-type rearrangements of both ketyl radical anions and neutral free radicals. Despite the differing structure/reactivity trends discussed above, it is noteworthy that the activation/driving force trends for ring opening of neutral free radicals parallel those of radical anions, though at comparable driving force, ring opening of the radical anions is generally slower.[11]

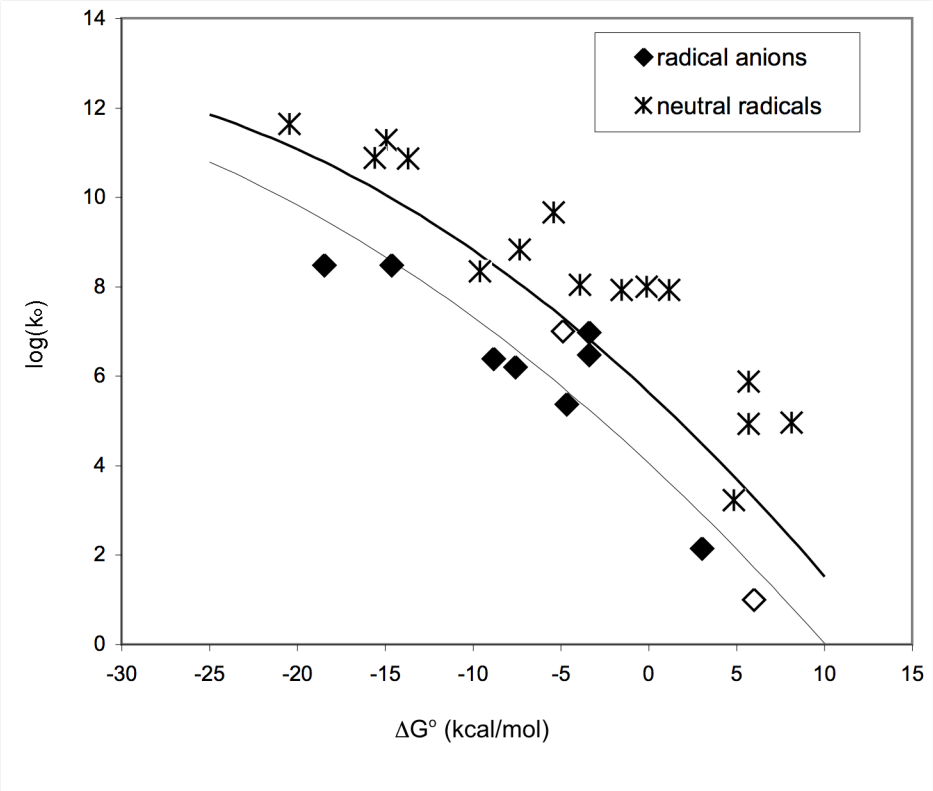

Figure 1.2. Structure/reactivity relationships for the cyclopropylcarbinyl →homoallyl-type rearrangement of radical anions generated from carbonyl compounds and neutral free radical (unshaded data points are based on estimates of k_o).

Savéant has developed theory pertaining to radical anion fragmentations which occur in a stepwise manner (e.g., R-X + e^- → R-$X^{\bullet -}$ → R• + X^-) which is applicable **(equation (1.6))**, where $\Delta G_o^{\neq}$ refers to the intrinsic barrier (activation energy at zero driving force) and accounts for the reorganization of solvent and/or counter ion (external reorganization), or changes in the molecule itself (internal reorganization) which are required in order to achieve the transition state; k_B, h, R, and T have their usual meanings.[12] When applied to the data in **Figure 1.2**, several interesting conclusions emerge. For the radical anions, the intrinsic barrier (12 kcal mol^{-1}) is only slightly higher than that for the neutral free radicals (10 kcal mol^{-1}).

$$\log(k_o) = \log\left(\frac{k_B T}{h}\right) - \frac{\Delta G_o^{\mp}}{2.303RT}\left(1 + \frac{\Delta G^o}{4\Delta G_o^{\mp}}\right)^2 \qquad (1.6)$$

Assuming that the bond breaking/making contributions to the intrinsic barrier (*i.e.*, internal reorganization energy) are similar for both classes of paramagnetic intermediates, the small difference in rate is attributable to the contribution of a minor, *ca.* 2 kcal mol^{-1} solvent reorganization component for the radical anion ring opening. This conclusion makes sense because for these ring openings, the negative charge is closely associated with the electronegative oxygen atom in the ring closed and ring opened forms, and a major reorganization of solvent is not needed to stabilize the negative charge in the progression from reactant → transition state → product. In contrast, higher intrinsic barriers (*ca.* 16 kcal mol^{-1}) are found for radical anion fragmentations where the negative charge migrates significantly, e.g., $Ph(C{=}O^{\bullet -})CH_2X$ → $Ph(C{=}O)CH_2\bullet + X^-$.[13]

There has been a great deal of interest in the current literature in the mechanistic details of dissociative electron transfer (DET), i.e., electron transfer which results in bond cleavage. The radical anion ring openings discussed thus far are examples of this phenomenon, and until recently, were all believed to occur in a stepwise fashion (**Scheme 1.7**, path a). However, it now appears that certain 1,2-disubstituted cyclopropanes undergo concerted, dissociative electron transfer (i.e., electron transfer occurs simultaneously with bond cleavage, path b, **Scheme 1.7**). The fact that the process is stepwise when R = Ph as opposed to concerted when R = CH_3 is readily accounted for by resonance stabilization provided by the phenyl group in the former.[14]

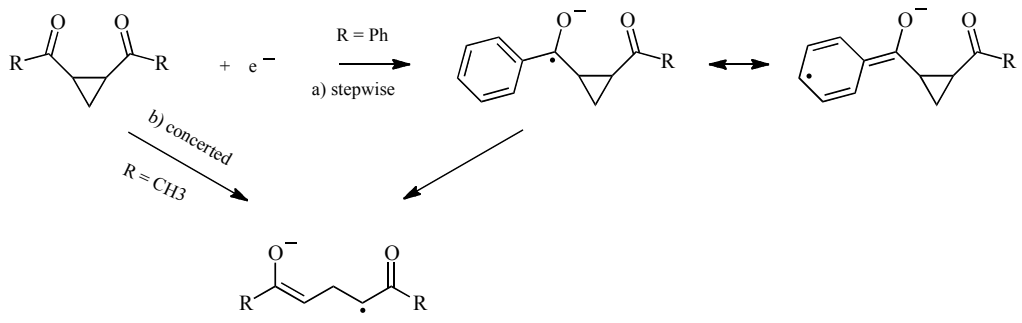

Scheme 1.7. Stepwise and concerted dissociative electron transfer. Reproduced by permission of the American Chemical Society **.**[15]

1.2.2 Cyclopropyl Substituted Radical Cation Ring Openings

1.2.2.1 Aliphatic *N*-cyclopropylamine radical cations: structure and mechanism of cyclopropane ring opening

Compared to the chemistry of radical anion and neutral radical analogs, our understanding of reactivity of cyclopropane substituted radical cations is in its infancy. Kinetic data is virtually non-existent for aliphatic amine radical cations. Theoretical and experimental studies demonstrate cyclopropylamine radical cation undergoes barrierless ring openings in both gas and solution (Freon) phase.[16] The distonic ring opened radical cation isomerizes via successive 1,2-hydrogen migration **(Scheme 1.8).**[16a, 17] Ring opened cyclopropylamine radical cations preferentially form the radical cation of allylamine **10.**

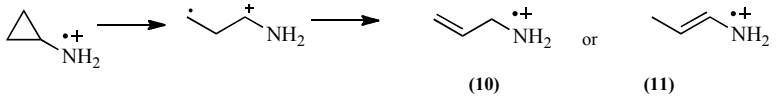

Scheme 1.8. Ring openings of aliphatic cyclopropylamine radical cation and subsequent 1,2-hydrogen migration. Reproduced by permission of the American Chemical Society **.**[18]

Notably, ring opening products undergo further dissociative steps to achieve more stable structures in the gas phase, but not in solution. This difference is presumably attributable to stabilizing interactions with solvent.[15-16] Cyclopropylamine

radical cations pass through a perpendicular transition state when ring opening. Extremely facile ring opening prevents the molecule from rearranging to the bisected conformation before ring opening. Computational analysis of the relative rates of ring opening for the cyclopropoxyl radical, cyclopropylcarbinyl radical and cyclopropylaminyl radical cation confirmed barrierless radical cation ring opening is most facile, followed by a preference for ring opening of the cyclopropoxyl radical over cyclopropylcarbinyl radical in a ratio of 3.1×10^6 to 1.[16b]

The unique structural features of alkylcyclopropylamines likely to govern reactivity and stability were highlighted in ESR and computational studies by de Meijere and co-workers. In *N,N*-diisopropyl,*N*-cyclopropylamine the cyclopropyl group adopts a perpendicular geometry and the molecule has C-N-C bond angles of about 113.3^{o} because the cyclopropyl group prefers to accept electron density into its LUMO.[19] In triisopropylamine, replacement of isopropyl groups with cyclopropanes, results in significant increases in the ionization energy for the radical cation. The ionization energy increased from a value of 7.18 eV for trisopropylamine to 8.44 eV for tricyclopropylamine, as determined experimentally. A similar increase of 7.13 eV to 8.26 eV was determined by computational work.[19] Generally, trialkylamine radical cations prefer planar orientations that facilitate donation of electron density to the electron deficient nitrogen center.[20] Neutral tricyclopropylamine is significantly more pyramidal than the corresponding radical cation. The cyclopropyl groups in tricyclopropylamine radical cations are in a bisected conformation relative to the N's partially filled orbital. A large structural reorganization from the perpendicular

conformation of the neutral analog is required to form the radical cation (**Figure 1.3**).[19-20]

Figure 1.3. Neutral tricyclopropyl amine adopts a perpendicular conformation; structural reorganization upon formation of the of radical cation yields a bisected conformation.

Alkyl substituted analogs typically exhibit conformations where the singly occupied N orbital is eclipsed by a H from an adjacent alkyl substituent affording stabilization by delocalizing spin through hyperconjugative interactions (**Figure 1.4**).[20] The preference for the bisected conformation in tricyclopropylamine radical cation means that these hyperconjugative interactions do not exist because the H on the cyclopropane is twisted about 90^{o} from the nitrogen center into a nodal plane of the half filled p orbital.[20] (In the bisected conformation, the cyclopropyl group is a potent p-electron donor).

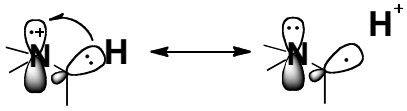

Figure 1.4. Hyperconjugative stabilization characteristic of aliphatic amine radical cations.

While there is much to be learned about the chemistry of aliphatic cyclopropylamine radical cations, it is interesting to note that a) bi and tricyclopropylamines deviate significantly from the planarity characteristic of the corresponding trialkylamines and require structural rotations upon formation of the radical cation, b) these changes likely accompany alignment of the partially filled orbital

on nitrogen with the adjacent p system of the cyclopropane, c) ring opening for cyclopropylamines has a low barrier and products undergo further rearrangement in gas phase. Analogous rearrangements do not occur in solution. Taken as a whole, kinetic data available for ring opening of aliphatic cyclopropylamine radical cations comes from computational work and suggests that ring opening is concerted and extremely rapid.

1.2.2.2 Application: *N*-cyclopropyl ring opening in ring expansions of arylcyclopropanes

Cyclopropane substituted radical cation ring openings are also useful in synthesis. In non-aromatic *N*-cyclopropyl substituted radical cations, the driving force for ring opening is stability imparted by separation of the radical and cation on different atoms, as well as the relief of ring strain. Blackstock and coworkers exploited this in the study of a series of cyclopropylamines (**Figure 1.5**) by generating the radical cation of the amines via photoinduced electron transfer.[18]

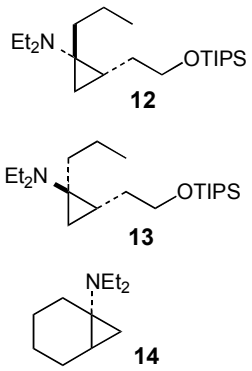

Figure 1.5. Structures of cyclopropylamines investigated as potential precursors to ketones.

Efficient ring opening and product formation was observed for **12** and **13**, although reaction of **13** was slower.[18] The mechanism of these reactions proceed from the N-centered ring closed radical cation to the ring opened product; which undergo a subsequent 1,5 hydrogen atom shift **(Scheme 1.9).** Intramolecular hydrogen transfer

was confirmed via isotopic labeling studies. Subsequent deactivation of the radical ion pair partner 1,4 dicyanobenzene radical anion ($DCB^{\bullet-}$) via single electron transfer is followed by generation of a ketone product through hydrolysis of the neutral ring opened amines during work up. With the exception of bicyclic compound **14**, these aminocyclopropane radical precursors are used as synthetic analogs of enamines, affording high yields of ketones.

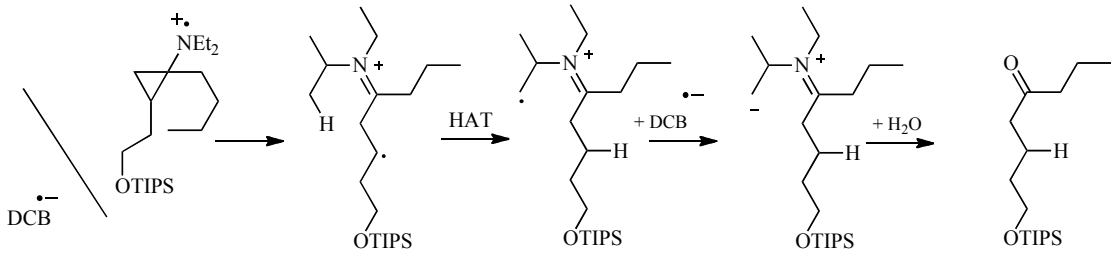

Scheme 1.9. Ring opening of photo-generated cyclopropylamine Reproduced by permission of the American Chemical Society **.**

1.2.2.3 Application: vinyl and siloxy substituted cyclopropyl ring opening in ring expansions

Chemically induced one electron oxidation of vinylcyclopropanes leads to radical cations that rearrange to the corresponding cyclopentene radical cations; the rate is much greater than the comparable thermally induced vinyl cyclopropane → cyclopentene rearrangement.[21] Neither *cis*-1-*p*-anisyl-2-vinylcyclopropane nor *trans*-1-*p*-anisyl-2-vinylcyclopropane undergo ring expansion to 4-*p*-anisylcyclopentene because the s-*trans* radical cation formed can not ring expand. The former undergoes cis → trans isomerization. In contrast, the spiro compound forms the desired cyclopentene product via a mechanism involving ring opening of the spirocyclic vinylcyclopropane radical cation intermediate (**Scheme 1.10**). Similar to the cis → trans isomerizations, the rate of rearrangement is enhanced by single electron transfer. Half lives of 10^{12} min compared to $\leq$ 1 min were observed for the thermal and SET-induced

processes, respectively. SET-induced ring expansion of cis and trans 1-*p*-anisyl-2-methyl,2-prop-1-en-cyclopropane demonstrates that this chemistry is not limited to structurally rigid cyclopropanes, although it is unclear why these compounds ring expand and the *p*-anisyl-vinylcyclopropanes do not.[21]

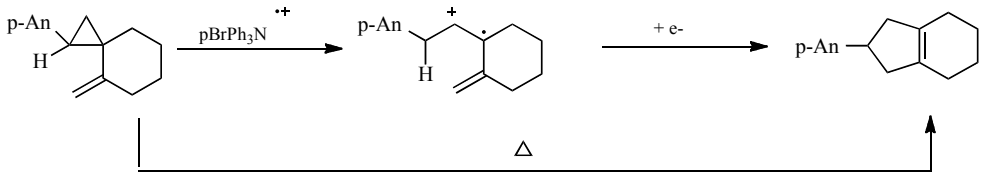

Scheme 1.10. Ring expansion via ring opening of spirocyclic vinylcyclopropane. Reproduced by permission of the American Chemical Society **.[21]**

Siloxy cyclopropane radical cations are also key intermediates in synthesis of larger ring systems wherein the radical cation ring opens, without nucleophilic assistance, to a distonic radical cation, subsequent loss of the silane group forms a b-keto radical.[22] These b-keto radicals have proven useful in the formation of polycycles through intramolecular addition to pi systems. Transition state calculations by Mattay and coworkers on (bicycle[4.1.0]heptan-1-yloxy)trimethylsilane determined endocyclic bond cleavage of the cyclopropane ring occurs.[23] This result supports experimental work with analogous compounds, by Hasegawa.[24] Further study of the regioselectivity of the cleavage of the bonds in these bicyclic compounds (**Scheme 1.11**) revealed a) that photochemically induced electron transfer and chemically induced oxidation (by tri-bromophenylaminyl radical cation) caused ring opening to occur via different pathways, as evidenced by observed products, and b) the presence of a nucleophile in chemically oxidized systems enhances the ability of the radical cation to undergo desylation thus increasing reaction efficiency.[24] In addition to utility in synthesis, *N*-cyclopropyl substituted radical cations have been controversial and interesting target molecules for use as mechanistic probes and radical clocks.

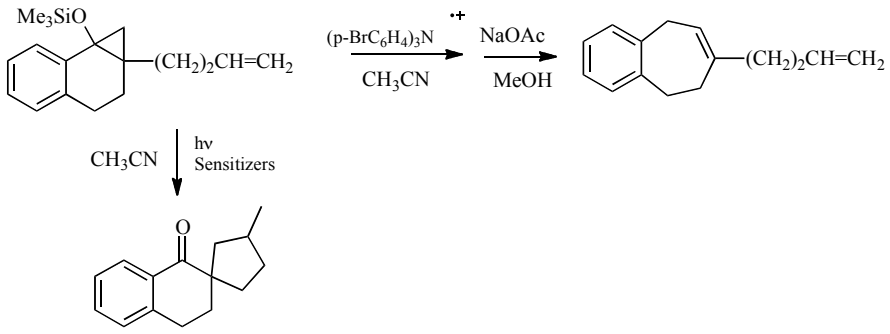

Scheme 1.11. Spirocyclic cyclopropane radical cation exhibits regioselectivity during ring opening as determined by mode of radical cations generation. Reproduced by permission of the American Chemical Society **.[24]**

1.2.2.4 Application: *N*-benzyl,*N*-cyclopropylamine radical cation mechanistic inhibitors in single electron transfer enzymes

In the late seventies, the single electron transfer mechanism was first invoked to explain irreversible inhibition of P450s by *N*-benzyl-*N*-cyclopropylamine substrates.[25] The potential of this class of substrates to resolve controversy between the hydrogen atom transfer (HAT) and single electron transfer (SET) mechanisms (**Schemes 1.12 and 1.13)**, for oxidation of tertiary amines by P450s and monoamine oxygenases, stimulated significant interest in mechanistic inhibitors containing cyclopropane moieties to probe for single electron transfer in enzymes.[25b, 26],[27] The metabolism of *N*-benzyl-*N*-cyclopropylamine and the 1-methyl substituted analog show similar inhibitory behavior toward P450 suggesting the hydrogen of the cyclopropane is not involved in inhibition; and further decreasing the probability of HAT for benzylcyclopropyl amine.[28] Consistently low deuterium isotope effects for dealkylation of tertiary amines by P450 provided further evidence for the SET pathway.[29],[30]

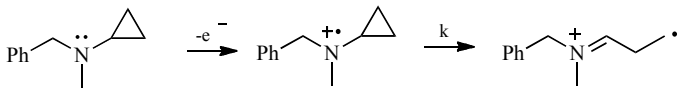

Scheme 1.12. SET generation of ring opening of N-cyclopropylbenzylamine radical cation. The ring opened form is proposed to inhibit SET enzymes by covalent interaction with a residue in the active site. Reproduced by permission of the American Chemical Society **.[27]**

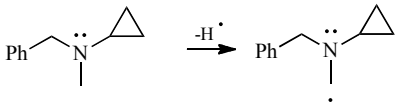

Scheme 1.13. With HAT, hydrogen abstraction yields a neutral carbon centered radical which is not expected to ring open. Reproduced by permission of the American Chemical Society **.[27]**

1.2.2.5 Application: *N*-cyclopropylaniline radical cations as mechanism-based inhibitors in single electron transfer enzymes

Hanzlik and coworkers set out to demonstrate, using Horse Radish Peroxidase (HRP), that mechanism based inactivation and ring opening of aryl-*N*-cyclopropylamines occurs exclusively through the single electron transfer pathway.[28] Because HRP's oxidation potential (0.75 V) is less than P450's (1.7-2.0 V); *N*-methyl-*N*-cyclopropylaniline (which is easier to oxidize) was used in lieu of *N*-methyl-*N*-cyclopropylbenzylamine.[28] Products arising from ring opening were detected, although the yields suggested the ring opening pathway accounts for less than 25% of *N*-methyl-*N*-cyclopropylaniline consumed in the reaction. The consumption of this substrate also followed a first order decay indicating inactivation of the enzyme is not occurring to an appreciable degree.[28] Radiolabeled cyclopropylaniline inhibitors (**Figure 1.6**) and radical traps were employed to determine the fate of the cyclopropyl group. In HRP, trapped products were unambiguously ascribed to SET.[28] Products derived from HRP

oxidation of *N*-methyl-*N*-cyclopropylbenzylamines **15,19** suggested a unimolecular rearrangement, as different products are expected from a nucleophile assisted ring opening.[25b] In contrast, for *N*-methylaniline **16** and *N,N*-dimethylaniline **17** both undergo deprotonation of the *N*-methyl group after SET.[28] In P450 neither inhibition nor ring opening products were observed with *N*-methyl-*N*-cyclopropylanilines **18**.[27] Experiments with P450 and the *N*-benzyl-*N*-cyclopropylamines produced the ring opened metabolite of the SET pathway in 57% yield![27] Interestingly, analogous investigation of *N*-methy-*N*-cyclopropylbenzylamine was first order showing no inhibition or ring opened product, rather dealkylation to form *N*-cyclopropyl-*N*-benzylamine, was observed.[27]

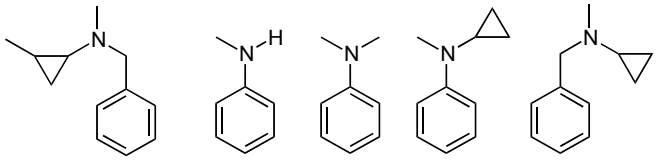

15 **16** **17** **18** **19**

Figure 1.6. Structures of aryl cycloproplyamines investigated in enzymatic systems.

Key to the viability of aromatic N-cyclopropyl substituted amines as mechanistic inhibitors is validation that a) ring opening is competitive with other modes of decay for the radical cation, such that inhibition due to ring opening occurs with a frequency that can be easily detected relative to normal modes of catalysis and b) ring opening and the resultant enzymatic inhibition are irreversible processes.

1.2.2.6 Cyclopropane ring opening in chemical systems: *N*-cyclopropylaniline radical cations

A comprehensive understanding of all factors that govern the mechanism, kinetics and energetics of cyclopropane radical cation reactions, as well as the relative

propensity of these oxidized species to decay by one pathway or another, is integral to unlocking their potential as mechanistic inhibitors, radical clocks and photosensitizers. Recently, our group studied the ring opening of electrochemically generated *N*-methyl-*N*-cyclopropylaniline radical cations, and curiously, ring opening occurred much slower than deprotonation.[31] Based upon the variation of peak potential with sweep rate and concentration, it was concluded that decay of the radical cation is first order (as expected for a ring opening process). Notably, decay is zero order in CH_3OH, which effectively rules out the nucleophile assisted pathway for Nu^- = CH_3OH.[31] Indirect electrochemical studies using various substituted ferrocenes were performed, and in all cases, the kinetics were controlled by the chemical step (i.e., cyclopropane ring opening). These two sets of experiments enable both the oxidation potential (+0.528 V vs. 0.1 M Ag^+/Ag) and the rate constant for ring opening (k_o = 4.1 x 10^4 s^{-1}) to be resolved.[31] LFP experiments (direct photoionization at 266 nm) showed that the radical cation of *N*-cyclopropyl-*N*-methylaniline was detected at a λ_{max} of 480 nm, and the lifetime for the radical is not perturbed upon introduction of a *N*-cyclopropyl group (in place of an *N*-methyl) suggesting that ring opening occurs on a time scale too long for LFP, meaning that k is less than 1 x 10^6 s^{-1}.[31] Thus, rather than being more easily oxidized, *N*-cyclopropyl-*N*-methylaniline is actually slightly more difficult to oxidize than *N,N*-dimethylaniline (E_{ox} = +0.491 V). The sluggish rate of ring opening, and the fact that the cyclopropyl group seems to have exerted little effect on the oxidation potential is easily explained; in *N*-cyclopropyl-*N*-methylaniline radical cation, the perpendicular conformation is lower in energy than the bisected conformation.[31] In the perpendicular conformation, overlap between the HOMO of the cyclopropyl group and adjacent π-

system is minimal.[31] Thus, the radical cation does not enjoy thermodynamic stabilization afforded by the cyclopropyl group, and is in the wrong conformation for ring opening to occur. This system is of particular interest because *N*-cyclopropyl-*N*-methylaniline, and several structurally related derivatives, were used to probe for single electron transfer in amine oxidations mediated by P450. Information regarding the low rate and unfavorable stereoelectronic factors for ring opening was not available for these studies.[5,13-17] Based upon this new information, it is likely that even if electron transfer were occurring in these systems, the sluggish rate of ring opening would be unable to compete with other processes such as radical cation deprotonation (**Scheme 1.14**).

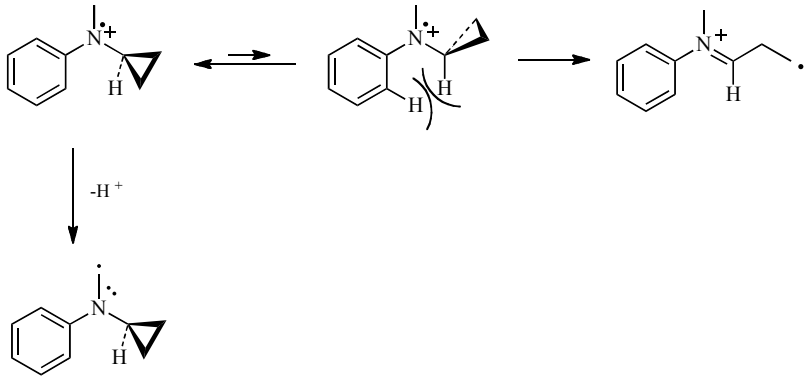

Scheme 1.14. Ring opening and deprotonation are non-competitive for N-methyl,N-cyclopropylanilines.

N-alkyl-*N*-cyclopropylaniline radical cations have been employed as mechanistic probes in nitrosations of aromatic amines where ring opening is an indicator of radical cation intermediates in nitrosation of *N,N*-dialkyl aromatic amines. Nitrosation of *N*-alkyl-*N*-cyclopropylanilines in acidic media (**Scheme 1.15**) proceeds through an aminyl radical cation intermediate. This intermediate undergoes regioselective ring opening and reacts further to form *N*-alkyl-*N*-nitroanilines.[32] Studies of acidity effects on decomposition pathway revealed the preferential mode of reactivity is de-ethylation

(versus de-methylation) when solution pH is above 2.[33] With addition of base α-deprotonation emerges, a favored pathway of decay; when the acidity is high deprotonation is suppressed and *N*-alkyl-*N*-cyclopropylanilines ring opening dominates.

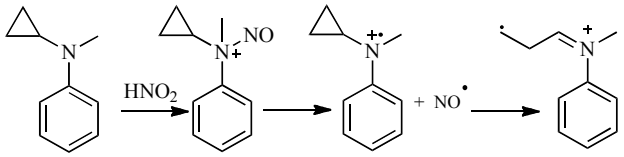

Scheme 1.15. Nitrosation mechanism for N,N-dialkylanilines. Reproduced by permission of the American Chemical Society **.**[31]

1.2.2.7 Cyclopropane ring opening in chemical systems: cyclopropylarene radical cations

In the past decade, kinetic studies of arylcyclopropane radical cations have emerged shedding light on their reactivity.[12,23,25-29] One very notable feature of cyclopropylaryl compounds is the stability provided by cyclopropanes in the plane of the p system containing the radical.[34] Crystallographic data in addition to molecular mechanics calculations for several aryl cyclopropane radical cations suggest cyclopropanes can act as electron donors when the cyclopropane is in the bisected conformation (**Figure 1.7**).

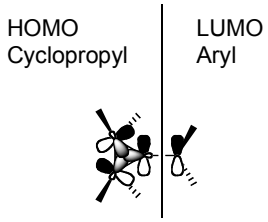

Figure 1.7. Walsh model for the cyclopropane HOMO in the bisected conformation mixes with the LUMO of the aryl group, also coplanar, allowing it to donate electron density to the conjugated ring. Reproduced by permission of the American Chemical Society.[34]

The equilibrium conformation for cyclopropyl naphthyl and phenyl compounds is bisected while the 9-anthryl compounds adopt a perpendicular geometry (**Figure 1.8**).[34] The cyclopropylanthrancenes are forced into this conformation by unfavorable steric interactions between the cyclopropane and peri-hydrogens on the adjacent anthracene. For the naphthyl and phenyl compounds the preference for the bisected conformation enables interaction of the aryl groups p system with the sp^2 orbital of the cyclopropyl carbon.[34] When the molecule is strongly electron deficient, as in the case of a radical cation, the p orbital on the aryl carbon adjacent to the cyclopropane is twisted out of conjugation with the cyclopropane the perpendicular conformation, markedly decreasing propensity for ring opening.[34]

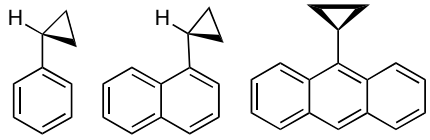

Figure 1.8. Cyclopropylarenes.

Dinnocenzo et al. demonstrated that ring opening of phenylcyclopropane radical cation occurs via a nucleophile-assisted, overall second-order process as delineated in **equation (1.7)[35] (reproduced by permission of** the American Chemical Society**)**.

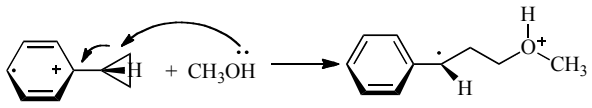

(1.7)

Inversion of configuration was observed in the nucleophile assisted ring opening of 1-phenyl-2,3-dimethylcyclopropanes, phenylcyclopropane reacting with methanol, isopropanol, tert-butanol, pyridine, water and cyanide ion.[35-36] Stereoinversion is attributed to positive overlap between the non-bonding orbital of the nucleophile and the σ^* orbital of the radical cation's one electron bond favoring a backside (σ^*) rather than

frontside (σ) interaction.[36a, 37] Interestingly, the rate constants in **Table 1.1** for substitution on 1,1-diphenylcyclopropane translate to a reactivity ratio 5:3:1, or less, going from primary to tertiary alcohol.[36a]

Table 1.1. Rate constants for ring opening of phenylcyclopropane radical cation by various nucleophiles at 23°C. Reproduced by permission of the American Chemical Society.[35-36]

Nucleophile	k, $[M^{-1}s^{-1}]$
CH_3OH	1.6×10^7
CH_3CH_2OH	1.4×10^7
$(CH_3)_2CHOH$	1.1×10^7
$(CH_3)_3COH$	$.73 \times 10^7$

Structural distortion inherent to radical cations formed by one electron oxidation leads to an early transition state with a large carbon-nucleophile distance lessening the effect of the nucleophile's steric bulk on kinetics.[36a] Additionally, the electronic environment of the carbon is significantly more important in determining the site of substitution than in four electron S_N2 reactions. Rate constants in **Table 1.2** for the reaction of 1,1-diphenyl-*2*-alkylcyclopropane radical cations present a counter intuitive trend, in that reaction rate constants actually increase as the degree of substitution is increased at the site of attack.

Table 1.2. Rate constants for methanol assisted ring opening for 1,1-dipheny-2-alkylcyclopropanes at 23°C in CH_3CN. Reproduced by permission of the American Chemical Society [38]

C2 Substituent(s)	k, $[M^{-1}s^{-1}]$
CH_3, CH_3	3.2×10^8
CH_3	1.5×10^8
CH_3CH_2	8.3×10^7
$(CH_3)_2CH$	3.0×10^7
$(CH_3)_3C$	4.8×10^6

The preference for anti-Markovnikov addition of methanol to substituted cyclopropanes was quite accurately predicted to be a result of weakening but not breaking of the C_a-C_b

bond by Hixson and cowokers.[39] Much later this supposition was confirmed by computational work that showed the C_{α}-C_{β} bond is about 10 kcal mol^{-1} in the transition state. Further it is noted that displacement preferentially occurs at the more substituted carbon.[38] Enhanced stabilization of the positive charge in the transition state on the more substituted carbon primarily drives the reaction to proceed at the more sterically hindered, but more electron rich, carbon on the cyclopropane ring as shown in **Scheme 1.16**.[38]

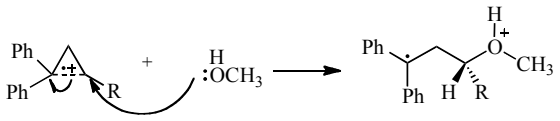

Scheme 1.16 Methanol adds at the more substituted carbon on an alkylsubstituted cyclopropane radical cation. Reproduced by permission of the American Chemical Society **.[32b]**

In the transition state increased C_a-C_b bond length, a 140° C_a-C_b-OMe bond angle, and a greatly increased localization of positive charge at the b position are predicted by both AM1 and PM3 calculations.[36b] The latter feature predicts the observed positive r value and high degree of correlation between *k* and the Hammett σ+ (rather than σ) parameter. *p*-Substituted phenyl groups at C_a stabilize the positive charge decreasing the importance of substitution at the C_b attack site on the cyclopropane effectively reintroducing the issue of steric bulk at the site of substitution and leading to an increased barrier to reaction as shown by the rate constant trend in **Table 1.2**. Although the structures of neutral cyclopropanes are relatively unresponsive to alkyl substitution, their radical cation counterparts are far more sensitive.

Cyclopropylbenzene and cyclopropylnaphthalene radical cations undergo nucleophile assisted ring opening,[36b, 40] whereas radical cations derived form cyclopropylanthracenes do not undergo ring opening.[40] Surprisingly low rate constants

for ring opening of cyclopropylnapthalenes have been observed, on the order of 10 $M^{-1}s^{-1}$. The decay occurs via a bimolecular pathway where the barrier to reaction is significantly affected by the magnitude of the positive charge on the cyclopropane in the transition state.[41] The ring openings of the analogous radical anions are unimolecular processes with rate constants several orders of magnitude larger(10^6–10^8 s^{-1}) than those observed for the aforementioned radical cations.[42] Electrochemically generated 9-cyclopropylanthracene and 9-bromo-10-cyclopropylanthracene radical cations show that nucleophilic attack on the aromatic ring occurs, rather than a nucleophile assisted ring opening, in the presence of methanol.[41b] While some cyclopropane ring-opened products were observed, in these studies, ring opened products were shown to arise from reaction of a primary product during work up of the reaction mixture.[41b]

A thermochemical cycle was used to estimate ΔG^o showing nucleophile-induced ring opening is extremely exoergic for all these radical cations (ΔG^o = -39, -28, and -20 for Ar = phenyl, α-naphthyl, and 9-anthryl, respectively). These results rule out the explanation that the sluggish rate of ring opening associated with the α-napthyl and 9-anthryl systems is simply attributable to the enhanced stability of these radical cations. Two major factors were found to contribute to ΔG_o for ring opening: a) the ability of the aryl group to stabilize the ring-closed radical cation (related to $E^o_{Ar\cdot/Ar}$) and b) the ability of the aryl group to stabilize the radical portion of the ring-opened (distonic) radical cation. On this basis, it was suggested that the reason that ring opening is slow for arylcyclopropane radical cations is a late (product-like) transition state, **Figure 1.9,** in which the positive charge is localized on the cyclopropyl group and thus, unable to benefit from stabilization offered by the aromatic ring.

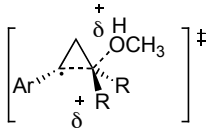

Figure 1.9. Charge localized transition state for ring opening of cyclopropylarenes. Reproduced by permission of the American Chemical Society.[36b]

The aromatic ring stabilizes the radical portion in the transition state, however, the effect of the aryl group on radical stability is miniscule compared to the effect of the aryl group on the stability of the ring-closed radical cation. (In the case of 9-cyclopropylanthracene radical cation, stereoelectronic factors may also contribute to the high barrier to ring opening; the cyclopropyl group in this system may exist in the perpendicular conformation, which does not meet the stereoelectronic requirements for ring opening). For a cyclopropane containing compound to act as an effective probe, for a SET mechanism with a radical cation intermediate, ring opening must occur faster than other possible decay processes. In the case of these radical cations the reactions proceed slowly through a product like transition state with significantly localized charge which severely limits their reactivity and dominates over the large thermodynamic stabilization that would otherwise suggest these molecules would make attractive substrates for use as mechanistic probes or radical clocks *(see Chapter 4)*.[43]

B3LYP calculations with a 6-31G(d) basis set suggest the structure of phenylcyclopropane radical cation has a cyclopropane containing 2 long and 1 normal length bond in contrast to the 1 long 2 normal bond length confirguration observed for the alkylsubstituted cyclopropanes in **Figure 1.10**.[36b] Additionally, with alkyl substitution at the β position the bisected conformation of the phenyl ring (which in the unsubstituted compound overlaps and stabilizes relatively equally the two C-C s bonds) moves into a conformation with a higher degree of overlap with the longer C_α-C_β bond.

Redistribution of charge accompanies these structural changes because the alkyl substituents are capable of stabilizing more of the positive charge associated with the radical cation character.[36b]

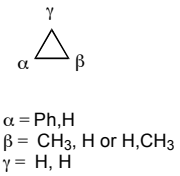

Figure 1.10 Substituted cyclopropanes studied in computations.

Photochemically generated three ring bridged allylcyclopropane radical cations undergo nucleophilic substitution in the presence of base. These substitution products are arrived at through a deprotonation mechanism, **Scheme 1.17**.[44] Deprotonation products are favored at position 2 because of resonance stabilization afforded by interaction with the neighboring functional groups.[44]

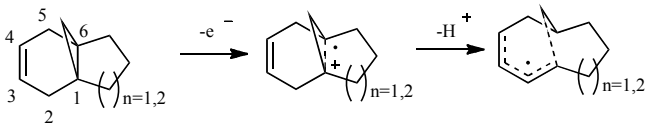

Scheme 1.17. Ally cyclopropanes deprotonation of the radical cation intermediate at position 2.

Like nucleophile assisted ring openings the cis/trans isomerization of 1,2-disubstituted cyclopropane radical cations proceeds through ring opened intermediates. These isomerizations occur via different mechanisms when the initial one electron oxidation to form the ring closed radical cation is induced photolytically or by a chemical oxidant.[45] The latter process (**Scheme 1.18**) is significantly more facile; the chemical oxidation of 1-phenyl-2-vinyl-cyclopropane by *p*-$BrPh_3N^{\cdot+}SbF_6^-$ experiences a rate increase of 10^{24} relative to the thermal process.[45a]

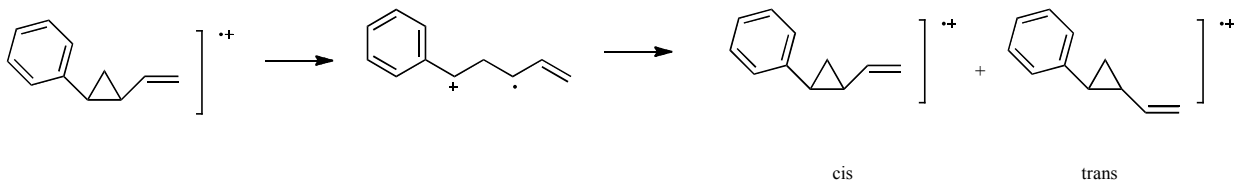

Scheme 1.18. Isomerization proceeds via ring openings of 1,2-disubstituted cyclopropropane radical cation. Reproduced by permission of the American Chemical Society **.**[38]

Furthermore, the chemically induced oxidation does not involve the biradical intermediate **(Figure 1.11)** implicated in the photochemical reaction; although both reactions do proceed through a ring opened intermediate.[45-46] The involvement of the biradical intermediate is easily eliminated in chemically induced isomerization as it is exothermic by only 0.7 kcal mol^{-1} and 32 kcal mol^{-1} are needed to form the biradical (estimated to be equal to the enthalpy of activation for the thermal process).[45a]

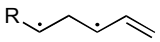

Figure 1.11. Biradical intermediate characteristic of isomerization of photochemcially generated 1,2-disubstituted cyclopropane radical cation.

The chemically oxidized cyclopropane isomerizes through a ring opened distonic radical cation intermediate. The reaction mechanism involves rotation at both stereocenters in a non-correlated way as shown in **Scheme 1.19**. These mechanistic conclusions are supported by isotopic labeling studies that show both possible trans products form. NMR analysis of the reactions proved that this is not a pre or post reaction equilibria. Additionally, accelerated isomerization of the chemically generated cyclopropane radical cation results from a decreased propensity to undergo back electron transfer thus favoring the competing isomerization.[45a] Additional reactions of chemically and

photochemically generated cyclopropane radical cations have been reported to be involved in cycloaddition reactions, although that is outside of the scope of this review as these mechanisms may involve ring intact intermediates.[47]

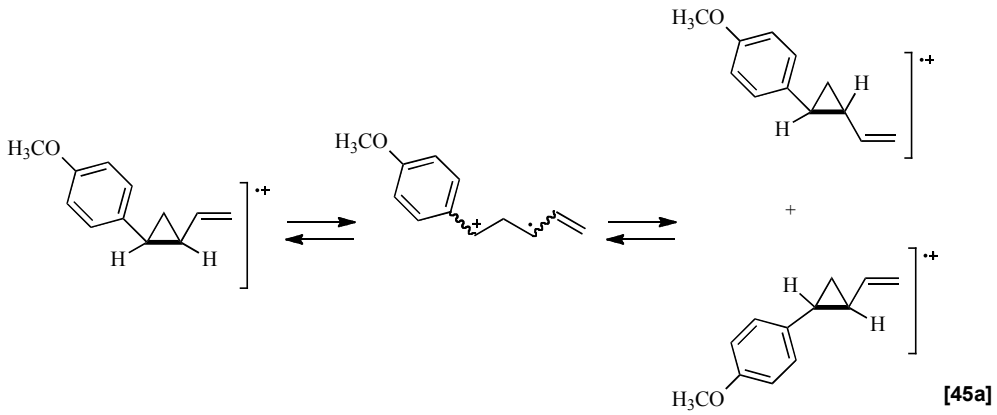

Scheme 1.19. Chemically oxidized 1-phenyl-2-vinyl-cyclopropane radical cation isomerization through a ring opened intermediate. Rotation at both stereo centers yield both trans products.

1.2.3 Comparison of Trends for Neutral Cation and Anion Radicals of Cyclopropane Substituted Compounds

The use of substituted cyclopropane substituted radicals and radical ions as mechanistic probes hinges largely on our understanding of their reactivity. Some notable parallels can be drawn from comparison of cyclopropane radicals, radical anions and radical cations ring openings. Alkyl radicals undergo rapid ring openings like their ketyl radical anion analogs. In some cases the ketyl radical anion ring openings are more facile because the oxygen is a potent electron donor, which can very effectively stabilize the ring opened product and transition state. While similar kinetic data is not available for aliphatic cyclopropyl radical cations, computations show that alkyl substitution can induce conformational changes in order to facilitate interaction and stabilization of charge. Similarly, no experimental kinetic data is available for aliphatic

amine radical cations but computations suggest that aliphatic aminyl radical cations ring open extremely rapidly and the ring closed form may not exist as a discrete species. Moreover, trialkyl amines adopt planar conformations maximize interactions of substituents with the radical center. Introduction of cyclopropyl groups induces conformational changes placing the cyclopropane in a bisected conformation facilitating ring opening and delocalizing spin through hyperconjugative interactions. In aliphatic radicals, ketyl radical anions and aliphatic radical cations the ability of a substituent to stabilize charge has important thermodynamic implications. In aminyl radical cations and ketyl radical anions charge stabilization is an important kinetic consideration as well. In aliphatic cyclopropylamine radical cations the ring closed radical cations prefer a bisected conformation but the ring closed form may not represent a potential energy minima and ring opening may proceed through a perpendicular transition state. Contrastingly, in aromatic cyclopropane cation radical systems significant evidence exists to suggest specific stereoelectronic requirements, namely a planar bisected conformation of the ring relative to the adjacent π system is necessary for ring opening to occur. These stereoelectonic constraints along with the enhanced radical cation stability afforded to the ring closed form by the aryl group lead to a markedly decreased propensity for ring opening of aryl (versus aliphatic) substituted cyclopropanes. These reactions proceed through a late transition state thus spin and charge delocalization in the reactant is not off set by similar stability in the transition state; in the transition state the charge is highly localized. Moreover, the perpendicular conformation of the reactant is more thermodynamically stable than the bisected conformation necessary for ring opening. The phenyl cyclopropyl radical anion ring openings rate constants are

similarly depressed and for similar reasons, highlighting the importance of resonance energy in the radical anion process as well. Substitution of electron donating groups on the cyclopropyl ring stabilizes the radical in the product causing a several order of magnitude increase in rate constant and again demonstrates the importance of spin delocalization. In all cases (radical anion, radical cation and neutral radical) relief of ring strain and delocalization of spin can drive ring opening. For both cyclopropane radical cations and radical anions delocalization of charge also affects reactivity significantly. In the case of the radical cations stereoelectronic requirements for ring openings, particularly in the aryl cyclopropanes, will dictate whether ring opening is a favorable process.

1.3. Δ-5-Hexenyl Radical/Radical Ion

1.3.1 Δ-5-Hexenyl Radical Cyclizations

The Δ-5-hexenyl radical reaction is the most widely studied radical cyclization mechanism. This is not surprising, as the stereo and regio selectivity of related intramolecular additions make these reactions extremely attractive from a synthetic perspective. Additionally, the Δ-5-hexenyl radical finds use as a radical clock and a mechanistic probe.[48] This reaction is known to be kinetically controlled for reasons discussed in the proceeding section. While extensive kinetic characterization for the corresponding 5-hexenyl radical anion cyclization has not been performed, product ratio analysis allows parallels between the two processes to be drawn. The next few pages will show that the reaction of 5-hexenyl radicals and their corresponding radical anions proceed similarly.

It is well established that the *Δ*-5-hexenyl radical preferentially undergoes intramolecular addition via the 5-*exo*-trig rather than 6-*endo*-trig pathway to yield the thermodynamically disfavored product (**Scheme 1.20**).[49] The 6-*endo* product is stabilized relative to the 5-*exo* product because it is a more substituted radical with less ring strain. In spite of thermodynamics; the exo product occurs in 98 to 2 excess over the endo product.[50]

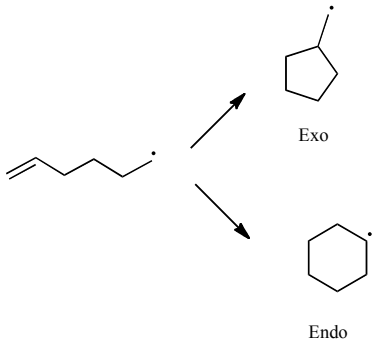

Scheme 1.20. Δ-5-hexenyl radical cyclization.

The pathway to the endo product proceeds through a boat-like transition state whereas the exo cyclization proceeds through a less strained chair-like transition state (**Figure 1.12**) that has been shown to be 2.8 kcal mol^{-1} or 1.7 kcal mol^{-1} lower in energy than the endo transition state (by calculation and experiment, respectively).[46] The chair conformation maximizes orbital overlap thus imposing a stereoelectronic demand for exo cyclization.

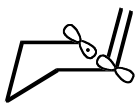

Figure 1.12. Proposed exo transition state for 5-hexenyl radical cyclization. Reproduced by permission of the American Chemical Society **.[51]**

Table 1.3 shows the 5-hexenyl cyclization was more facile than larger chains and more endo selective. Comparing an alkyne and alkene, addition is more facile for the alkene and more regioselective for the alkyne.

Table 1.3. Rate constants for formation of both regioisomers for radical cyclizations at 25°C. Regioselectivity varies as a function of chain length and bond order.[52]

Radical	$k_{Exo\ (calc)}$ [s^{-1}]	$k_{Endo\ (calc)}$ [s^{-1}]
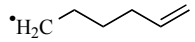	$2.3x10^5$	$4.1x10^3$
	$1.1x10^5$	$5.0x10^2$
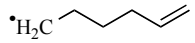	$2.8x10^4$	$<6x10^2$
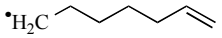	$5.2\ x10^3$	$8.3\ x10^2$
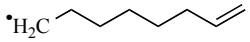	$1.2\ x10^2$	$<7\ x10^1$

1.3.1.1 Regioselectivity of *Δ*-5-hexenyl radical cyclization

Functionalization of the terminal end of the alkene, and the corresponding polarization of the scissile double bond, markedly affects kinetics and the preference for endo or exo cyclization. The 5-hexenyl radical is nucleophilic and polarization of the double bond affects preferential site of addition. The attraction between the nucleophile and the most electrophilic site on the cleavable double bond favors reaction through the more strained transition state structure and forms the thermodynamic product. Stabilizing groups at the exo attachment site introduce a steric effect which makes both regioisomers equally likely (**Table 1.4**). The endo selectivity is increased when a methyl group is present at the endo attack site.

Table 1.4. Changes in regioselectivity based on strain energy of the transition state due to substituents on the double bond at 25°C.[50]

Radical	ΔE_{Strain} Exo$_{(calc)}$ [kcal mol^{-1}]	ΔE_{Strain} Endo$_{(calc)}$ [kcal mol^{-1}]
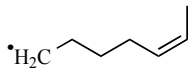	6.7	13.5
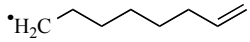	7.0	10.2
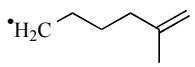	9.7	9.5

Geminal substitution increases *k* relative to the unsubstituted 5-hexenyl reaction (**Table 1.5**). The maximum effect was observed for the 3 position. The rate constant for the 1 substituted compound is lower than the other substituted compounds in **Table 1.5** because it involves cyclization of a secondary radical. Conversely, substitution of electron withdrawing groups at or near the radical site increases radical nucleophilicity and rate constant for cyclization. Donation of electron density to the radical decreases the rate and decreases selectivity. Substitution of a $Si(CH_3)_2$ for the 2 carbon stabilizes the radical to such an extent that it becomes exo selective.

Table 1.5. Rate constants displaying regio selectivity of 5-Hexenyl at 25°C. Cyclization trends with site of substitution and electron withdrawing/donating substituents. [50],[52],[53]

Radical	Solvent	$k_{Exo\ (expt)}$ [s^{-1}]	$k_{Endo\ (expt)}$ [s^{-1}]
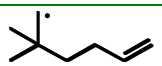	Hexane	$3.5x10^5$	$6.0x10^3$
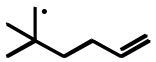	None	$3.6x10^{6a}$	$<1x10^{5a}$
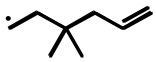	None	$5.1x10^{6a}$	$<1x10^{5a}$
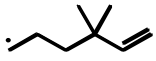	None	$3.2x10^6$	$<1x10^{5a}$
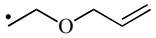	Benzene	$8.5x10^6$	$<1x10^5$
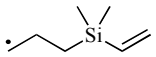	Benzene	$7.4x10^4$	$5.0x10^3$
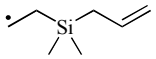	Benzene	$8.7x10^2$	$1.8x10^3$

a = calculated [52] T=25°C

1.3.1.2 Stereoselectivity of *Δ*-5-hexenyl radical cyclization

Substitiution not only plays a role in regioselectivity but also dictates stereoselectivity for these cyclizations. For 5-hexenyl radicals, substitution at the 1 or 3 position leads to the cis product while substitution at the 2 or 4 position favors the trans product **(Figure 1.13).**

Generally, substituents in the 2, 3 or 4 position prefer a chair like transition state placing bulky substituents in a pseudo-equatorial position. Moreover, selectivity increases with

geminal disubstitution at the 3 position.[51] Rate data for cyclization of various methyl substituted 5-hexenyl radicals is presented in **Table 1.6**. Placing substituents in an axial position is disfavored by destabilization imparted by Van der Waals interactions, bending and torsional strain in the transition state. Methyl substitution at the radical center leads to increased stereoselectivity. Similar substitution near the scissile alkene bond enhances production of the trans product. Interestingly, the strain energy of the transition state, assuming a chair conformation for both the stereoisomers, overestimates the cis contribution. The experimental partitioning ratio for the cis and trans product is in good agreement with computational work where the trans isomer proceeds through a boat-like transition state.

Table 1.6. Effects of substitution on stereoselectivity of 5-hexenyl radical cyclizations at 25°C.

Radical	Solvent	k_{cis}	k_{trans}	$k_{overall}$	cis:trans	
					Calc	Expt
 [54],[55],[56],[57]	Hexane Cyclopropane Cyclohexane Isopentane	-	-	2.3×10^{5} 1.1×10^{5} 1.0×10^{5} 1.0×10^{5}	-	-
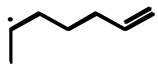 [50],[53]		1.1×10^{4}	4.2×10^{4}	1.5×10^{5}	66:34	67:33
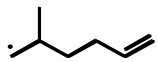 [50]	Benzene or Hexane	2.4×10^{5}	4.5×10^{5}	6.9×10^{5}	40:60	36:64
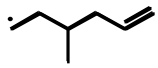 [50],[53]		7.0×10^{5}	2.4×10^{5}	9.4×10^{5}	63:37	71:29
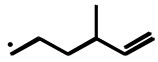 [50],[53]		7.5×10^{4}	3.6×10^{5}	4.4×10^{5}	19:81	17:83
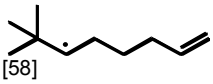 [58]		2.8×10^{4}	8.7×10^{4}	11×10^{4}		

Rate constants given in [s^{-1}]

Rate data for cyclization of alkenylaryl compounds (**Table 1.7**) showed the rate constants for these reactions to be 3 to 4 orders of magnitude greater than the corresponding alkenyl reactions. These aryl radicals are subject to lesser torsional strain and less energy is required to form the new bond. The aromatic radicals are isolated in an orbital adjacent to the π system. The corresponding ether exhibits an order of magnitude increase in rate constant. Substitution of the electrophilic double bond for the aryl ether causes a moderate decrease in the cyclization rate constant relative to the unsubstituted double bond.

Table 1.7. Aryl 5-hexenyl radical cyclization rate constants at 25°C.[50]

Radical Aromatic	$k_{Exo\ (expt)}$ [s^{-1}]	$k_{Endo\ (expt)}$ [s^{-1}]
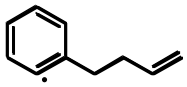	3.1×10^8	$<6 \times 10^6$
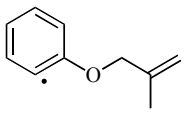	1.7×10^9	3.6×10^7
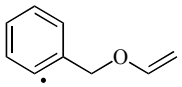	5.3×10^9	$<5 \times 10^7$

In 1-methyl-5-hexenyl radical cyclization the cis product is afforded because stabilizing torsional interactions between the the methyl and C6 outweigh the strain imposed by bending. For many years replacement of the methyl with a more sterically bulky group, such as t-butyl, was believed to introduce unfavorable Van der Waals interactions that would dominate torsional and bending effects and calculations suggested this cyclization would preferentially form the trans product (**Figure 1.13**). Upon reinvestigation, Curran and others were able to show that both experiment and higher level computational analysis evidenced a preference for the cis product.[51]

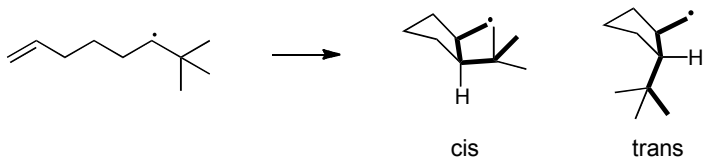

Figure 1.13. Isomeric products for cyclization of 1-t-butyl-5-hexenyl radical cyclization.

Comparing molecular mechanics and quantum mechanical calculations it was noted that only the latter computation accurately predicts the cis product preference; thus providing a basis for the assertation that both steric and electronic factors contribute to determination of product stereochemistry.[51] It has been noted in competition experiments that yields are affected by alkyl substitution of the scissile bond; with more cyclized product forming when the 5-hexenyl radical is more highly substituted.

1.3.1.3 Solvent effects on *Δ*-5-hexenyl radical cyclization

In some cases, as solvent polarity is increased the cis isomer becomes more predominate; notably, this is not the case for all hexenyl radical cyclizations in **Table 1.8**. The stereoselectivity of the cyclization of the 2,2-dimethyloct-en-3-yl radical exhibits a moderate dependence on solvent polarity**.** Similar trends have been observed for the hept-6-en-2-yl and the 1,1,1-trifluorohept-6-en-2-yl radical. The proportion of cis isomer increases with increasing solvent dipole moment; results likely indicative of a polar transition state.[58]

Table 1.8. Stereoselectivity ([cis/trans] ratios) of 5-hexenyl radical cyclizations in solvents of varying polarity at 25°C.[59]

Radical	Benzene/Hexane	1,2-dimethyoxyethane	1-propanol
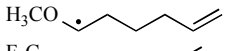	0.95	0.93	0.94
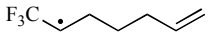	1.13	1.86	1.70
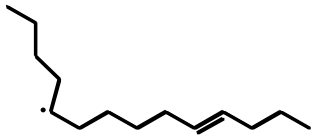	0.57	0.57	0.57
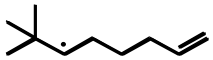	3.1	4.4	5.9

1.3.2 6-hepten-1-one radical anion cyclizations

Similar 6-hepten-1-one radical anion cyclizations **(equation (1.8)[60] reproduced by permission of** the American Chemical Society**)** have been investigated for their potential use in synthesis of cyclic molecules as well as intramolecular radical clocks; not unlike their neutral radical analogs.[61]

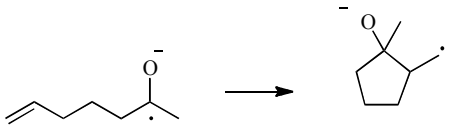

(1.8)

The dimethylpyrrolidinium (DMP) mediated reduction of substituted 6-hepten-1-ones shows these radical anions undergo regioselective cyclization to form the exo product, similar to the neutral radical analog. The analogous direct reductions of 6-hepten-1-ones form straight chain alcohols, not the cyclized alcohols characteristic of the mediated process. These products are thought to form because, at the oxidation potential of the direct reduction, the radical anion can undergo subsequent reduction to the dianion. The dianion of these ketones do not prefer the cyclization pathway.[60] Heterogeneously catalyzed reduction of *o*-(3-butenyl)fluorobenzene exhibits

regioselectivity similar to that observed for the aforementioned ketones.[48] The initial steps of the synthesis of cyclic molecules by DMP mediated reduction of ketones is shown in **Scheme 1.21**.[61]

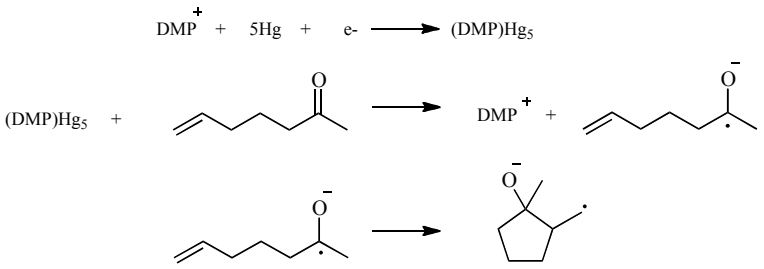

Scheme 1.21. DMP mediated reduction of subsequent cyclization of 6-hepten-2-ones. Reproduced by permission of the American Chemical Society **.[62]**

1.3.2.1 Regio/stereoselectivity of 6-hepten-1-one radical anion cyclizations

These radical ion cyclizations are known to be endo selective, reminiscent of a 5–hexenyl radical cyclization. The primary product of the radical ion reaction reaction for analog **20** is **21**; which is expected to come about through nucleophilic attack on the less sterically crowded face of the molecule.[61] Two isomeric radicals result; the trans radical leads to the minor product **22** because of an inability to undergo further cyclization **(equation** (**1.9**) **reproduced by permission of** the American Chemical Society).[61]

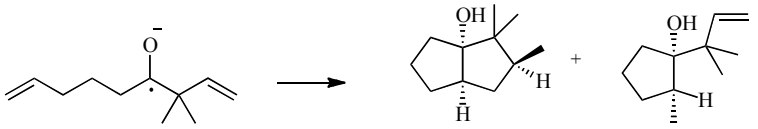

20 **21** **22** (1.9)

Other ketones **23-26**, shown in **Figure 1.14** are also reduced by DMP to yield radical anions exhibiting similar regio and stereospecificity in cyclization.[61]

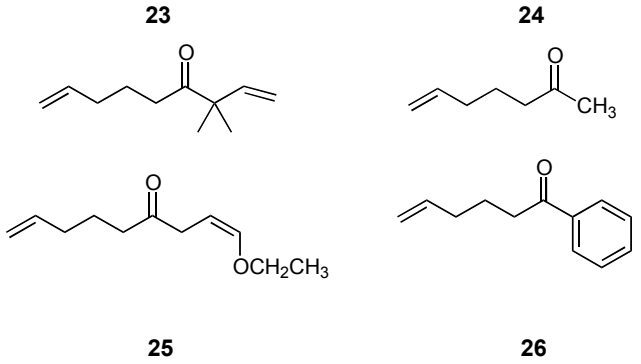

Figure 1.14. Structures of ketones known to undergo mediated reduction and subsequent cyclization.

Swartz and coworkers astutely noted that the plot of product yield as a function of molar equivalents of electrons consumed exhibits a linear relationship with a slope on the same order of magnitude as the previously reported rate constant for the corresponding cyclizations for both hexenyl and hexynl radical.[62] Moreover, **26** shows a retardation in rate constant of about an order of magnitude, as indicated by the analogous plot; this result is cogent as cyclization onto an arene would be expected to be subject to a rate decrease.

The reductive cyclization by DMP is highly stereoselective.[62] The homogeneously catalyzed reduction of 6-hepten-2-one has been shown to be sensitive to the concentration of water while the hetereogenous process is not. The heterogeneous process is extremely stereoselective so even if it was subject to an analogous effect it would be difficult to discern an increase in stereoselectivity that was statistically significant. Unlike the heterogeneous process the ratio of cis to trans product formed for the homogeneously catalyzed reduction can be increased by changing the concentration of water or catalyst or by using a different redox catalyst all together.

A similar mechanism is invoked to explain the homogeneous and heterogeneously catalyzed processes. The two mechanisms are differentiated by the reversibility of the cyclization step in the homogeneously catalyzed system. The observation of an appreciable amount of the thermodynamically favored product in the homogeneously catalyzed reaction results from differences in how the catalysts function.[60] The insoluble heterogenous catalysis complex will form the kinetic product at the electrode surface by extremely rapid subsequent irreversible reduction of the cyclized product.[60] Contrastingly, in the homogeneous system, the proportion of the product going to the kinetic product will be proportional to the concentration of catalyst in solution.[60]

1.3.3. Stereo and Regiochemical Trends for Δ-5-Hexenyl Radicals and Radical Anions

Comparatively, the radical anion and radical processes exhibit similar regio and stereoselectivity in cyclization. Generally, both reactions undergo exo ring closure and preferentially form the cis product. Of course, substituent effects and electronic effects lead to exceptions in both cases. Little kinetic data exist for the radical anion process but it has been proposed that the two processes occur through a similar step in their mechanisms; cyclization through the neutral radical center. Swartz suggests that the radical anion process is expected to occur with similar rate constants to Beckwith's measured 5-hexenyl cyclizations.[62] For the radical anion reactions the catalyst used is known to be a factor that could potentially allow for selective production of the thermodynamic product. For the neutral radical the most favored transition state resembles the cyclohexane chair conformation and maximizes overlap between the

singly occupied orbital containing the radical and the π^* orbital of the atom being attacked and minimizes ring strain in the transition state. Steric factors have been shown to play some role in both processes with steric demands and the placement of bulky groups in the transition state modulating stereochemistry of the products and kinetics of the cyclization. In some 5-hexenyl radical cyclizations increasing solvent polarity increases the preference for the cis product; although this is not true for all 5-hexenyl radical cyclizations. In light of the available evidence, it is reasonable to conclude that the neutral radical and the radical ion cyclization may proceed through similar transition states. This may indicate that, unlike the previously discussed cyclopropane ring openings, charge delocalization in the transition state is not a primary factor in determining reactivity. Similar to the cyclopropanes this may result from the stabilization afforded by the oxygen on the ketyl radical anions. Of course, these suppositions are simply that without further investigation of the radical anion reactions. Understanding the nature of the transition state for these intramolecular additions as well as determination of important kinetic parameters has facilitated their use in stereo and regioselective synthesis of cyclic compounds. Moreover, knowledge of the kinetic parameters for these reactions can aid in determination of useful kinetic parameters for other interesting reactions by acting as intramolecular radical clocks. One class of reactions where radical clocks like these are useful is in atom and group transfer reactions. The next section will address a particularly interesting class of atom transfers; namely deprotonation and hydrogen transfer reactions.

1.4. MECHANISMS OF HYDROGEN ATOM TRANSFER (HAT)

1.4.1 Modes of HAT

The most common, and seemingly simple, atom transfer reaction involving radicals is hydrogen transfer. The equivalent process for a radical cation is deprotonation. HAT reactions find widespread importance in both synthesis and biology.

Classical HAT is characterized by the simultaneous removal of a proton and one electron from the breaking bond. As of late, several authors report evidence suggesting alternative routes for hydrogen atom transfer (HAT) involving radicals and radical ions such as sequential proton loss electron transfer (SPLET), electron transfer followed by proton transfer (ET/PT), and proton coupled electron transfer (PCET).[63] Classical concerted HAT proceeds via direct transfer of a hydrogen atom between molecules via a three-electron transition state as shown in **Scheme 1.22**.

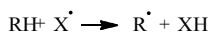

Scheme 1.22. Concerted hydrogen transfer.

1.4.1.1 Classic hydrogen atom transfer (HAT)

Many HAT reactions including the reaction of the *N*-hydroxylphthalimide radical (PINO•) with toluene and several other aliphatic and aromatic hydrocarbons proceed via classical HAT.[64] Since proton and electron transfer occur in a single molecular motion via a three electron transition state, neither will individually affect the rate of reaction. Instead, the rate is directly related to relative difference in the strength between the breaking and forming bond. The relationship between reaction kinetics and bond dissociation energy is quantified by the Evans Polyani postulate; a nice example of this is the HAT from hydrocarbons to PINO• in acetic acid.[64-65] For this process, a

reasonably linear correlation is noted with an alpha value of about 0.38 denoting a slightly exothermic process.[65] The Evans Polyani postulate is not well suited to represent the relationship between kinetics and thermodynamics of reactions when factors such as stereoelectronic effects, steric effects and polar effects influence enthalpy since these variables not considered in the corresponding equation.[66] One example where stereoelectronic factors significantly impact kinetics is in the reactions of the 1-hydroxyl-benzotriazole radical (BTNO•) with cyclic and acyclic alkylarenes. Bond scission is more facile in the former case as a result of hyperconjugative interactions between the breaking C-H bond and the aromatic system; these interactions weaken the C-H bond.[67]

1.4.1.2 Electron transfer followed by proton transfer (ET/PT)

One sequential alternative to classical HAT is the electron transfer followed by proton transfer mechanism. Studies of the reaction of several para substituted dimethylanilines with PINO• indicate sequential electron transfer proton transfer is a probable mechanism for HAT as shown in **Scheme 1.23**.[63e]

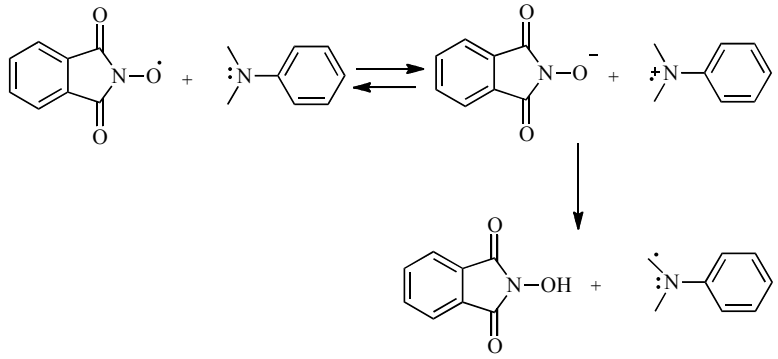

Scheme 1.23. ET/PT mechanism for the reaction of PINO radical with N,N-dimethylanilines. Reproduced by permission of the American Chemical Society **.**[68]

Baciocchi asserts differences in isotope effects observed for dideuteromethyl and monodeuteromethyl *N,N*-dimethylanilines suggest that electron transfer and proton

transfer are not concerted.[68] The intermolecular isotope effects observed for the former compounds were smaller than those observed for the corresponding monodeuteromethyl amines. KIE studies showed large primary isotope effects for monodeuteromethyl amines with electron withdrawing para substituents.[63e] In addition, the overall rate is also highly dependent on the electron donating ability of the substituent. Furthermore, the intramolecular KIEs are larger than the intermolecular, suggesting that removal of the hydrogen atom is not necessarily the rate determining step. These observations suggest electron transfer is followed by proton transfer. Electron transfer was shown to be rate limiting for substrates having electron donating substituents, whereas proton transfer could affect the rate for electron withdrawing substituents. Insomuch as electron donating substituents on a particular compound should correspond to a more favorable, and consequently exothermic process, the rate of reverse electron transfer is expected to be significantly less than the favored deprotonation.[63e] The magnitude of intramolecular deuterium isotope effect results from the decay route of the electron transfer product, either back electron transfer or deprotonation. For strongly electron donating substituents no intramolecular isotope effects were observed, further supporting a rate limiting electron transfer. Contrastingly, for electron withdrawing substituents, back electron transfer is expected to proceed faster as these substituents pull electron density from the radical cation making it less able to stabilize the electron deficiency of the nitrogen.[63e] In studying these particular compounds it is noted that significant intermolecular isotope effects emerge alluding to the significance of proton transfer in the rate of these reactions.[63e]. A similar mechanism was observed in the reaction of benzotriazole N-oxyl radical

reactions with para substituted *N,N*-dimethylanilines.[69] In contrast to this sequential process, previous studies by Espenson of deprotonation on phenols and several hydrocarbons suggest concerted HAT mechanisms with PINO•.[64-65, 70]

1.4.1.3 Sequential proton loss electron transfer (SPLET)

A second sequential mechanism proposed for HAT is SPLET. The SPLET mechanism was first proposed by Ingold and co-workers to explain a solvent induced effect on rate of deprotonation of phenols by 2,2-diphenyl-1-picryhydrazyl radical (dpph•).[71] In studying the kinetics of these reactions the authors observed a drastic increase in rate constant for hydrogen abstraction from phenols by dpph• in solvents with the ability to hydrogen bond to the phenol.[72] Moreover, studies in alkane solvents showed decreased rate constants, vide infra.[71b] One would expect that hydrogen bonding of the phenolic hydrogen would result in a stabilized reactant. As a result, the rate constant of the simple HAT would be expected to decrease. These counterintuitive results can be rationalized on the basis of a faster HAT proceeding via SPLET as shown in **Scheme 1.24**.

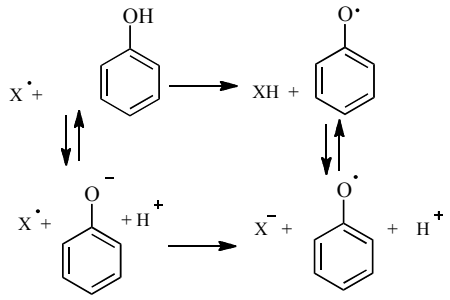

Scheme 1.24. SPLET mechanism for phenol with a neutral radical.

The SPLET mechanism is shown in contrast to HAT for the reaction of phenol with a radical. SPLET is facilitated by the ionization of the phenol; followed by proton loss then electron transfer to yield a phenoxyl radical and a neutral species. SPLET

reactions proceed much faster than HAT when favorable, and are favored by solvents that promote ionization of the phenol as shown in **Scheme 1.24**.[71d] In polar, hydrogen bond accepting solvents reaction rates are faster as hydrogen bonding favors protonation of the solvent and simultaneous ionization of the phenol. Studies by Ingold consistently show no change in the ratio of rate constants for deprotonation by a given radical in two different solvents when comparing reactions involving several phenols and several radicals of varying reactivity.[73] This result provides further affirmation that the radical and its reactivity is not the limiting factor in SPLET mechanisms. In acidic media when SPLET is not favored (because ArOH remains protonated), PCET emerges in some cases as an alternative route to simple HAT.[63e]

1.4.1.4 Proton coupled electron transfer (PCET)

PCET is characterized by transfer of a proton coupled to the transfer of a non-bonded electron. It is important to note that for this mechanism, the proton and electron are transferred from different orbitals in a single step. PCET was first proposed by Mayer in a theoretical investigation comparing the abstraction of hydrogen from toluene and phenol by their deprotonated radical counterparts and is shown in **Scheme 1.25**. [74]

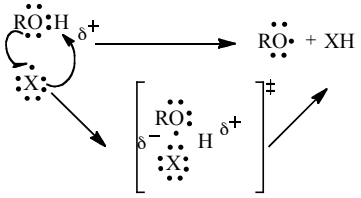

Scheme 1.25. PCET mechanism for the reaction of a neutral radical with an alcohol. Reproduced by permission of the American Chemical Society **.[75]**

Studies of deprotonation by dpph• from phenol displayed a much greater rate constant than the reaction with toluene.[73] The enhanced rate of H-abstraction from

phenol is because phenol has a non-bonding electron pair, and can react via proton-coupled electron transfer PCET, while toluene does not and can only react via classical H-abstraction.[73] Interestingly, in non-polar solvents reactions between dpph• and phenols are believed to proceed through a product like transition state and computations evidence the contribution of both HAT and PCET to the overall reaction mechanism.[76] For the reactions of dpph• and *N,N*-dimethyanilines a PCET mechanism is supported, rather than a sequential mechanism, by the observation of primary isotope effects.[77] During PCET, electron transfer occurs simultaneously with a transfer of a proton between pairs of electrons on both reactants.[71e] While both mechanisms involve the transfer of a proton and an electron, the difference between PCET and SPLET or ET/PT is that the former is concerted, while the latter two are stepwise.[73] Mayer suggests that stepwise processes do not necessarily proceed through intermediates with a lower energy than concerted PCET. The increase in energy required to move both a proton and electron in concert (as opposed to just the electron as in a ET/PT) is often more than compensated for by the reduction in solvation energy displayed by the concerted process. In addition to the intrinsic barrier to reaction, the Gibb's free energy of PCET is consistently lower and the mechanism is thermodynamically favored over a stepwise process. [78]

1.4.1.5 Role of hydrogen bonding in determining mode of HAT

In the analysis of self-decomposition reactions, phenol exhibited severely increased rates or reaction with the phenoxyl radical, relative to the carbon centered benzyl radical reaction with toluene. It has been suggested that the rate of hydrogen abstraction from phenol by phenoxyl radical was greater because hydrogen bonding

between reactants created a short lived intermediate complex.[79] It should be noted that researchers suggest that hydrogen bonding between the two phenolic reactants does lend stability to the reactants and, in effect, decreases the reactivity of these species although this stabilization is offset by the closer proximity and enhanced accessibility of the two reacting species to one another.[71e, 79] The increase in rate for the phenol reaction is attributed to the increased accessibility of the oxygen resultant from the smaller radius of an oxygen in the phenol relative to the carbon being deprotonated on toluene.[71e] In addition, Ingold highlights another well known consequence of a narrow reaction barrier, the increased probability of tunneling.[63a] Proton tunneling in this case results from the closeness of the hydrogen bonded reacting molecules. The SPLET mechanism occurs so readily with phenols, to observe the PCET pathway, ionization must be prevented by performing the reaction in the presence of acetic acid or another readily ionzable solvent. Favoring ionization of the solvent over the phenol disfavors the SPLET pathway.[71e]

1.4.2 Radical Cation Deprotonations

1.4.2.1 Radical cation deprotonation: Thermodynamics

Radical cations, because of their electron deficient nature, are not likely to participate in HAT; instead they undergo the analogous radical ion fragmentation, proton transfer. Factors that influence proton transfer are also significant for sequential HAT. In sequential HAT radical ion intermediates undergo deprotonation as an elementary step of the overall HAT. In deprotonations, in addition to the alkalinity of the base and strength of the breaking bond, the acidity of the radical is a factor that may significantly impact kinetics. Acidities for for selected aromatic hydrocarbons, phenols

and amines are displayed in **Table 1.9**. The pK_a's estimated using thermodynamic cycles show solution phase acidity is drastically decreased relative to the gas phase; ionization is less favored because energy is required to solvate solution phase ions.[80] Analogous results would be expected for all radical cations as a result of the increased electrophilicity of a cation relative to a neutral radical. A comparison of phenol in both DMSO an H_2O can be made; data suggests that in the less polar protic solvent the phenol is more acidic. These highly acidic compounds are known to react in hydrogen atom transfer processes via either SPLET or PCET.

Table 1.9. Acidities for selected radical cations and their neutral analogs

Compound	pK_a	p$K_a^{\cdot+}$	Proton Affinity
C_6H_6			147+ 1[81]c
$C_6H_5CH_3$	43[82]a	-20[82]a	191[82]b
			139+1[81] c
C_6H_5OH	9.99[47a]d	-2.0[83]e	200[82]b
	18.3[82]a	-8.1[82]a	
$C_6H_4(OH)_2$	9.	-0.75[83]	a DMSO
$C_6H_5NH_2$	30.6[84]	6.4[84]f	b,c Gas phase proton affinity
$C_6H_5NHCH_3$	29.5[84]	4.2[84]f	d H_2O
$C_6H_5N(CH_3)_2$		9[75]f	e Gas phase proton affinity, error ±5%
		18.8[85]g	f CH_3CN
$(C_6H_5)_2N$		3.6 [86]d	g CH_3CN/.5 M H_2O
$(CH_3CH_2)_2N$		5.3[86]d	

The predominate mechanism of HAT is largely dependent on reaction conditions and the ability of the phenol to ionize, as reflected by its pK_a. As radical cations are very acidic relative to their neutral counterparts, electron transfer might be a good mechanism for catalysis especially when a C-H bond is broken during the reaction because a highly ionizible radical cation favors the subsequent deprotonation step. In **Table 1.10**, pK_a's calculated for several anilines radical cations are presented.

Table 1.10. pK_as of aromatic amines.

Aromatic Amine	p$K_a^{\cdot+}$ CH_3CN[75]	p$K_a^{\cdot+}$ 0.5M H_2O/CH_3CN[85]
$C_6H_5N(Me)_2$	9	18.8
p-$MeOC_6H_5N(Me)_2$	13	23.2
p-$MeC_6H_5N(Me)_2$	12	19.5
p-$ClC_6H_5N(Me)_2$	9	16.6
p-$CF_3C_6H_5N(Me)_2$	-	14.6

These compounds are of interest as a result of their structural similarity to several substrates for SET enzymes. In fact, until recently *N*-cyclopropyl,*N*-methylanilines were thought to be attractive mechanistic probes for mechanism of catalysis for these enzymes, vide supra. As expected the radical cations are extremely acidic relative to the neutral bases. On average for substituted anilines the radical cation is more than 20 orders of magnitude more acidic than the neutral counterpart! The large difference between the pK_a of the anilines and their radical cations displays this increased acidity; analogous results would be expected for all radical cations as a result of the increased electrophilicity of a cation relative to a neutral radical. It is this increased acidity that puts forth PCET as a mechanism for catalysis involving these substrates in SET enzymes. The authors use this evidence to assert the idea that this decreased acidity decreases the possibility that HAT from the parent compound will proceed via a route involving deprotonation of a radical cation intermediate.[86] Although values were not available for the pK_a's of the neutral dimethylanilines, discussed these molecules are expected to exhibit alkalinity similar to other aromatic amines to a normal aliphatic C-H bond. **Table 1.10** presents the acidities of several dimethylaniline radical cations and pK_a refers to the acidity of a C-H bond not a quaternary protonated amine this point is further clarified by **Scheme 1.24** showing the acid and its conjugate base. Moreover,

the acidity of the aniline radical cations are greater than those of the corresponding dimethylaniline radical cations. From the values in **Table 1.10** some general structure acidity relationships are apparent. Values for pK_a's, calculated by Bordwell and Dinnocenzo, for both sets of compounds show similar trends, in that as the electron donating ability of the substituent decreases, the pK_a also increases, indicating the most electron withdrawing para substituents are the most acidic. This result is expected as electron donating para substituents stablize the cationic character of these aminyl radical cations. Again, as noted for the anilines the dimethylaniline radical cations are not extremely acidic as might be expected. Although pK_a's were not provided for tertiary aliphatic amine radical cations, a study by Nelsen *et al*. states several acidities calculated via a thermodynamic cycle show that the trialkyl amine radical cations exhibit average pK_a's of 15 suggesting tertiary alkyl amines radical cations are also not as acidic as might be expected.[86] These species do exhibit drastically lowered C-H bond dissociation energies in the radical cation attributed to orbital mixing between the C-H bond and the nitrogen's p orbital containing the unpaired electron.[86] The authors further note that the stability of the resultant carbon centered neutral radical is high due to resonance in support of the conclusion that acidity of the radical cation is not a primary factor in deprotonation. Griller noted in the study of deprotonation of alkyl radical cations by their parent compound that the amines were not basic enough to cause facile deprotonation to occur. Other studies of tertiary alky amine radical cations indicate stronger bases could significantly increase rates.[87] Nelsen poignantly asserts that a probable reason for this is that weaker bases do not deactivate the radical cation by deprotonation at a rate competitive with other means of decay.[86] In **Table 1.11**, strictly

for comparison, the experimentally determined aqueous pK_a's of several secondary aliphatic amine radical cations are shown, displaying weakly acidic behavior, more acidic though than values calculated for their tertiary counterparts.

Table 1.11. pK_as of some aliphatic amines. [86]

Aliphatic Amines	p$K_a^{\cdot+}$ H_2O
Diphenylamine	3.6 ± 0.2
Diethylamine	5.3 ± 0.5
Dimethylamine	6.8 ± 0.5
Piperidine	5.8 ± 0.5
Pyrrolidine	5.5 ± 0.5

As the degree of substitution increases, the acidity of the amine decreases because alkyl substituents donate electron density to the nitrogen disfavoring deprotonation and a further increase in electron density on the nitrogen adjacent to the alpha carbon attached to the protic hydrogen.

1.4.2.2 Radical cation deprotonation: Kinetics

The kinetics of deprotonation of radical cations are dependent on several factors discussed above such as bond strength and pK_a of the radical cation; the strength of the base can also impact kinetics. For radical cations that have a low thermodynamic acidity, deprotonation may occur on a time scale slow enough that other routes of decay are plausible.[86, 88] Further convoluting kinetic analysis is difficulty distinguishing radical cation deprotonation from other processes such as the preceding electron transfer process which generates the radical cation.[86] As dynamics of deprotonation has long been a topic of interest there is a vast amount of literature pertaining to the topic.

Rate constants for deprotonation of dimethylaniline radical cations by acetate and pyridine have been determined previously by electrochemical and photochemical

means.[85, 89] Parker noted decay of the *N,N*-dimethylaniline radical cations by dimerization without base present, likewise noting this occurrence even for para substituted derivatives.[89] In the presence of base, facile deprotonation of these radical cations is observed and attributed to the positive charge on the nitrogen being relatively close to the alpha carbon deprotonated by the base.[89] Hammett and Bronsted analysis was performed for reactions with both bases. Hammett and Bronsted plots display linear free energy relationships of acidity of the radical cation with the nature of substituents, and base strength with rate constant for deprotonation.[90] The acetate deprotonation proceeds with a rate constant several orders of magnitude greater than the corresponding reaction with pyridine as shown in **Table 1.12**.[89]

Table 1.12. Rate constants for the reactions of *p*-substituted *N,N*-dimethylaniline radical cations with acetate and pyridine at 25 °C in CH_3CN with 0.5 M *n*-Bu_4ClO_4. Reproduced by permission of the American Chemical Society.[75]

Substituent	$k_{pyridine}$ [M^{-1} s^{-1}]	$k_{acetate}$ [M^{-1} s^{-1}]
CH_3O	0.94	3.5×10^6
Cl	1.0×10^3	6.2×10^8
CN	2.5×10^5	1.0×10^9
NO_2	1.4×10^5	3.0×10^9

Reactions of both bases with *para*-substituted *N,N*-dimethylanilines in acetonitrile show sensitivity to substituents effects giving linear Hammett plots displaying the relationship between rate constant and $\sigma+$ yielding ρ values of 1.7 and 3.5 for acetate and pyridine, respectively.[85, 89] Although these reactions are affected by the nature of the substituent, it should be noted that the magnitude of this effect decreases for the more energetically favorable, and consequently faster deprotonation by acetate. Bronsted analysis was also performed and alpha values were determined to be 0.24 and 0.51 for

acetate and pyridine, correspondingly.[89] Because the alpha value is a measure of transition state location, a low value of alpha suggests an early transition state, consistent with acetate being more reactive.[89] Also, this explains the lower ρ value because acetate is more reactive, the rate is less sensitive to the nature of the substitutent. Building on these observations and evidence from previous studies of radical cation kinetics, the authors suggest the mechanism for proton transfer shown in **Scheme 1.26**.

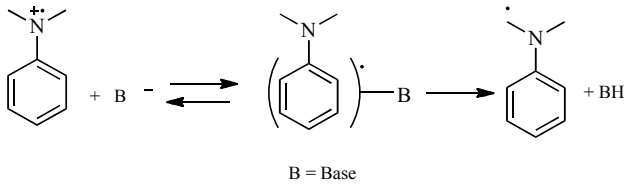

Scheme 1.26. Mechanism of proton transfer from *N,N*-dimethylaniline radical cations.

This mechanism is characterized by a fast reversible formation of an adduct followed by rate determining proton transfer as the complex breaks apart.[75, 85, 89] Parker also uses this mechanism to account for observed experimental results for proton transfers involving several arene radical cations, and in these studies provides further support for a mechanism involving adduct formation.[75, 91]

Later, photochemical analysis by Dinnocenzo of the acetate deprotonations of several substituted *N,N*-dimethylaniline radical cations revealed similar trends in rate constants for the para substituted compounds as previously noted by Parker, although, the magnitude of the photochemically acquired rate constants was greater in all cases than those attained electrochemically. Differences are to be expected as ionic strength was maintained with different electrolytes and in the latter experiments a different solvent system was employed. The second order rate constants for the reaction of

several substituted dimethylaniline cations with acetate in 0.5M H_2O in CH_3CN are shown in **Table 1.13**.[85]

Table 1.13. Rate constants for deprotonation of *o,p*-substituted *N,N*-dimethylaniline at room temperature in 0.5 M H_2O in CH_3CN with 0.5 M *n*-$BuClO_4$.[85]

Substituent		k [M^{-1} s^{-1}]
Para	OCH_3	1.1×10^7
	CH_3	4.1×10^7
	H	1.2×10^8
	Cl	1.7×10^8
	CF_3	1.4×10^8
Ortho	CH_3	2.4×10^8
	t-Bu	4.9×10^9
	CH_3, CH_3	3.6×10^9

In the Dinnocenzo experiments, 0.5 M H_2O in acetonitrile in lieu of neat acetonitrile was the solvent used in an effort to maintain polarity as, in these studies, it was observed that the rate of deprotonation was significantly affected by ionic strength and polarity.[85] Small primary deuterium kinetic isotope effects were noted in kinetic studies of *N,N*-dimethylanilines with deuterated alpha carbons suggesting that the barrier to reaction is governed by the C-H bond breaking and an early transition state.[85] Dinnocenzo performed Bronsted analysis; an alpha value of 0.23 was observed, providing further support for the reactant like transition state.[85] In addition, the effect of electron donating ability showed similar trends to those observed by Parker. Notably, the effect of ortho substituents is an increase in acidity of the amine.[85] This occurs for steric reasons as the nitrogen twists, consequently breaking up the conjugation with the aromatic ring, and concentrating electron density on the nitrogen as shown in **Figure 1.15**.[85]

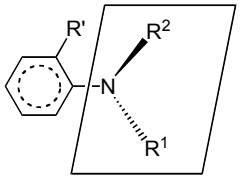

Figure 1.15. Ortho substituents increase amine acidity by twisting α-carbon out of the plane of the aromatic ring.

This supposition was confirmed via density functional theory calculations that displayed a rotation of the nitrogen in the ortho substituted compounds.[85] Dinnocenzo further suggests this localization may lend an increased acidity to the analogous radical cation as charge and spin will also be localized in close proximity to the protic hydrogen supporting a more facile deprotonation.[85]

1.4.3 Comparing Mechanisms: HAT and Deprotonation

When proton and electron transfer occur in concert, whether it be involving a single hydrogen atom or a proton and an electron in a nearby orbital, the reaction is typically more facile than a stepwise HAT because the solvation cost for involving deprotonation (and ions) outweighs the increase in reaction barrier for both processes to occur in a single step. Also these processes have been shown to be more thermodynamically favorable than their sequential counterparts.[78] The Evans-Polyani relationship is a great linear free energy relationship to describe simple concerted hydrogen transfer reactions. However, many reactions, especially sequential HAT processes, are effected by complicating stereoelectronic or polar effects making this type of data treatment ineffective and necessitating investigation of kinetic dependence

on other structural features such as thermodynamic acidity of the molecule undergoing HAT.

Generally, attempts to differentiate between deprotonation and HAT require careful and innovative experimental strategies. In sequential HAT mechanisms where deprotonation is the rate limiting step it is impossible to elucidate the actual mechanism in some cases. In these cases, the elementary step with the greatest barrier is deprotonation. Therefore, factors governing deprotonation control the reaction thus making sequential HAT and deprotonation indistinguishable. This ambiguity is not limited to differentiating between sequential processes and deprotonation; concerted HAT and deprotonation can also be extremely difficult to discriminate as the transition states for a concerted HAT and deprotonation process are isoelectronic. Like the rearrangements discussed in the preceeding sections the radical process (HAT) is intimately related to the radical ion process (deprotonation). In all cases transition state similarities predict similar kinetic trends and often times thermodynamic parameters that predict how specific structural features influence reactivity will trend similarly with kinetics for both the radical and radical ion processes. This is a lucky and important observation for many of us who study radical ion processes making assumptions predicated on assumptions that these charged species will behave similarly to their neutral analogs.

1.5. CONCLUSIONS

In the preceding pages a relatively comprehensive comparison of some radical and radical ion processes is presented. Two classes of radical reactions are discussed, rearrangements and atom transfers. In the context of atom transfer, routes

leading to hydrogen transfer for neutral radicals are compared to the complementary radical ion process, deprotonation. Many sequential hydrogen transfer reactions involve deprotonation as an elementary step in their mechanism. What is more, concerted hydrogen transfer and deprotonation proceed through isoelectronic transition states; often times leading to difficulties discriminating the processes experimentally. Both classes of unimolecular rearrangements discussed, cyclopropyl ring openings and *Δ*-5-hexenyl cyclizations, have been utilized in synthesis and as radical clocks. Many trends observed for the well characterized *Δ*-5-hexenyl radical cyclizations extrapolate accurately to predicting the regio and stereoselectivity of the lesser known radical anion siblings. Likewise, there is much to be gleaned about radical ion reactivity from the extensive work on cycloropylcarbinyl → homoallyl rearrangements. The role of torsional strain, ring strain and the stereoelectronic requirements for ring opening show both marked similarities as well as notable differences comparing the reactivity of radicals, radical anions and radical cations of cyclopropyl substituted compounds. These particular reactions stand out from the others discussed because there is a rather complete data set for both radicals and radical anions. The cyclopropyl rearrangements provide an excellent example of how similar factors may influence a radical and its complimentary radical ion reactions while also clearly demonstrating the need for caution when extrapolating reactivity trends as the relative importance of factors influencing reactivity may change significantly with the introduction of charge. The similarities observed in the reactions discussed herein are not fortuitous but rather indicative of similar activation or driving force trends for the complementary processes.

Prudently used, these reactivity relationships are an excellent predictive tool when studying the radical ion analog of a previously characterized radical process.

REFERENCES:

[1] A. N. Hancock, J. M. Tanko, in *Encyclop, Vol. 1*, John Wiley and Sons, ???, **2011**.

[2] aA. L. J. Beckwith, V. W. Bowry, *Journal of Organic Chemistry* **1989**, *54* 2681-2688; bA. Effio, D. Griller, K. U. Ingold, A. L. J. Beckwith, A. K. Serelis, *Journal of the American Chemical Society* **1980**, *102*, 1734-1736; cL. Mathew, J. Warkentin, *J. Am. Chem. Soc.* **1986**, *108(25)*, 7981-7984; dM. Newcomb, A. G. Glenn, *J. Am. Chem. Soc.* **1989**, *111(1)*, 275-277.

[3] J. M. Tanko, R. E. Drumright, *J. Am. Chem. Soc.* **1990**, *112*, 5362-5363.

[4] J. M. Tanko, R. E. Drumright, *J. Am. Chem. Soc.* **1992**, *114*, 1844-1854.

[5] J. M. Tanko, R. E. Drumright, N. K. Suleman, L. E. Brammer, *J. Am. Chem. Soc.* **1994**, *116*, 1785-1791.

[6] aT. J. M., L. E. Brammer, M. Hervas, K. Campos, *Journal of the Chemical Society, Perkins Transactions 2* **1994**, 1407-1409; bJ. P. Phillips, J. G. Gillmore, P. Schwartz, L. E. Brammer, D. J. Berger, J. M. Tanko, *J. Am. Chem. Soc.* **1998**, *120*, 194 - 202.

[7] M. Chahma, X. Li, J. P. Phillips, P. Schwartz, L. E. Brammer, Y. Wang, J. M. Tanko, *Journal of Physical Chemistry A* **2005**, *109*, 3372 - 3382.

[8] J. M. Tanko, L. E. Brammer, *J. Chem. Soc., Chem. Commun.* **1994**, 1165 - 1166.

[9] J. M. Tanko, L. E. Brammer, *J. Org. Chem.* **1997**, *62*, 5550 - 5556.

[10] J. P. Stevenson, W. F. Jackson, J. M. Tanko, *J. Am. Chem. Soc.* **2002**, *124*, 4271 - 4281.

[11] J. M. Tanko, J. G. Gillmore, R. Friedline, M. Chahma, *J. Org. Chem.* **2005**, *70*, 4170 - 4173.

[12] J. M. Saveant, *Accounts of Chemical Research* **1993**, *26*, 455 - 461.

[13] C. P. Andrieux, J. M. Saveant, A. Tallec, R. Tardivel, C. Tandy, *Journal of the American Chemical Society* **1996**, *118*, 9788 - 9789.

[14] J. M. Tanko, X. Li, M. Chahma, W. F. Jackson, J. N. Spencer, *J. Am. Chem. Soc.* **2007**, *129*, 4181 - 4192.

[15] M.-T. Nguyen, D. Odile, C. Alcaraz, G. Bouchoux, *Journal of the American Chemical Society* **1998**, *120*, 152-160.

[16] aM.-T. Nguyen, S. Creve, T.-K. Ha, *Chemical Physics Letters* **1998**, *293*, 90-96; bW. F. Richardson, H. F. King, A. L. Cooksy, *Journal of Organic Chemistry* **2003**, *68*, 9441-9452.

[17] X. Z. Qin, F. Williams, *Journal of the American Chemical Society* **1987**, *109*, 595-597.

[18] J. K. Cha, S. C. Blackstock, S. U. Jong, J. Lee, *Journal of the American Chemical Society* **1997**, *119*, 10241-10242.

[19] A. d. Meijere, V. Chalinski, H. Winsel, M. A. Kusnetsov, P. Rademacher, R. Boese, T. Haumann, M. Traetteberg, P. v. R. Schleyer, T. Zywietz, H. Jiao, P.

Merstetter, F. Gerson, *Agewandte Chemie International Edition* **1999**, *38*, 2430-2433.
[20] A. d. Meijere, V. Chalinski, P. Merstetter, F. Gerson, E. Haselbach, *Journal of Organic Chemistry* **1999**, *64*, 6951-6959.
[21] J. P. Dinnocenzo, D. A. Conlon, *Journal of the American Chemical Society* **1988**, *110*, 2324-2326.
[22] B. H. Lee, J. M. Sung, S. C. Blackstock, J. K. Cha, *J. Am. Chem. Soc.* **2001**, *123*, 11322-11324.
[23] J. Mattay, P. A. Waske, H. Rinderhagen, *Tetrahedron* **2006**, *62*, 6589-6593.
[24] E. Hasegawa, N. Yamaguchi, H. Muraoka, H. Tsuchida, *Organic Letters* **2007**, *9*, 2811-2814.
[25] aT. L. Macdonald, K. Zirvi, L. T. Burka, P. Peyman, F. P. Geungerich, *Journal of the American Chemical Society* **1982**, *104* 2050-2052; bR. P. Hanzlik, V. Kilshore, R. Tullman, *Journal of Medicinal Chemistry* **1979**, *22*, 760-761; cR. P. Hanzlik, R. H.Tullman, *Journal of the American Chemical Society* **1982**, *104*, 2050-2052; dT. L. MacDonald, L. E. Richards, J. P. Shea, R. J. Willard, F. P. Guengerich, *Journal of the American Chemical Society* **1984**, *106*, 6446-6447; eR. P. C. Hanzlik, M. A., *Archives of Biochemistry and Biophysics* **2005**, *436*, 265 - 275.
[26] N.S.Scrutton, A. W. Munro, D.Leys, M.J.Sutcliffe, A. v. Theil, H. Toogood, A. W. Mohsen, J. P. Combe, J. Basran, S. E. Rigby, *Biochemical Society Transaction* **2005**, *33*, 754-757.
[27] R. P. Hanzlik, M. A. Cerney, *Journal of the American Chemical Society* **2006**, *128*, 3346-3354.
[28] R. P. Hanzlik, M. D. Morton, C. L. Shaffer, *Journal of the American Chemical Society* **2001**, *123*, 8502-8508.
[29] aG. T. Miwa, J. S. Walsh, G. L. Kedderis, P. F. Hollenberg, *Journal of Biological Chemistry* **1983**, *258*, 14445-14449; bR. P. Hanzlik, R. A. Totah, *Journal of the American Chemical Society* **2001**, *123*, 10107-10108.
[30] R. P. Hanzlik, M. A. Cerny, *Archives of Biochemistry and Biophysics* **2005**, *436*, 265-275.
[31] J. M. Tanko, N. C. Jr., K. Igarashi, M. L. Grimm, X. Li, *Chem. Commun.* **2007**, 2648-2650.
[32] aR. N. Loeppky, T. Theiss, R. Hastings, S. Elomari, S. P. Singh, *Journal of the American Chemical Society* **1998**, *120*, 5193-5202; bR. N. Loeppky, S. Elomari, *Journal of Organic Chemistry* **2000**, *65*, 96-103.
[33] R. N. Loeppky, E. L. Teuten, *Organic Biomolecular Chemistry* **2005**, *2005*, 1097-1108.
[34] J. M. Tanko, J. S. Merola, R. E. Drumright, *Journal Of Organic Chemistry* **1990**, *55*, 4098-4102.
[35] J. P. Dinnocenzo, T. R. Simpson, H. Zuilhof, W. P. Todd, T. Heinrich, *Journal of the American Chemical Society* **1997**, *119*, 987-993.
[36] aJ. P. Dinnocenzo, W. P. Todd, T. R. Simpson, I. R. Gould, *Journal of the American Chemical Society* **1990**, *112*, 2462-2464; bJ. P. Dinnocenzo, H. Zuilhof, D. Lieberman, T. R. Simpson, M. W. McKechney, *Journal of the American Chemical Society* **1997**, *119*, 994-1004.

[37] S. S. Shaik, J. P. Dinnocenzo, *Journal of Organic Chemistry* **1990**, *55*, 3434-3436.
[38] J. P. Dinnocenzo, D. R. Lieberman, T. R. Simpson, *Journal of the American Chemical Society* **1993**, *115*, 366-367.
[39] S. S. Hixson, V. Ramachandea-Rao, *J. Am. Chem. Soc.* **1979**, *101*, 6458-6459.
[40] Y. J.M. Tanko Wang, *Journal of the Chemical Society of Perkins Transactions* **1998**, *2*, 2705-2711.
[41] aJ. M. Tanko, Y. Wang, *Journal of the American Chemical Society* **1997**, *119*, 8201-8208; bK. M. W. J.M.Tanko McLean, Y., *Journal of Organic Chemistry* **1998**, *63*, 628-635.
[42] J. M. Tanko, J. P. Phillips, *Journal of the American Chemical Society* **1999**, *121*, 6078-6079.
[43] aJ. M. Tanko, N. C. Jr., K. Igarashi, M. L. Grimm, X. Li, *Journal of the American Chemical Society* **2007**, *Accepted Submission*; bJ. M. Tanko, N. C. Jr., K. Igarashi, M. L. Grimm, X. Li, *Journal of the American Chemical Society* **2007**, *Accepted Submission*.
[44] H. D. Roth, J. Chou, D. Zhou, *J. Phys. Org. Chem.* **1999**, *12*, 867-874.
[45] aJ. P. Dinnocenzo, M. Schmittel, *Journal of the American Chemical Society* **1987**, *109*, 1561-1562; bH. D. Roth, M. L. Manion-Schilling, *J. Am. Chem. Soc.* **1981**, *103*, 7210-7217; cH. D. Roth, M. L. Manion-Schilling, *J. Am. Chem. Soc.* **1980**, *102*, 7956-7958; dP.C.Wong, D. R. Arnold, *Tetrahedron Letters* **1979**, 2101.
[46] S. S. Hixson, J. Boyer, C. Gallucci, *Chemical Communications* **1974**, 540-542.
[47] aP.H.Mazzocchi, R. S. Lusting, *J. Am. Chem. Soc.* **1973**, *95*, 7178-7180; bP. H. Mazzochi, C. Somich, M. Edwards, T. Morgan, H. L. Ammon, *J. Am. Chem. Soc.* **1986**, *108*; cP. H. Mazzocchi, C. Somich, M. .Edwards, T. Morgan, H. L.Ammon, *J. Org. Chem.* **1990**, *55*, 2624-2630; dP. H. Mazzocchi, H. L. Tamburin, *J. Am. Chem. Soc.* **1970**, *92*, 7221-7222.
[48] E. Kariv-Miller, J. E. Swartz, D. M. Loffredo, *Journal of Organic Chemistry* **1989**, *54*, 5953-5957.
[49] A. L. J. Beckwith, *Tetrahedron* **1981**, *37*, 3073-3100.
[50] A. L. J. Beckwith, C. H. Schiesser, *Tetrahedron* **1985**, *41*, 3925-3941.
[51] J. C. Tripp, C. H. Schiesser, D. P. Curran, *Journal of the American Chemical Society* **2005**, *127*, 5518-5527.
[52] A. L. J. Beckwith, C. H. Schiesser, *Tetrahedron Letters* **1985**, *26*, 33-376.
[53] K. N. S. Houk, D.C., *Journal of Organic Chemistry* **198**, *52*, 959-974.
[54] A. L. J. Beckwith, C. J. Easton, T. Lawrence, A. K. Serelis, *Australian Journal of Chemistry* **1983**, *36*, 545-556.
[55] K. U. Ingold, D. Griller, P. Schmid, *International Journal of Chemical Kinetics* **1979**, *XI*, 333-338.
[56] K. U. Ingold, D. J. Carlsson, *Journal of the American Chemical Society* **1968**, *90*, 7047-7055.
[57] K. U. Ingold, D. Griller, S. Husband, *Journal of the American Chemical Society* **1974**, *96*, 6455-6357.
[58] J. M. Tanko, X. Li, M. Chahma, W. Jackson, J. N. Spencer, *Journal of the American Chemical Society* **2007**, 4181-4192.

[59] A. J. Beckwith, C. H. Schiesser, *Organic and Biomolecular Chemistry* **2011**, *9*, 1736-1743.
[60] J. E. Swartz, E. Kariv-Miller, S. J. Harrold, *Journal of the American Chemical Society* **1989**, *111*, 1211-1216.
[61] F. Lombardo, H. Maeda, E. Kariv-Miller, *Journal of Organic Chemistry* **1989**, *4*, 4022-4024.
[62] J. E. Swartz, T. J. Mahachi, E. Kariv-Miller, *Journal of the American Chemical Society* **1988**, *110*, 3622-3628.
[63] aG. Litwinienko, K. U. Ingold, *Accounts of Chemical Research* **2007**, 222-230; bD. G. Nocera, J. Stubbe, J. M. Hodgkiss, S. Y. Reece, *Philosophical Transactions of the Royal Society* **2006**, *361*, 1351-1364; cG. Litwinienko, M. Musialik, *Organic Letters* **2005**, *7*, 4951-4954; dV. Lukes, E. Klein, *Journal of Molecular Structure:THEOCHEM* **2007**, *805*, 153-160; eE. Baciocchi, M. Bietti, M. F. Gerini, O. Lanzalunga, *Journal Of Organic Chemistry* **2005**, *70*, 5144-5149.
[64] J. H. Espenson, K. Nobuyoshi, B. Saha, *Journal of Organic Chemistry* **2003**, *68*, 9364-9370.
[65] J. H. Espenson, Y. Cai, N. Koshino, *Journal of Physical Chemistry A* **2003**, *107*, 4262-4267.
[66] B. P. Roberts, A. J. Steel, *Journal of the Chemical Society of Perkins Transactions 2* **1994**, 2155-2162.
[67] P. Brandi, C. Galli, P. Gentili, *Journal of Physical Organic Chemistry* **2006**, *19*, 552-554.
[68] E. Baciocchi, M. Bietti, M. F. Gerini, O. Lanzalunga, *Journal of Organic Chemistry* **2005**, *70*, 5144-5149.
[69] E. Baciocchi, M. Bietti, O. Langzalunga, A. Lapi, D. Raponi, *Journal of Organic Chemistry* **1998**, *75*, 1378-1385.
[70] J. H. Espenson, B. Saha, N. Koshino, Y. Cai, *Journal of Organic Chemistry* **2004**, *70*, 238-243.
[71] aG. L. Malgorzata Musialik, *Organic Letters* **2005**, *7*, 4951-4954; bK. U. I. Gregorz Litwinienko, *J. Org. Chem.* **2003**, *68*, 3433-3438; cK. U. I. Gregorz Litwinienko, *J. Org. Chem.* **2004**
, *69*, 5888-5896; dK. U. I. Gregorz Litwinienko, *J. Org. Chem.* **2005**, *70*, 8982-8990; eK. U. I. Gregorz Litwinienko, *Acc. Chem. Res.* **2006**.
[72] aC. D. M.C. Foti, *Chemical Communications* **2006**, *3252-3254*; bD. B. O. Friaa, *Organic and Biomolecular Chemistry* **2006**, *4*, 2417-2423.
[73] K. U. I. Gregorz Litwinienko, *Accounts of Chemical Research* **2007**, 222-230.
[74] J. M. Mayer, D. A. Horvat, J. L. Thomas, W. T. Borden, *Journal of the American Chemical Society* **2002**, *124*, 11142-11147.
[75] V. D. Parker, M. Tilset, *Journal of the American Chemical Society* **1991**, *113*, 8778-8781.
[76] M. C. Foti, C. Daquino, I. D. Mackie, G. A. DiLabio, K. U. Ingold, *Journal of Organic Chemistry* **2008**, *73*, 9270-9282.
[77] E. Baciocchi, A.Calcagni, O. Lanzalunga, *Journal of Organic Chemistry* **2008**, *73*, 4110-4115.
[78] J. M. Mayer, *Annual Reviews of Physical Chemistry* **2004**, *55*, 363-390.

[79] Schulster, in *Advances in Electron Transfer Chemistry, Vol. 1*, JAI Press Ins., **1991**, pp. 163-197.
[80] aA. d. Martin, R. J. Boyd, D. Arnold, *Canadian Journal of Chemistry* **1982**, *60*, 3011-3018; bA. d. Martin, P. Nicholas, D. Arnold, *Canadian Journal of Chemistry* **1982**, *60*, 2165-2179
[81] F. G. Bordwell, *Journal of the American Chemical Society* **1988**, *110*, 1229-1231.
[82] F. G. Bordwell, J. P. Cheng, *Journal of the American Chemical Society* **1989**, *111*, 1792-1795.
[83] W. T. Dixon, D. Murphy, *Journal of the Chemical Society, Faraday Transactions* **1976**, *72*, 1221-1230.
[84] F. G. Bordwell, X. M. Zhang, J. P. Cheng., *Journal of Organic Chemistry* **1993**, *58*, 6410-6416.
[85] J. P. Dinnocenzo, G. W. Dombrowski, P. A. Zielinski, S. Farid, Z. M. Wosinska, I. R. Gould, *Journal of Organic Chemistry* **2005**, *70*, 3791-3800.
[86] S. F. Nelsen, T. J. Ippoliti, *Journal of the American Chemical Society* **1986**, *108*, 4879-4881
[87] aD. Griller, F. P. Lossing, *Journal of the American Chemical Society* **1981**, *103*, 1586; bF. D. Lewis, T. I. Ho, J. T. Simpson, *Journal of the American Chemical Society* **1982**, *104*, 1924-1929.
[88] J. P. Dinnocenzo, T. E. Banach, *Journal of the American Chemical Society* **1989**, *111*, 8646-8653.
[89] V. D. Parker, Y. Chao, B. Reitstoen, *Journal of the American Chemical Society* **1991**, *113*, 2336-2338.
[90] E. V. Anslyn, D. A. Dougherty, in *Modern Physical Organic Chemistry* (Ed.: J. Murdzek), University Science Books, Sausalito, **2006**, pp. 397-402.
[91] aV. D. Parker, Y. Lu, Y. Zhao, *Journal of the American Chemical Society* **2001**, *123*, 5900-5907; bV. D. Parker, Y. T. Chao, G. J. Zheng., *Journal of the American Chemical Society* **1997**, *119*; cV. D. Parker, Y. Lu, Y. Zhao, *Journal of Organic Chemistry* **2005**, *70*, 1350-1355.

Contributions:

The following chapter comprises original work toward the Ph.D. of Amber Hancock. Acknowledgement and thanks to the others who contributed toward the identification of the surprising and new mechanism presented is given here. Both Professor Jim Tanko, chair of the thesis committee, and Professor Hayati Celik, a former post doctoral researcher, contributed significantly to the intellectual content of this work as well as the conceptual and experimental education of the student performing the work. Selected syntheses and kinetics experiments were reproduced by Ms. Jeneffer England. Experimental data involving ferrocenes are borrowed from the work toward the Ph.D. of Jared Spencer. Electrochemical diffusion measurements were performed by Dr. Michelle Grimm. Collaboration with Ms. Zhiyang Zhang and her advisor, committee member Professor Louis Madsen, resulted in the measurement and interpretation of diffusion coefficients integral to unambiguously ascribing the correct mechanism to the reaction discussed in the proceeding pages.

ABSTRACT

To date, the available literature states that para-substituted *N,N*-dimethylaniline radical cations undergo α-carbon deprotonation in the presence of carboxylate bases. The results reported herein provide compelling evidence in contrast to the reported mechanistic preference. Instead of deprotonation, electron transfer is the preferred mode of reaction. In the case of more reactive *N,N*-dimethylaniline radical cations not bearing electron-donating para-substituents, a more complex mechanism occurs where

deprotonation constitutes a minor competing reaction path. The effect of solvent on mechanistic preference was shown to be negligible comparing the reaction in both CH_3CN and 0.5 M H_2O in CH_3CN. Consequently, it is unlikely that a polarized transition state is involved. Using pulsed field gradient (PFG) NMR the diffusion coefficients of a protonated amine and the neutral parent compound were measured to be different. This difference is explained on the basis of an increased cost associated with solvation during transport of the charged molecule. The difference in diffusion coefficients, while significant in terms of transport properties, is not so large as to have an effect on the availability of the substrate at the electrode surface or the corresponding reaction mechanism.

2.1 Introduction: Amminium Radical Cations

2.1.1 Chemistry and Biology of Aminyl Radical Cations

Over the past century, the ubiquitous nature of amine oxidations in chemistry, materials science and biological systems has been revealed. Exploited for numerous applications including the synthesis of photosensitizing azo-dyes, formation of persistent N-centered radical spin traps, as antioxidants, polymerization inhibitors and even in abatement of release of greenhouse gases; the versatile utility of amines can be largely credited to the intrinsic nucleophilicity or electron donating ability imparted by the lone pair on nitrogen.[1]

In the case of aryl amines the nucleophilicity is decreased by interaction with the pi system; instead, these molecules readily undergo single electron transfer forming the corresponding aminyl radical cations. Recent scrutiny into the mechanism of deprotonation of amine radical cations results from their suspected role in several

enzymatic processes. Amine radical cations are potential intermediates in catalysis by several porphyrin containing proteins such as horseradish peroxidase (HRP), monoamine oxidase (MAO) and the cytochrome P450 family of enzymes.[2]

Cytochrome P450s are a family of thousands of enzymes belonging to the oxygenase class.[3] P450s are known to play a central role in drug metabolism, and almost certainly involve either radicals or radical ions as intermediates in their oxidation of amine substrates.[4] A mechanistic understanding of P450 catalysis is essential to the design of drugs targeted to inhibit the P450s responsible for metabolism of a variety of xenobiotics. Moreover, several naturally occurring neurotransmitters and psychotropic drugs are amine based. An understanding of catalysis by P450 may also lend insight to the mechanism for monoamine oxidase (MAO); similar catalytic mechanisms have been proposed for their oxidation of certain amines.[5] MAOs are also very important enzymes as they are responsible for oxidation of various neurotransmitters such as dopamine and serotonin. In addition, MAO-catalyzed oxidation is known to play a role in several degenerative conditions such as Parkinson's disease.[5] Two mechanisms are proposed for catalysis involving MAO and P450, single electron transfer and hydrogen atom transfer (***see Chapter 1.2.2.4 and 1.2.2.5***). The initial step of the SET pathway is characterized by the transfer of an electron from the substrate to the enzyme, **Scheme 2.1**. The initial electron transfer is shown to result in formation of the amminum radical cation. Subsequent ring opening then forms the distonic radical shown on the right and this radical cation can irreversibly inhibit the enzyme by binding to a histidine in the active site.[4] The SET mechanism is proposed for catalysis of tertiary amine substrates, in particular.

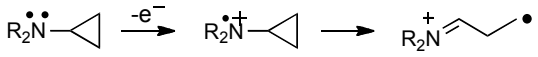

Scheme 2.1. Electron transfer from the amine to the active site of the enzyme will generate a ring opened distonic radical cation that can act as an irreversible mechanistic inhibitor. This inhibition can be used to provide evidence for the electron transfer and thus aid in resolving controversy regarding the mechanism of P450 and related enzymes.

N-methyl-*N*-cyclopropylanilines have been utilized as mechanistic probes for single electron transfer in these important enzymatic systems on the assumption that the kinetics of ring opening and deprotonation were competitive. An opportunity to assess this assumption seemed attractive. Moreover, derivitization of a series of *N*-methyl-*N*-cyclopropylanilines and analysis of the kinetics of the two reaction pathways was expected to 1) produce and characterize a new and interesting class of intramolecular radical clocks 2) provide identification of structural features that modulate the preference for either pathway promised to lend insight into the structural features governing the reactivity of these new radical clocks. Our goal was to determine the rate constant for ring opening for several *N*-methyl-*N*-cyclopropylanilines radical cations shown in **Figure 2.1**.

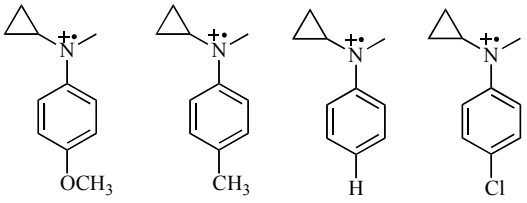

Figure 2.1. Amine radical cation precursors intended for use in this study (other substitutions and stereochemical constraints on the orientation of the ring would be considered after analysis of this simple series of para-substituted compounds).

2.1.2 Purpose

In the initial stages of this project the intention was to study the kinetics of ring opening of *N*-methyl-*N*-cyclopropylanilines radical cations by competition with deprotonation by a carboxylate base. These studies had potential to produce a new class of intramolecular radical clocks as well as assess the supposition used in enzyme elucidation studies, that ring opening of these *N*-methyl-*N*-cyclopropylaniline radical cations were viable mechanistic probes by determining if the rate constants for the two processes were competitive (**Scheme 2.2**).

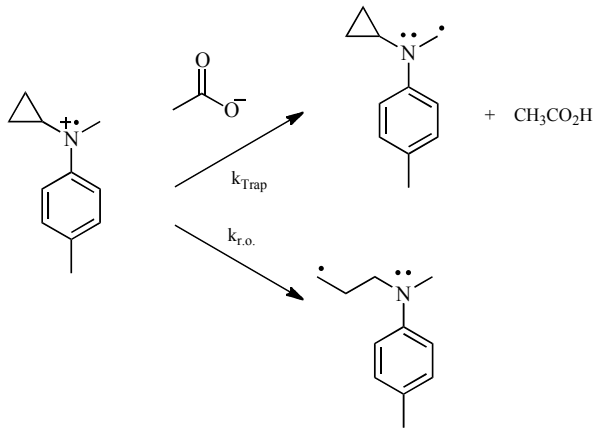

Scheme 2.2. Competition kinetics experiments were intended to be utilized to determine a) if ring opening could be competitive with deprotonation, (Was the assumption that these processes competitive correct? Was data obtained by their use are mechanism based inhibitors meaningful?) b) would substitution significantly impact kinetics of ring opening (Could these ring openings be used as intramolecular radical clocks?).

The late Thomas H. Huxley was quoted as once saying “The great tragedy of science is the slaying of a beautiful hypothesis by an ugly fact”. Herein we report a superb example of this concept. Use of the amine/carboxylate system was predicated on the assumption that the primary mode of decay for *N,N*-dimethylanilines in the presence of carboxylate bases was deprotonation, as reported in several studies.[6] In

reproduction of these original control studies it was realized that something was awry with the reported mechanism. That is not to say that the previous investigators data was erroneous. We were simply afforded the opportunity to identify the true mechanism because of a fortuitous instrumental limitation that forced us to use a different approach to the initial kinetics control experiments. The use of multiple sweep CV to study kinetics provided mechanistic insight unobtainable via flash photolysis for this reaction.

2.2 Results

2.2.1 Sensitized Photolysis: Failed Approaches to Generation of Radical Cations

As noted, the original goal of this study was to generate a series of intramolecular radical clocks. These radical clocks were intended to calibrate ring opening versus deprotonation of derivatized *N*-cyclopropyl,*N*-methylaniline radical cations. Seemingly advantageous was the fact that Dinnocenzo and Mariano had characterized the kinetics of deprotonation of *N,N*-dimethylaniline radical cations by acetate anion using the laser flash photolysis **(*see Chapter 1.4.2 and 4.2.1*)**,. It was reported that these radical cations could be generated by sensitized laser flash photolysis **(Figure 2.2)** wherein at 308 nm excitation would generate an excited state of dicyanoanthracene; this in turn would initiate a cascade reaction that would produce the desired amine radical cation.[6a, 6c]

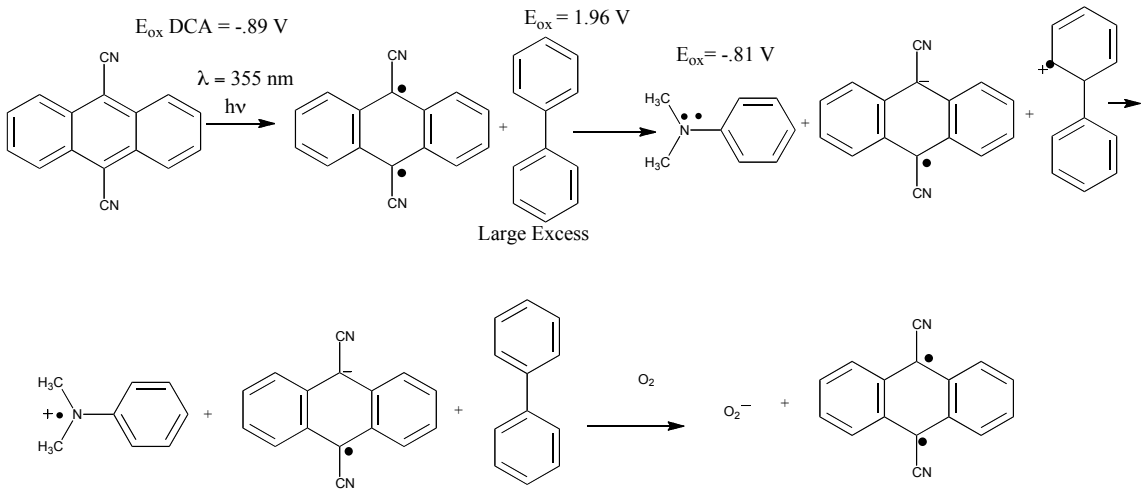

Figure 2.2. Indirect sensitization scheme proposed for generation of N,N-dimethylaniline radical cations. Dicyanoanthracene is excited by absorption of a photon. This excited state then undergoes electron transfer from biphenyl generating the biphenyl radical cation. The biphenyl radical cation then removes an electron from the amine substrate generating the desired N,N-dimethylaniline radical cation.

A subtle difference in our laser flash photolysis system existed; we would employ a solid-state Nd:YAG laser that was tunable to four wavelengths 266nm, 355 nm, 532 nm and 1064 nm but unable get to access the wavelength of 308 nm employed by previous researchers using an organic dye laser.[6a] The UV-vis spectrum of 9,10-dicyanoanthrace, the sensitizer to undergo direct photo-excitation, is shown in **Figure 2.3**. Promisingly, a broad absorption maximum was observed corresponding to 9,10-dicyanoanthracene that spanned a range including both the literature excitation wavelength as well as wavelengths accessible with the instrument in this lab. This observation was encouraging as we envisaged use of a similar approach in our photochemical kinetic studies.

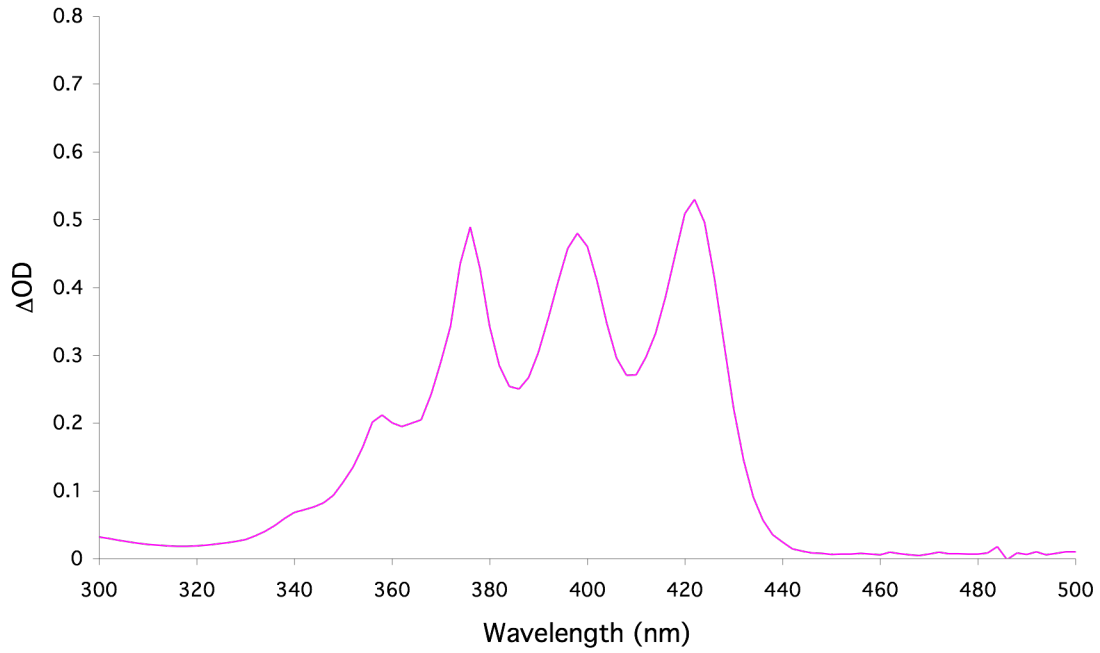

Figure 2.3 UV-vis spectra for dicyanoanthracene.

Spectroscopic data gathered for reactive intermediates generated by our laser flash photolysis was distinctively dissimilar to that observed by previous researchers. We rationalized this to mean the four bands in the peak seen between 344 nm and 444 nm represent several distinct vibrationally excited state within the single electronically excited state for dicyanoanthracene are seen in **Figure 2.3**. Interestingly, when studying the decay of 9,10-dicyanoanthracene, O_2 is unable to quench the resulting absorption at 470 nm. The presence of oxygen is reported to deactivate 9,10-dicyanoanthracene radical anion. The UV-vis spectra for the excited state we generated and monitored with the 9,10-dicyanoanthracene irradiation are inconsistent with that observed for the neutral analog as well as the published spectra for dicyanoanthracene radical anion, further suggesting that the 355 nm wavelength generates a different excited state than 308 nm, **(Table 2.1).**

Table 2.1. λ_{max} for the species generated by our 355 nm excitation are inconsistent with either starting material or the literature spectra for the radical anion of dicyanoanthracene in CH_3CN.

Compound	λ_{max} (nm)
Biphenyl	280
Biphenyl radical cation	650
9,10-dicyanoanthracene	376, 392, 422
9,10-dicyanoanthracene•−	510, 640, 710
Observed	440,470

Notably, the DCA excited state absorbed exhibits a persistent absorption at the wavelength of maximum absorbance around 470 nm, similar to that expected for the *N,N*-dimethylaniline radical cations. Importantly, this persists longer than the reported lifetime of the *N,N*-dimethylaniline radical cations. We were unable to conclude whether this reaction generates the radical cation in an appreciable quantity because its absorption is coincident with that the sensitizer excited state. Several other sensitizers were tried but also proved unsuccessful for similar reasons.

2.2.2 Direct Photolysis

In spite of the difficulties encountered with sensitized methods, direct generation of the desired radical cation seemed a promising alternative as *N,N*-dimethyl-*p*-toluidine and *N,N*-dimethylaniline were reported to exhibit UV absorptions of 225-380 nm and 200-350 nm, respectively, and our instrument produced a 266 nm excitation beam.[7] The primary motivation for use of sensitized photolysis was two fold: 1) it appeared an easy route to experiment as the experimental nuances had been worked out by previous researchers[6a, 6c] and 2) other researchers in our laboratory were simultaneously performing experiments at the wavelength (355 nm) that would be used for sensitized studies (as opposed to 266 nm needed for direct photo-excitation thus affording the practical advantage of eliminating the need to frequently change the optics

in the instrument). Direct excitation at 266 nm was successful in generating the radical cations of *N,N*-dimethylaniline and *N,N*-dimethyl-*p*-toluidine (**Figure 2.4**).

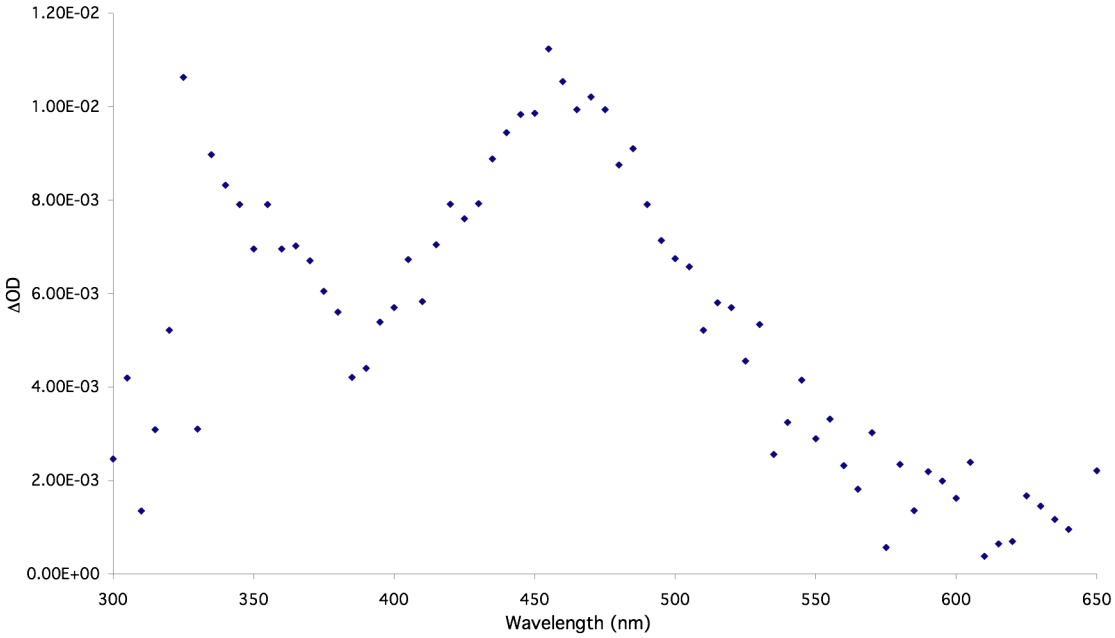

Figure 2.4. UV spectra for *N,N*-dimethyl-*p*-toluidine in 0.5M H_2O, 0.5 M *n*-Bu_4NClO_4 in CH_3CN at 25 ^oC under an argon atmosphere.

Experiments were performed to determine the optimal concentration of amine to generate a high starting absorbance and maximize the signal to noise ratio. As displayed in **Figure 2.5** 8 x10^{-4} M amine gave the highest starting absorbance.

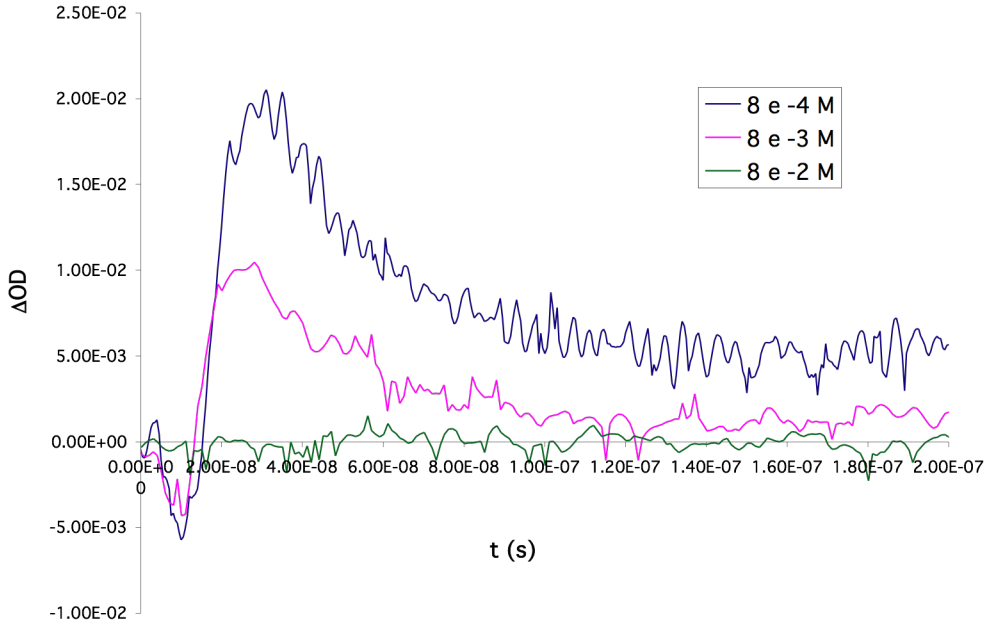

Figure 2.5. The lowest concentration of *N,N*-dimethylaniline photolyzed provided the highest starting absorbance. Suggesting this concentration would afford more accuracy and was used for kinetic analysis in 0.5M H_2O, 0.5 M *n*-Bu_4NClO_4 in CH_3CN under argon.

Moreover, a two order of magnitude increase in amine concentration resulted in no noticeable signal. In flash photolysis too high concentrations of a radical precursor can result in generating a thick wall of excited species in the portion of the sample closest to the excitation beam thus precluding excitation of the molecules farther into solution that are in the path of the excitation beam.

The decay **(Figure 2.6)** of the aminyl radical cation of interest was monitored at 470 nm with varying carboxylate concentrations. Determination of concentration dependent rate constants (hereafter referred to as observed rate constants) was achieved by non-linear curve fitting for transient traces collected at each concentration.

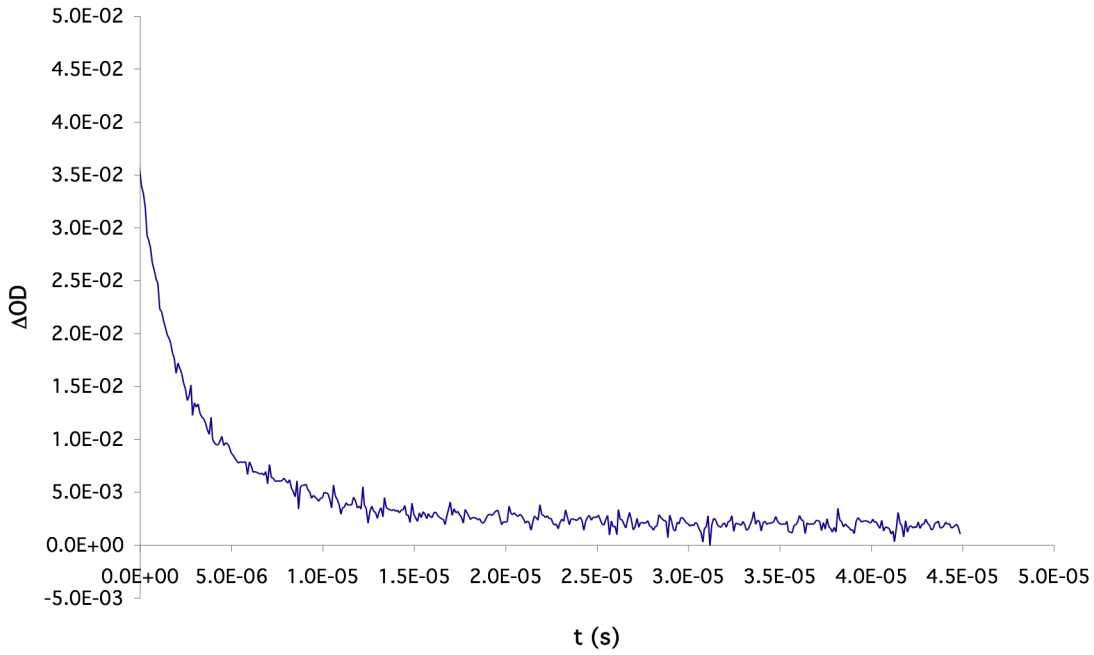

Figure 2.6. Transient at 470 nm for the decay of 3 mM *N,N*-dimethyl-*p*-toluidine in 0.5M H_2O, 0.5 M *n*-Bu_4NClO_4 in CH_3CN under argon.

Kinetics experiments were performed under the conditions specified in **Scheme 2.3.**

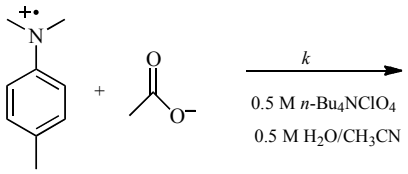

Scheme 2.3. Spectroscopic kinetics experiments were performed in the solvent and electrolyte system shown here. The high concentration of supporting electrolyte was chosen because previous reports indicate ionic strength has an effect on kinetics.

Acetate([B]) concentrations were varied over an order of magnitude and used in concentrations in at least a 10-fold excess relative to the radical cation precursor concentration; thus under pseudo-first order ***(see 4.1.2.)*** conditions with respect to the amine([A]) **(equation (2.1)).**

$$[B]_o >> [A]_o$$

$$-\frac{d[A]}{dt} = k_{obs}[A] \qquad \textbf{(2.1)}$$

$$k_{obs} = k[B]_o \qquad \textbf{(2.2)}$$

According to **equation (2.2)** absolute rate constants were determined the linear dependence of k_{obs} on acetate concentration **(Figure 2.7)**.

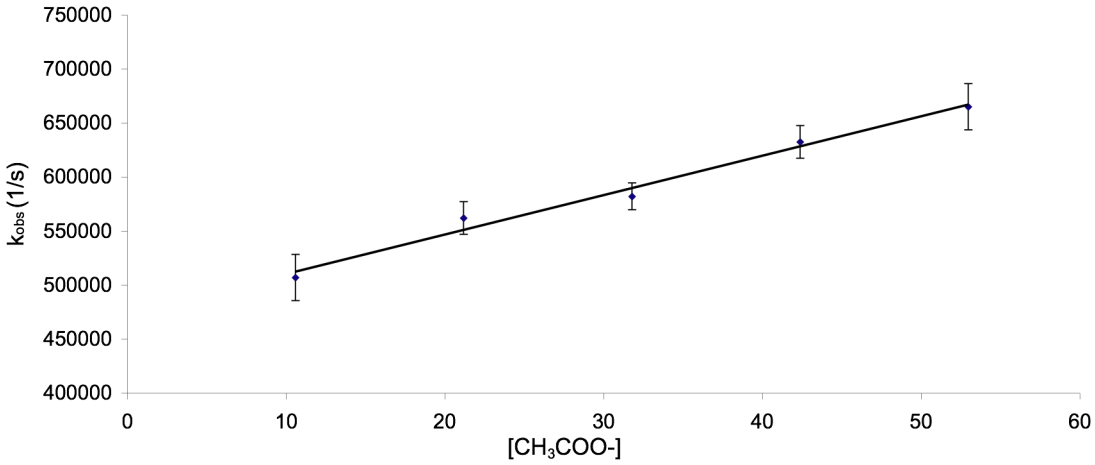

Figure 2.7. Rate constants were determined for the reaction of *N,N*-dimethyl-*p*-toudine radical cation and acetate anion in 0.5M H_2O, 0.5 M *n*-Bu_4NClO_4 in CH_3CN from the slope of the plot of k_{obs} as a function of concentration of the flooding species (*n*-Bu_4NOAC).

Utilizing this method we were able to determine the desired rate constants, hydrogen isotope effects, as well as probe the effect of solvent on reaction (comparing .5M H_2O in CH_3CN and anhydrous CH_3CN). These results are reported in comparison to the electrochemical results later in the text. Similar kinetic parameters were desired for other *p*-substituted amines that were not suitable for study by laser flash photolysis. The *p*-chloro-*N,N*-dimethylaniline radical cation was unable to be generated in sufficient quantities by laser flash, and the *p*-OCH_3–*N,N*-dimethylaniline radical cation decayed

too slowly to be measured on a time regime within the instrument capabilities. In order to expand our range of substrates and comprehensively assess the effect of para substituent on deprotonation kinetics CV coupled to digital simulations was utilized as a kinetic tool. This limitation at first appeared to be undesired but later proved to be quite a serendipitous failure of technique. Had these experiments not been performed by cyclic voltammetry, the behavior suggesting a surprising mechanistic incongruity, in contrast to the reported results, would not have been discovered.

2.2.3 Cyclic Voltammetry (Part 1: Dimerization Kinetics)

Electrochemical simulations (***see Chapter 4.3***) are a powerful tool affording researchers the ability to investigate a number of plausible mechanisms, providing input parameters related to the experiments are accurate. In order to perform cyclic voltammetry simulations properly all competing processes must be accounted for.

Initially, experiments were performed to determine the apparent dimerization rate constants for the *N,N*-dimethylaniline radical cations under the exact conditions of the experiment. These values were necessary for precise simulation of the deprotonation rate constants. It has been reported on several occasions that N,N-dimethylaniline radical cations undergo dimerization. This is evidenced by the quasireversible voltammogram for the oxidation of *N,N-p*-toluidine in **Figure 2.8**.

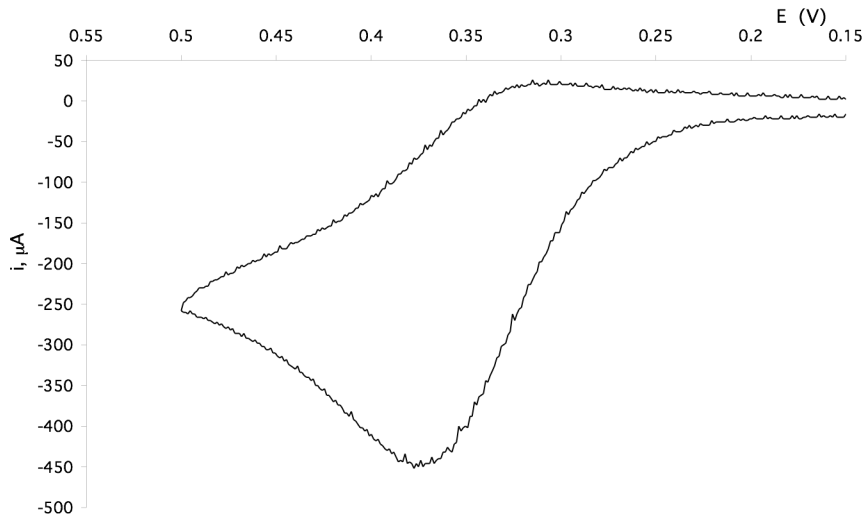

Figure 2.8. Quasireversible cyclic voltammogram for the oxidation of *N,N*-dimethyl-*p*-toluidine in 0.5 M H_2O, 0.5 M *n*-Bu_4NClO_4 and CH_3CN under argon at 23 ($\pm$1)^{o}C and a scan rate of 600 mV/s. The small reverse wave indicate the amine radical cation generated is being consumed by reacting to some extent before reaching the potenital at which the radical cation can be reduced back to the neutral parent amine. No acetate is present in these reactions.

Similar experiments were performed with all amines excluding *N,N*-dimethylaniline. This compound was not accessible by electrochemical means. The lack of a para substituent means that it undergoes a significantly more facile dimerization than the other amines who contain substituents at the 4 position and thus prevent or slow dimerization at this position. In order to measure the rate constant for dimerization, the magnitude of the reverse peak must be a function of scan rate. That is to say, the time frame for the dimerization cannot be so fast that the process gives the appearance of a completely irreversible voltammogram. The change in reverse peak current as a function of scan rate is the factor used to measure the dimerization rate constants. The rate constants for dimerization determined by direct comparison with simulations based on experimental parameters are presented in **Table 2.2.**

Table 2.2. Rate constants for apparent dimerization of para-substituted N,N-dimethylanilines in 0.5 M H_2O, 0.5 M n-Bu4$NClO_4$ in CH_3CN under argon at 23 (±1) °C.

Compound	k_{Dimer} 22°C (1/Ms)
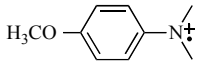	201(±78.7)
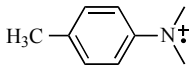	600(±200)
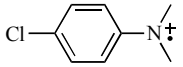	785 (±242)

2.2.4 Cyclic Voltammetry (Part 2: Catalyzed Kinetics Part 1)

Having the rate constant for the other reaction known to be happening in solution, experiments were undertaken to measure the deprotonation kinetics by monitoring the reaction of the electrochemically generated aminyl radical cation in the presence of acetate anion. The voltammogram was not cogent with what was expected for an irreversible deprotonation process. Intriguingly, an oxidative peak distinct from the main peak was observed and the potential at which this peak oxidizes is less positive than the potential for the normal oxidation of the amine, suggesting this is a kinetic shift **(Figure 2.9)**.

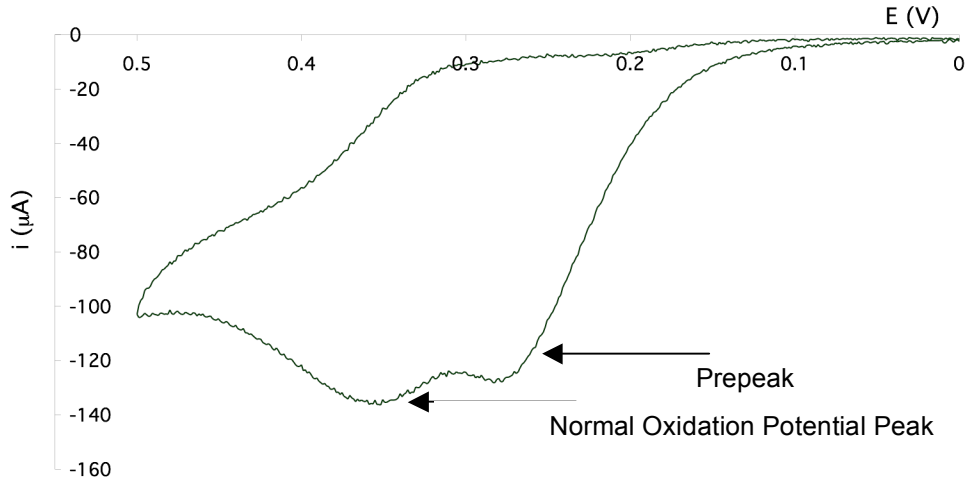

Figure 2.9. Cyclic voltammogram for the reaction of 3.0 mM *N,N*-dimethyl-*p*-toluidine with n-Bu_4NOAc under argon at 23 ($\pm$1) ^oC in 0.5 M H_2O, 0.5 M *n*-Bu_4NClO_4 and CH_3CN and at a scan rate of 600 mV/s.

Oddly, the kinetically shifted peak is distinct from a separate peak present at the normal oxidation potential of the amine. Because of the "prepeak" present in the voltammogram, a more comprehensive investigation of the behavior of the system was performed by way of multiple sweep experiments. In these experiments it was expected that over the longer time frame and several subsequent cyclic voltammetry scans insight into why this incongruous "prepeak" was present could be gleaned. These experiments only produced more confounding results **(Figure 2.10)**.

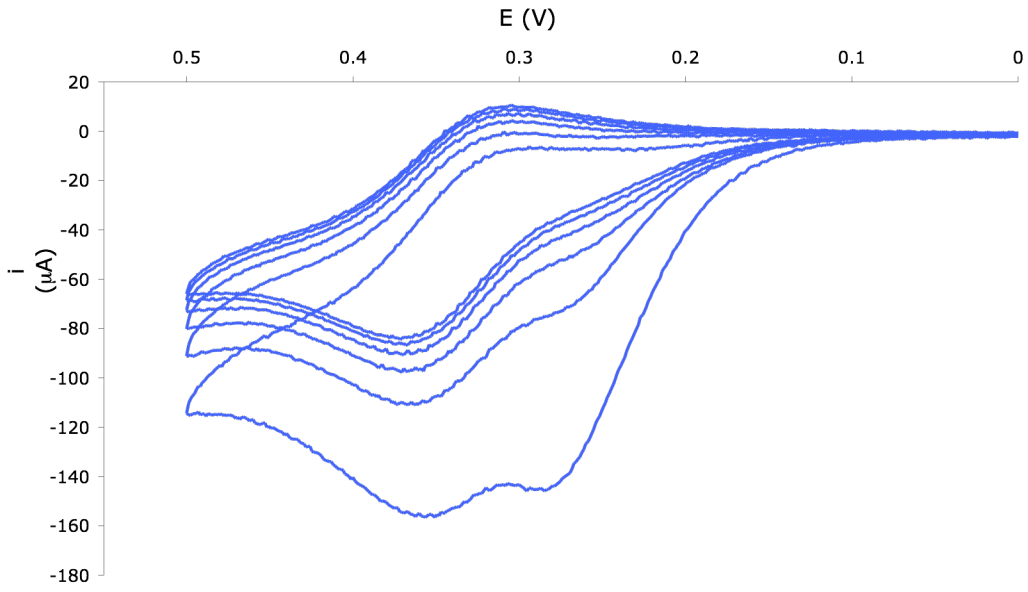

Figure 2.10. Multiple sweep cyclic voltammogram for the reaction of 3.0 mM *N,N*-dimethyl-*p*-toluidine with *n*-Bu_4NOAc under argon at 23 (±1) °C in 0.5 M H_2O, 0.5 M n-Bu_4NClO_4 in CH_3CN at a scan rate of 600 mV/s.

After several scans the kinetically shifted oxidative wave disappears and the voltammogram begins to resemble the voltammogram observed in the dimerization experiments where a quasireversible voltammogram was observed. This suggests that the after several scans there is no acetate anion present in the vicinity of the electrode but there is still amine near the electrode. In the case of deprotonation, reversibility should not be observed as it is a rapid irreversible chemical process! Three essential questions needed to be answered: 1) Why does the voltammogram contain this unexpected "prepeak" on initial scans? 2) Why does the relative magnitude of this "prepeak" diminish with each subsequent scan? 3) Why does dimethylaniline persist on later scans behaving as the uncatalyzed dimerization reaction did? Two likely reasons exist for the observed behavior: 1) Acetate is being consumed via deprotonation at a rate faster than it is diffusing to the surface of the electrode. 2) The mechanism of

reaction is more complex than previously expected. To answer question one and determine if an unusually low diffusion coefficient for acetate was responsible for this behavior, the diffusion coefficients of all species involved in the deprotonation process were reinvestigated using convolution voltammetry and pulsed-field-gradient NMR (hereafter referred to as PFG-NMR).

2.2.5 Diffusion Coefficient Measurements

Diffusion coefficients for species involved in the reaction of *N,N*-dimethylaniline with acetate anion were studied in an effort to investigate the assumption that neutral molecules and their electroactive counterparts exhibit approximately the same diffusion coefficients. Moreover, comparison of the charged species and their neutral counterparts is of interest to determine if, in the case that differences do exist, these differences are significant enough that transport kinetics will affect reaction kinetics.

N,N-dimethylaniline and protonated *N,N*-dimethylaniline were studied by PFG-NMR. These experiments were intended to address whether charge significantly affects rates of transport. Protonated *N,N*-dimethylaniline was studied as a model for the radical cation; it was assumed that solvation of charge would be the most significant factor affecting diffusion. The results obtained from these studies suggest that a protonated amine is a poor model for a radical cation because hydrogen-bonding interactions rather than charge solvation is the mitigating the key factor determining the rate of diffusion for the amines studied.

Using NMR, diffusion coefficients (D_o) were determined for the analyte of interest (*N,N*-dimethyl-*p*-toluidine or protonated *N,N*-dimethyl-*p*-toluidine **(Figure 2.11)**) as well as H_2O and CD_3CN in each sample.

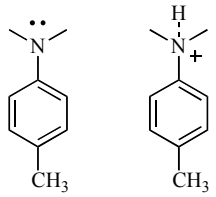

Figure 2.11. Amines whose diffusion coefficients were determined by PFG-NMR.

Diffusion coefficients are reported relative to the diffusion of H_2O in each particular sample (**equation (2.3**)) for the purpose of comparison. Diffusion of the analyte is reported relative to the diffusion of water and is normalized to account for the change rate of diffusion of water in the system under study relative to neat water. In our system water diffused notably faster than neat water. We postulate this results from the inability to form hydrogen-bonding networks that retard the diffusion of individual water molecules in neat water or systems containing higheoncentrations of water. **Equation (2.3**) was used to normalize diffusion coefficients for our analytes to account for this change in the apparent *Do*.

$$D_x = \frac{D_{analyte} \cdot D_{H_2O(Neat)}}{D_{H_2O(Sample)}} \qquad \textbf{(2.3)}$$

These values do not account for the presence of high concentrations of supporting electrolyte present in our electrochemical systems; inclusion of this factor is not necessary for the purpose of this analysis. Moreover, this role of supporting electrolyte in diffusion is addressed later in the text.

The apparent D_o of *N,N*-dimethyl-*p*-toluidine and its protonated counterpart were determined to be 7.28($\pm$.02) x 10^{-6} cm^2/s and 1.46($\pm$.03) x 10^{-5} cm^2/s, respectively, in 0.5 M H_2O and CD_3CN. Interestingly, this suggests the neutral amine diffuses slower than its protonated counterpart, a result counter-intuitive to expectations based on increasing energetic cost of solvation, and the associated transport, for an ion

compared to the neutral molecule. The observation of a difference in diffusion coefficient of this magnitude can be assumed to be negligible with regards to electrochemical kinetics *(vide infra).*

To rationalize the surprising result regarding the direction of change in diffusion coefficient, it is conjectured that protonation of the amine decreases the hydrogen bond accepting ability of the N, facilitating easier transport in a polar solvent. Water molecules are present in 17-fold excess relative to amine in these experiments. In the case of a neutral amine, hydrogen bonding interactions between the water's H and N of the amine are reported to have gas phase enthalpies of 6.9 kcal/mol. In the case of the protonated amine, two types of hydrogen bonding interactions would be observed; namely, interactions between protonated and neutral water, or interactions between the aminyl proton and the H-bond donor O of water. The gas phase enthalpies of these types of hydrogen bonds are reported to be 1.9 kcal/mol and 4.3 kcal/mol, respectively.[8] The former hydrogen bonding should not have a notable effect on the energetics of transport for the amine as the amine is not involved in these hydrogen bonding interactions. Nor is it competing with hydronium ion for hydrogen bonds to water, as water is in roughly a two fold excess to free H^+ in these experiments.

If hydrogen bond enthalpies trend similarly in solution and have similar differences in magnitude our results can be justified on the basis of a 5 kcal/mol increase in enthalpy of solvation associated with each hydrogen bond formed or broken as the neutral species moves through solution because it participates in stronger H-bonding interactions with the water in the sample mixture than does its protonated counterpart.

The primary reason for studying the diffusion coefficients in this work was to determine if the diffusion of acetate was unexpectedly slow. If the diffusion of acetate were unexpectedly slow, this may account for the separation of the kinetically shifted oxidative wave relative to the main wave as well as the reversibility observed on later scans. To be sure that the distinction between the two waves does not result from the rapid consumption of acetate at the surface of the electrode and slow replenishing of the reaction layer with acetate anion for further reaction, the diffusion coefficient of acetate was studied by two techniques. These experiments answer three important questions: 1) Is the diffusion of acetate and acetic acid (a deprotonation product) significantly different? 2) Does the change in viscosity resultant from the change in solvent (CD_3CN, 0.5M H_2O versus CH_3CN, 0.5 M H_2O, 0.5 M *n*-Bu_4NClO_4 have an appreciable effect on diffusion coefficient for the analyte of interest? 3) Is the diffusion of acetate slower than expected and likely to be the cause of the anomalous electrochemical behavior?

To answer question 2, both voltammetry and NMR were employed in diffusion coefficient determination. Convolution voltammetry affords a D_o for acetate in 0.5 M H_2O and CH_3CN of 1.80($\pm$.16)x 10^{-5} cm^2/s which compares favorably to the PFG-NMR value of 1.58 ($\pm$.03)x 10^{-5} cm^2/s. Voltammetry experiments comparing anhydrous and 0.5 M H_2O CH_3CN as solvent afford D_o values of 1.73 ($\pm$.11)x 10^{-5} cm^2/s and 1.80($\pm$.16)x 10^{-5} cm^2/s suggesting that the addition of water to these solutions does not significantly effect the kinetics of transport.

Importantly, the diffusion coefficients measured by convolution voltammetry were in the presence of 0.5 M *n*-Bu_4NClO_4. The addition of electrolyte is likely to slightly

increase viscosity of the sample and likely accounts for the insignificant but observed retardation of diffusion in the values measured by voltammetry relative to the PFG-NMR experiment. Diffusion coefficients in 0.5 M *n*-Bu_4NClO_4/0.5M H_2O/CH_3CN versus 0.5M H_2O/CD_3CN is reduced by 13%. Similar experiments performed by Alligrant *et.* al comparing 0.2 M *n*-Bu_4NPF_6/CH_3CN versus CD_3CN exhibit a 7.5% increase in viscosity.[8b],[9] We suggest that the difference in our values observed by the two methods (voltammetry and NMR) is also the result of viscosity changes as the increase in D_o observed in the absence of supporting electrolyte is congruent with what may be expected accounting for the 2.5 fold increase in electrolyte concentration relative to the literature. We are conscious of the fact the radii of the two anions (PF_6 and ClO_4) differ. Nevertheless, considering the exceptional agreement of the two techniques not even accounting for the minor change in viscosity these factors seem insignificant. Accounting for viscosity difference, our values show an outstanding agreement between the two techniques affording affords a D_o for acetate in of 1.80($\pm$.16)x 10^{-5} cm^2/s and 1.78 ($\pm$.03)x 10^{-5} cm^2/s by convolution voltammetry and PFG-NMR, respectively.

Alligrant and coworkers also investigated the magnitude and direction of the change in D_o resulting from protonation of a carboxylate anion. These compounds exhibit respective D_o of 3.95 x 10^{-5} cm^2/s and 2.67 x 10^{-5} cm^2/s; showing a factor of 1.47 difference between the values for the acid and its conjugate base, respectively.[8] Due to overlap of the CH_3 protons and the residual CH_3CN peak and rapid exchange of the OH protons in our 0.5 M H_2O/CH_3CN solutions PFG-NMR experiments to determine the D_o for acetic acid were unsuccessful. Voltammograms and rate constants determined for the reaction of *N,N*-dimethy*l*-*p*-toluidine radical cation with acetate anion in both

anhydrous CH_3CN and 0.5 M H_2O/CH_3CN are extremely similar suggesting that hydrogen bonding induced changes on diffusion coefficients are not significant for our reaction. This result is expected because in CH_3CN H bonding interactions to between the OH proton and the solvent(CH_3CN) N (6.9 kcal/mol) are stronger than those that would be observed between the OH proton and the water oxygen (5.0 kcal/mol) so the addition of water is not likely to induce a significant change in diffusion coefficient. This supposition can be easily investigated through comparison of phenylacetic acid and *n*-$Bu_4NPhOAc$ by PFG-NMR. Acetate and acetic acid should exhibit a similar difference in D_o in 0.5 M H_2O solution as the differences are attributable to similar molecular phenomena; ion solvation costs and hydrogen bonding. The hydrogen bonding ability of the aliphatic and aromatic carboxylate are likely to be similar as there are no other hydrogen bond donors present in the aryl system and both molecules are similar carboxylate ions.

Notably, the observation of a 2-fold difference in D_o for a molecule and its charged counterpart, on first inspection, does appear to challenge a key assumption of digital electrochemical simulations (diffusion coefficients for the electroactive species is assumed to be equal to that for the parent compound). Although based on our results the reason this assumption can be made is that the magnitude of these changes in D_o are insignificant on the timescale of the kinetics measured. The reaction layer for a process occurring with a rate constant on the order of magnitude of our reactions, 10^4 to 10^7, 1/Ms will give a reaction layer thickness of 10^{-5} to 10^{-6} relative to the thickness of the diffusion layer; therefore, the concentration of the electroactive species at the surface of the electrode will be constant be constant over the course of the reaction. Britz suggest

that even for the slowest reactions capable of being measured by cyclic voltammetry a reaction layer thickness of no greater than 10^{-2} the thickness of the diffusion layer is observed.[10]

In summary, excellent agreement among diffusion coefficients observed by both techniques was observed. Additionally, the diffusion coefficients for the charged and uncharged species are somewhat different but these differences are insignificant on the timescale of electrochemical kinetics. The protonated amine does not provide an adequate model for determination of diffusion coefficient of the amine radical cation because of significantly different factors likely to affect transport for the two species. The most significant result determined here is the diffusion coefficient of acetate anion is not unexpectedly slow. It is in fact slightly higher than that for the amines measured **Table 2.3**.

Table 2.3. Diffusion coefficients at 25°C corrected for viscosity of a 0.5 M n-Bu_4NClO_4 containing solution. [a] measured by PFG-NMR [b] measured by voltammetry

Compounds	D_o Corrected for Viscosity cm^2/s
N,N-dimethyl-*p*-toluidine [a]	8.22(±.02) x 10^{-6}
Acetate Anion [b]	1.80(±.16)x 10^{-5} cm^2/s and
Acetate Anion [a]	1.78 (±.03)x 10^{-5} cm^2/s

It stands to reason that if amine is still present at the surface of the electrode after 6 scans and acetate is not this is not the result of the inability of acetate being depleted more rapidly than it can diffuse. Therefore, the observed electrochemical behavior is not a diffusion effect.

2.2.6 Cyclic Voltammetry (3: Kinetic Analysis)

Having eliminated a surprisingly low diffusion of acetate as the cause of the interesting electrochemical behavior, the focus was turned on analysis of possible mechanistic incongruities between our results and the literature reports. Reinvestigation of the reaction mechanism was performed with the aid of digital electrochemical simulations ***(see 4.3)***. Considering what mechanism could occur between the two reagents, it was determined that electron transfer or deprotonation were the most likely pathways for reaction **(Scheme 2.4)**.

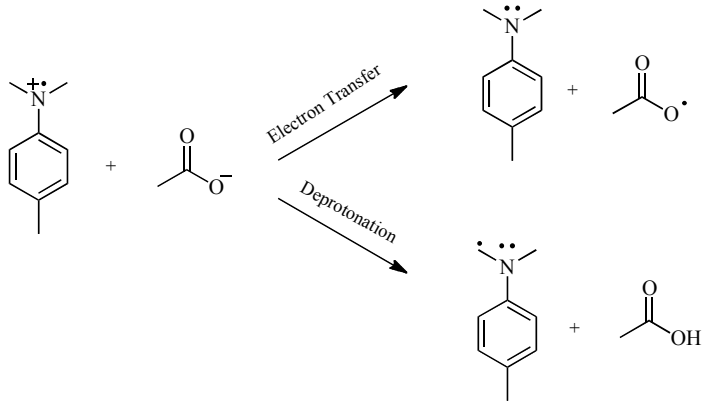

Scheme 2.4. Possible modes of reaction for *N,N*-dimethylaniline radical cations and acetate anion.

The supposition that electron transfer was a feasible mechanism of reaction was further supported by the fact that electron transfer would yield an unstable acetoxyl radical. Unstable acetoxyl radicals have been reported to undergo facile decarboxylation, providing an additional thermodynamic driving force for this pathway.[11] A qualitative depiction of the electrode process for an electron transfer is shown in **Scheme 2.5**.

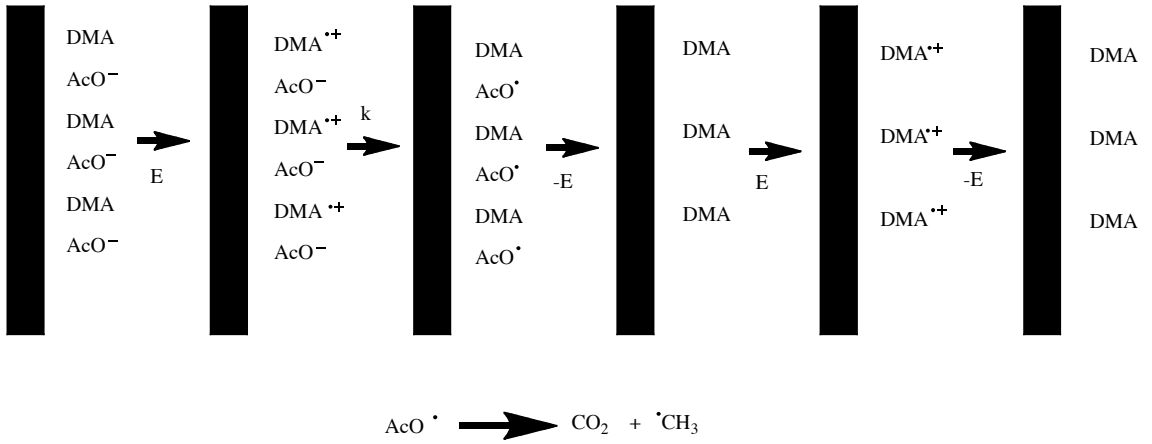

Scheme 2.5. Rationale for electrochemical behavior based on an electron transfer mechanism. E represent applying potential.

At the surface of the electrode the radical cation is generated. This radical cation undergoes reaction with the acetate anion in solution. The supposition of an electron transfer reaction being feasible was further supported by the fact that electron transfer would regenerate the neutral amine and yield an unstable acetoxyl radical, which would be irreversibly consumed in a subsequent and rapid decarboxylation. After several scans the acetate is consumed (loss of kinetically shifted peak) but the amine is catalytically regenerated. The amine can then undergo oxidation to form the amine radical cation. This radical cation can, in turn, be reduced to form the parent amine (return of the reverse wave).

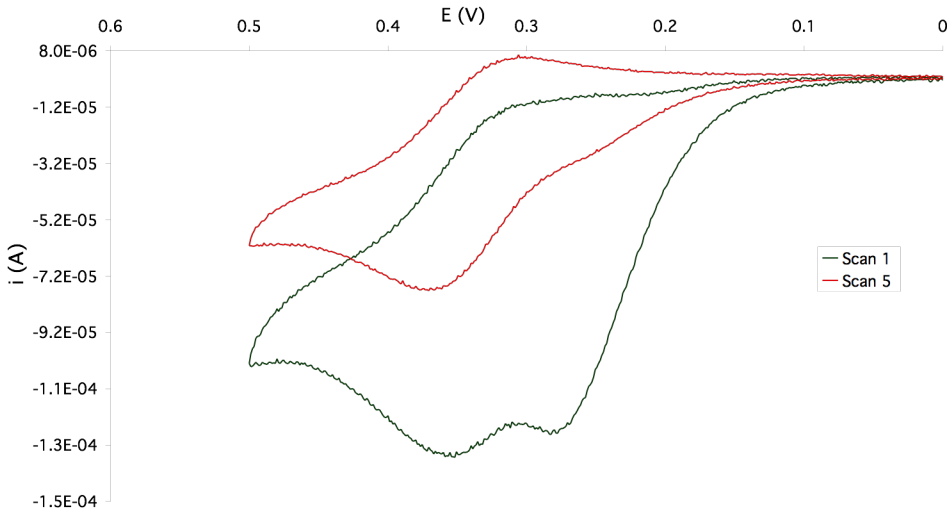

Figure 2.12. The electrode process in scheme 5 is well represents by the cyclic voltammetry data attained in analysis of 3.0 mM *N,N*-dimethyl-*p*-toludine and 3.45 mM *n*-Bu_4NOAc in 0.5M H_2O, 0.5 M *n*-Bu_4NClO_4 in CH_3CN.

Inputting the necessary experimental parameters (E_o, D_o, electrode area) and utilizing the rate constants determined by laser flash photolysis (where available) simulations were performed. To provide unbiased assessment the feasibility of both deprotonation and electron transfer, simulations for both systems were performed for a multiple sweep cyclic voltammetry experiment. The similarities between the simulated voltammograms for the electron transfer mechanism and the experimental data was undeniably clear. Additionally, the differences between the simulated voltammograms and the deprotonation mechanism show that this mechanism is extremely unlikely to be the primary mode of reaction as the voltammograms are remarkably dissimilar. The voltammograms comparing the two mechanisms and the experimental data for *N,N*-dimethyl-*p*-toluidine are shown in **Table 2.4**.

Table 2.4. Simulated versus experimental data for the reaction of 3 mM *N,N*-dimethyl-p-toluidine and 3.45 mM *N,N*-dimethyl-*p*-toluidine at a scan rate of 600 mV/s.

Deprotonation Simulation	Experiment	Electron Transfer Simulation
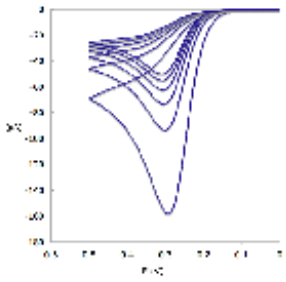	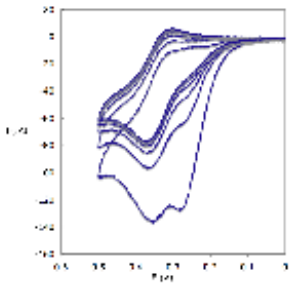	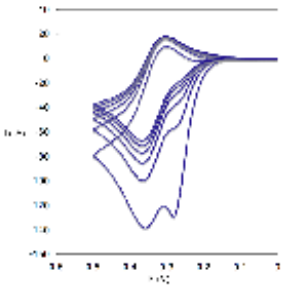

The voltammogram for a deprotonation mechanism would be expected to look like that that afforded by the simulation and no reversibility would be expected because oxidation is followed by a chemical step where the amine is consumed irreversibly. In the case of electron transfer the simulation of the electron transfer reaction would be expected to show some reversibility because the chemical step regenerates the neutral starting material. In some simulations particularly those involving amines without electron donating para substituents a pure electron transfer mechanism over estimated the magnitude of the reverse wave. This observation led us to expect that some degree of deprotonation may be occurring. The faster reacting (less stable) radical cations were expected to be most reactive and apt to be less selective in their preference for mode of reactivity. This supposition is supported by the rate constant data presented in **Table 2.5.**

Table 2.5. Rate constants for electron transfer reactions from acetate anion to para-substituted *N,N*-dimethylaniline radical cations in 0.5 M H_2O, 0.5 M *n*-Bu_4NClO_4, CH3CN, under argon. All rate constants are given in 1/Ms.

Compound	k_{total}	k_{dep}	k_{ET}
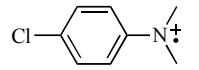	5.0(±0.3) x 10^{7} [a]	≤ 5 x 10^{6} [a]	5.0(±0.3) x 10^{7} [a]
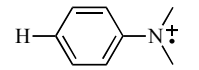	2.9(±0.3) x 10^{6} [b]	-	-
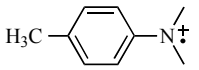	2.7(±0.6) x 10^{6} [a]	6.5(±4.7) x 10^{4} [a]	2.7(±0.6) x 10^{6} [a]
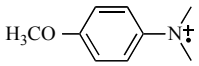	4.1(±.9) x 10^{4} [a]	0	4.1 x 10^{4} [a]

[a] Measured by cyclic voltammetry. T=23 (±1)°C
[b] Measured by laser flash photolysis. T= 25 °C

Rate constant data for deuterated dimethylanilines is given in **Table 2.6**.

Table 2.6. Rate constants for electron transfer reactions from acetate anion to para-substituted *N,N*-di(deutero)methylaniline radical cations in 0.5 M H_2O, 0.5 M *n*-Bu_4NClO_4 in CH_3CN. All rate constants are given in 1/Ms.

Compound	k_{total}
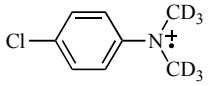	2.4(±1.1) x 10^{7} [a]
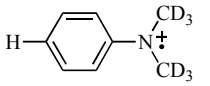	1.5(±0.6) x 10^{6} [b]
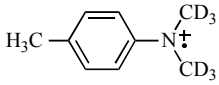	1.0(±0.4) x 10^{6} [a] 7.2(±0.7) x 10^{5} [b]
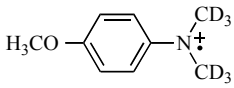	4.7(±0.3) x 10^{3} [a]

[a] Measured by cyclic voltammetry. T=23(±1)°C
[b] Measured by laser flash photolysis T=25°C

Notably the rate constant data suggests that deprotonation is detected as a competing pathway in some reactions. The rate constant for deprotonation is greatest in the case of *N,N*-dimethyl-*p*-aniside which also exhibits the largest rate constant for electron transfer. The introduction of a methoxy substituent at the para substituent that stabilizes the radical cation and decreases the rate constant for its reaction relative to the most destabilized compound by 3 orders of magnitude relative to the para chloro

compound. It is also possibly that the methoxy compound was also undergoing deprotonation to some degree however, because the total rate constant was so low the simulation may have been insensitive to the contribution of this minor contributing pathway. It was desired that all compounds be analyzed by both techniques; however, practical considerations prevented the fulfillment of this want. Nevertheless, some compounds were able to be analyzed by both laser flash photolysis and multiple sweep cyclic voltammetry. In these cases the two techniques provided kinetic parameters in excellent agreement with regards to k_{Total}.

While laser flash photolysis lacks the ability to distinguish between the two processes cyclic voltammetry experiments where the concentration of the two reactants are in a ratio such that the "prepeak" can be resolved from the normal peak can be used to provide a measure of the rate constant for both deprotonation and electron transfer. Parker astutely noted, in the only other electrochemical analysis of these systems, that the shift of the prepeak from the normal oxidative wave is a measure of k_{Total}.[6b, 12] We too, in our simulations, have found this to be true as increased separation of the two peaks indicates a greater overall reaction rate constant as shown in **Figure 2.13.**

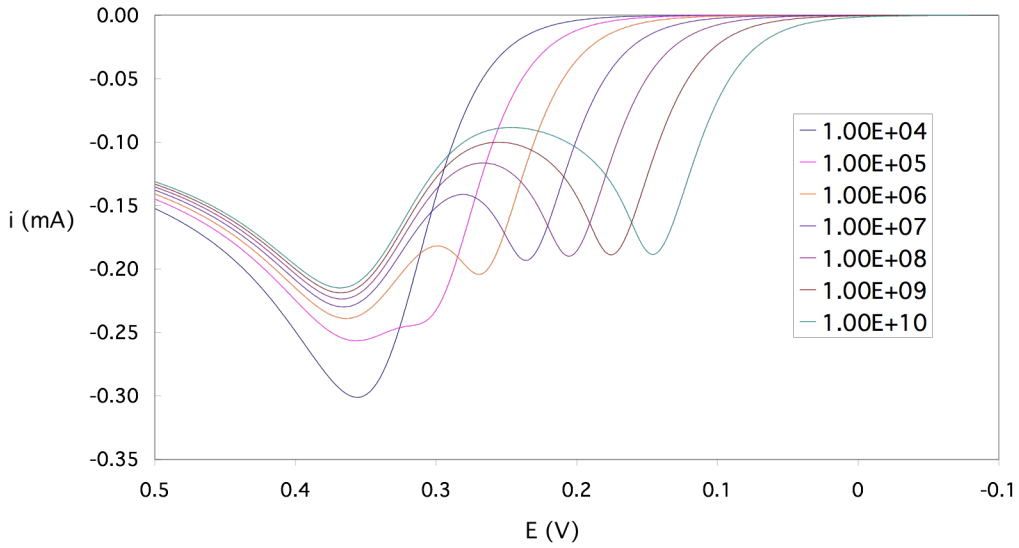

Figure 2.13. The separation of the normal oxidative peak and the "prepeak" potential are a measure of the total rate constant for the reaction between acetate and the dimethylanilines studied.

Additionally, we noted that the difference in height of the two peaks provides a clear indicator of the ratio of the rate constant of deprotonation relative to electron transfer **(Figure 2.14)**. The larger the height of the prepeak relative to the main peak the higher the amount of deprotonation occurring. It should be noted that in the system studied here the rate constant for deprotonation was found to be no greater than 3% relative to the rate constant for electron transfer occurring in the system.

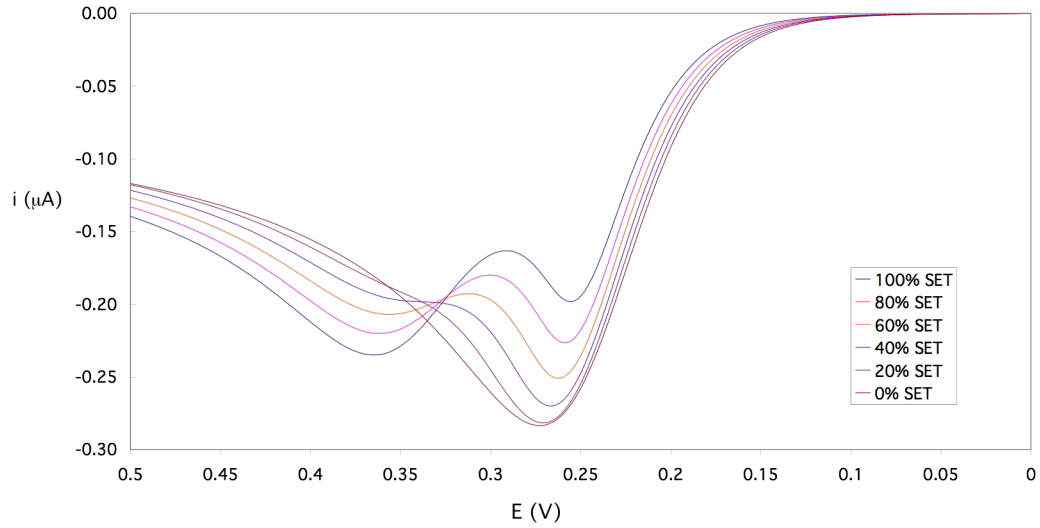

Figure 2.14. SET simulations demonstrate the relative height of the peak at the normal peak potential and the "prepeak" potential is an accurate measure of the partitioning between the two pathways, electron transfer and deprotonation.

Schemes 2.6 and **2.7** are the complete mechanistic schemes utilized in the simulations. Notably in the simulations where electron transfer was considered as the dominate reaction mode both the deprotonation and electron transfer process were included in the simulation. The rate constant for the two processes were adjusted to determine three values k_{Total}, k_{ET} and k_{-H+}. Other experimentally determined parameters including k_{Dimer} were held constant as the other desired kinetic parameters were varied. First, electron transfer was considered to occur in the absence of deprotonation. These simulations were performed until the seperation between the kinetically shifted peak and the oxidative peak were modeled to match the seperation observed in the experimental voltammogram being fit. A second set of simulations was then performed using $k_{E.T.}$ from the first set of simulations to serve as k_{Total} (k_{Total}=k_{ET} + k_{-H+}). The ratios of k_{ET} and k_{-H+} were adjusted so that kinetically shifted peak and main peak height as well as the magnitude of the reverse wave matched the experimental data as closely as possible.

Electrode:

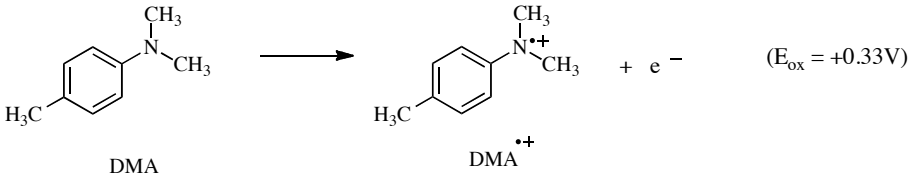

Solution:

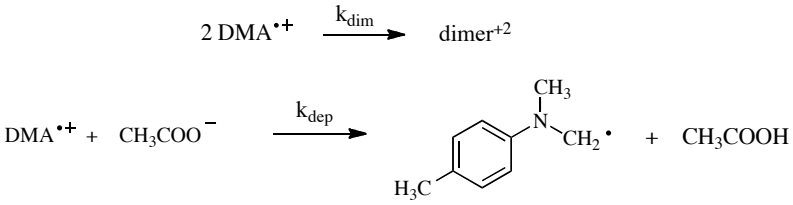

Electrode:

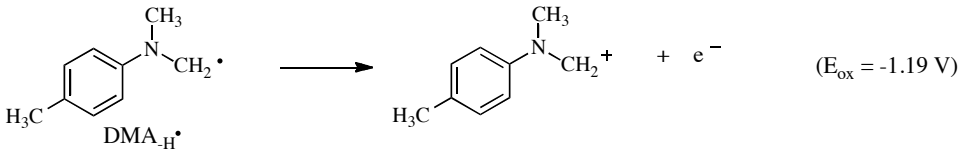

Scheme 2.6. The deprotonation mechanism consumes two equivalents of electrons. The amine is oxidized to the radical cation at the electrode surface and subsequently undergoes deprotonation to form an easily oxidizable ã-aminylalkyl radical which can undergo subsequent oxidation to form the corresponding cation at the electrode surface.

Electrode:

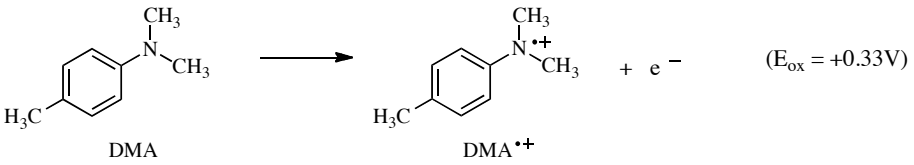

Solution:

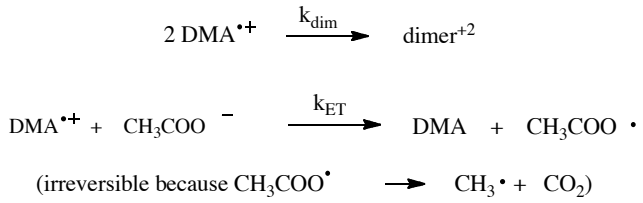

Scheme 2.7. Electron transfer mechanism involves passage of two equivalents of electrons. Each mole of neutral amine is oxidized twice at the electrode surface; it is catalytically regenerated by oxidation of the carboxylate and the neutral amine is oxidized a second time. After the second oxidation, if no carboxylate is present in solution it undergoes an irreversible dimerization and no further electrode reaction can occur.

In all electrochemical kinetic studies two or three different molar ratios of amine to carboxylate were studied. For each set of experiments several different scan rates between 100 to 2000 mV/s were studied by multisweep cyclic voltammetry. Reaction rate constants were determined by simulating voltammograms adjusting both $k_{\text{-H+}}$ and $k_{\text{E.T.}}$ to give the best fit to experimental data for each scan rate, at each molar ratio and for each replicate of the experiment. Overall rate constants and experimental error were determined from the average and 95% confidence interval for the entire data set analyzed in this way. Each voltammogram was fit independently and weighted equally in determining kinetic parameters.

2.2.7 Isotope Effects

Isotope effects were also determined for deuterated compounds **(Figure 2.15)** to address further the significance of previously reported isotope effects.

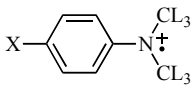

X=Cl,H, CH_3 or OCH_3

L=H or D

Figure 2.15. Site of deuteration of amines studied.

The isotope effects measured in this work are reported in **Table 2.7** below.

Table 2.7. Experimentally determined isotope effects in 0.5 M H_2O, 0.5 M *n*-Bu_4NClO_4 and CH_3CN

Compound	k_H/k_D
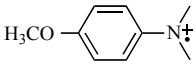	1.6[a]
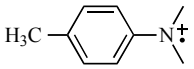	2.7[a] 1.9[b]
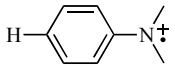	1.9[b]
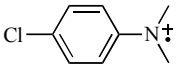	2.1[a]

[a]Measured by cyclic voltammetry.
[b]Measured by Laser Flash Photolysis

The isotope effects measured in our studies compare favorably to those reported by previous researchers **(Table 2.8)**.

Table 2.8. Reported isotope effects for the reaction of *N,N*-dimethylaniline radical cations with *n*-Bu_4NOAC is various solvent.

Compound	CH_3CN[6b]	60:40 CH_3OH:CH_3CN[6c]	0.5M H_2O/CH_3CN[6a]
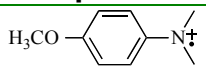	5.3		
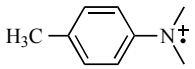			1.6
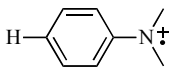		3.6	2.1
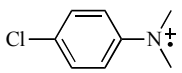	3.6		2.4

[a] Measured by cyclic voltammetry T=23(±1) °C
[b] Measured by laser flask photolysis T=25°C

On the basis of the similarities of the magnitudes of these values, we conjecture that the isotope effects observed in both our studies and the previous studies are principally secondary isotope effects. In cases where some contribution from both deprotonation and electron transfer these isotope effects may be a combination of the primary and secondary isotope effects for the respective processes. Isotope effects of the magnitude we report here have been observed by other researchers in electron transfer reactions involving methyl substituted aryl radical cations; in these reports the secondary isotope effects are said to result from hyperconjugative interactions involving the radical cation center and adjacent methyl protons.[13].

2.2.8 Solvent Effects

The rate constants for these reactions have been reported in various solvent systems from 60:40 Methanol to anhydrous acetonitrile resulting in rate constants ranging from 10^5 to 10^7 1/Ms for *N,N*-dimethyl-*p*-toluidine it was necessary to determine if these rate constant variations were due to a change in mechanism. Studies of *N,N*-dimethyl-*p*-toluidine in both 0.5 M H_2O in CH_3CN and dry acetonitrile were performed **(Table 2.9).**

Table 2.9. Rate constants and isotope effects for the reaction of *N,N*-dimethyl-*p*-toluidine radical cations and *n*-Bu_4NOAc. Deuterated compounds are deuterated at the methyl groups a to the amine nitrogen. Experiments are performed in 0.5 M *n*-Bu_4NClO_4. When water is included in the solvent mixture the concentration is 0.5M.

Solvent		k_{ET} (1/Ms)	$k_{Deprotonation}$ (1/Ms)	k_{Total} (1/Ms)
CH_3CN	L=H	5.6(±1.1) x 10^6 [a]	1.5(±0.5) x 10^5 [a]	5.8(±1.2) x 10^6 [a] 3.7(±0.8) x 10^6 [b]
	L=D	2.1(±0.3) x 10^6 [a]	2.2(±1.6) x 10^4 [a]	2.1(±0.3) x 10^6 [a] 1.2(±0.2) x 10^6 [b]
		k_H/k_D =2.8[a]	k_H/k_D = 7.0[a]	k_H/k_D =2.8[a], 3.0[b]
CH_3CN/ H_2O	L=H	2.7(±0.6) x 10^6 [a]	6.5(±4.7) x 10^4 [a]	2.7(±0.7) x 10^6 [a] 1.3(±0.2) x 10^6 [b]
	L=D	1.0(±0.4) x 10^6 [a]	(not detected) [a]	1.0(±0.4) x 10^6 [a] 0.72(±0.12) x 10^6 [b]
		k_H/k_D = 2.6[a]	$k_H/k_D \geq$ 6.0[a]	k_H/k_D = 2.7[a], 1.9[b]

both solvent systems the same “prepeak” behavior was observed. Only a small decrease in rate constant occurred with the addition of water to the reaction mixture. Moreover, the magnitude of isotope effects observed were similar in both systems. Aromatic amines are less likely to participate in hydrogen bonding interactions than their aliphatic counterparts so it is not expected that a notable solvent effect would manifest in these studies. The amine radical cation is likely highly delocalized over the ring so may be afforded less stabilization by hydrogen bonding. We expect the small solvent effect observed can be attributed to minor stabilization of acetate anion due to hydrogen bonding in water.

Oxidation of aromatic and aliphatic carboxylates can be catalyzed using ferrocene radical cations has been studied by others and reported to occur via electron transfer. Rapid decarboxylation of the acetoxyl radicals leads to radicals that can be useful in electrochemical syntheses. These decarboxylations proceed under diffusion control, suggesting this may be a thermodynamic driving force for our reactions. Importantly, our preliminary investigation of the electrochemical kinetics of the reaction

of *N,N*-dimethylaniline radical cations with an aryl carboxylate (phenyl acetate) exhibits similar behavior via cyclic voltammetry (**Figure 2.16)** and is likely to also proceed via and analogous mechanism.

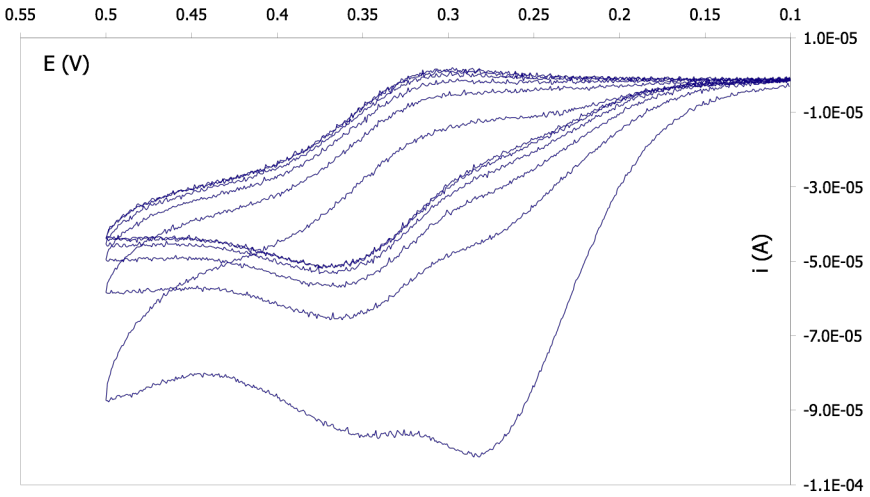

Figure 2.16. 1:1 experiments with phenyl acetate exhibit prepeak behavior similar to that observed in the acetate oxidations of *N,N*-dimethylanilines. Conditions: 3.0 mM *N,N*-dimethyl-*p*-toludine and 3.0 mM n-$Bu_4NPhOAc$ in 0.5 M H_2O, 0.5 M n-Bu_4NClO_4, CH_3CN at 23 (±) 1 ^oC and 500 mV/s.

As stated previously, we believe our reaction is proceeding by an electron transfer mechanism therefore to provide additional evidence for the proposed electron transfer mechanism we fit our data to the Marcus equation in combination with the data for several ferrocenes oxidation of acetate anion. The work term was not included in the equation as it was expected to make a negligible contribution in our system and the reorganization energy was determined by fitting the generated curve to the experimentally obtained points. The ferrocene/acetate system was investigated under analogous experimental conditions with acetate anion by another researcher in our laboratory. The Marcus plot **(Figure 2.17)** exhibits a striking fit for our data to the curve generated for the oxidation of acetate via an electron transfer mechanism suggesting

that the reaction under study is an authentic electron transfer process. This result provides substantial circumstantial evidence that an electron transfer mechanism is appropriate to describe the observed electrochemical behavior.

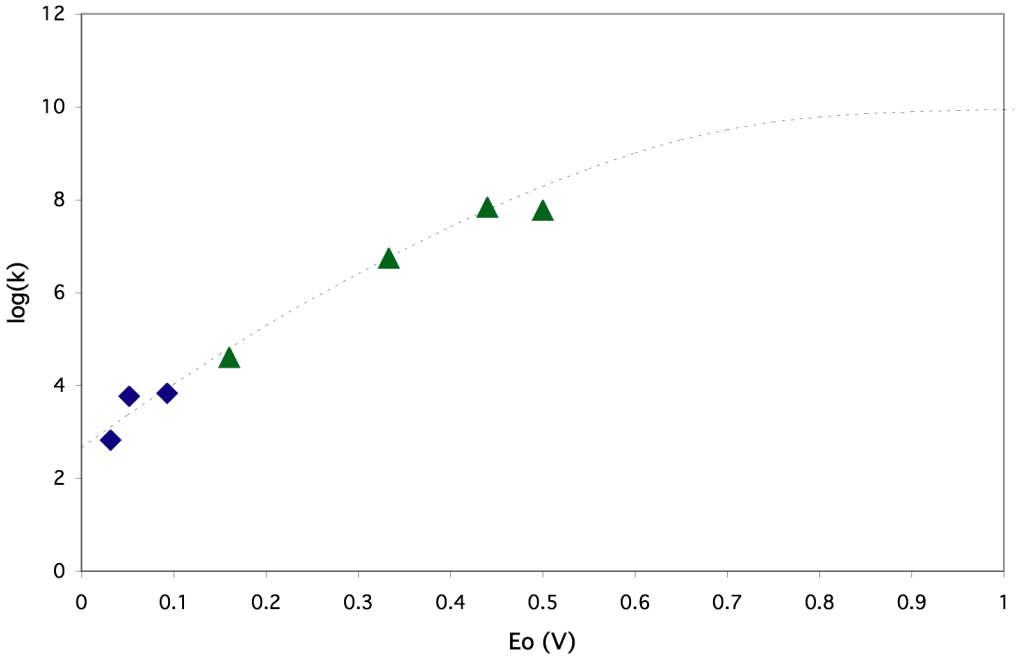

Figure 2.17. Marcus plot for the oxidation of acetate. Comparison of a genuine electron transfer to ferrocenes and the proposed oxidation involving the *N,N*-dimethylaniline radical cations all fall on the same plot. This analysis does not include a contribution of the work term of the Marcus equation. (Ferrocenes studied by Jared Spencer in Blue, *N,N*-dimethylanilines studies by author in green)

2.2.9 Product Study (Constant Potential Coulometry)

Product studies were carried out to assist in mechanistic assignment for the reactions of para-substituted *N,N*-dimethylaniline radical cations and carboxylate bases. Our study was intended to determine if the amine is catalytically regenerated as it is in the proposed electron transfer mechanism. The published and proposed mechanisms (***see 2.2.6***) both consume two moles of electrons per mole of amine**.**

Exhaustive constant potential electrolysis at the oxidation potential of *N,N*-dimethyl-*p*-toludine (478 mV) of solutions containing 1:2 molar equivalents of *N,N*-dimethyl-*p*-toludine: phenyl acetate consumed 1.44(±0.18) equivalents of electrons before the current measurements indicated the amine has been completely consumed. It may be reasoned that the contribution of the competing "dimerization" reaction may involve one mole of neutral amine and one mole of radical cation thus decreasing the number of electrons consumed by the overall process (if this "dimerization" makes a significant contribution to the mechanism). At low excess factor such as the factor of two used in this experiment allows the concentration of carboxylate to decrease significantly over the timeframe of the experiment thus allowing the emergence of the competing dimerization pathway. It is equally likely that the amine radical cation can react with carboxylate oxidation products.

Solutions containing one equivalent of *N,N*-dimethy-*p*-toludine and ten equivalents of carboxylate were electrolyzed at the prepeak potential (280 mV) until two equivalents of electrons had passed. Providing a large excess of carboxylate was envisaged to favor the amine radical cation oxidizing acetate rather than the significantly less facile self-decomposition via dimerization. It was expected that the concentration of carboxylate would not become sufficiently low that the dimerization process would dominate and irreversibly consume the amine radical cation. Using a modified electrochemical cell, electrolysis solutions were able to be analyzed by CV before and after constant potential experiments to provide qualitative evidence for the presence or absence of *N,N*-dimethyl-*p*-toludine in these solutions. Satisfyingly, we were able to detect a current increase at the peak potential of *N,N*-dimethyl-*p*-toludine's oxidation

after the solution consumed two equivalents of electrons (**Figure 2.18**). This result indicates the amine was not irreversibly consumed as it would be if deprotonation were the primary or only reaction occurring. Because an extremely high concentration of carboxylate was used, no reverse wave or prepeak was observed in the resultant voltammograms.

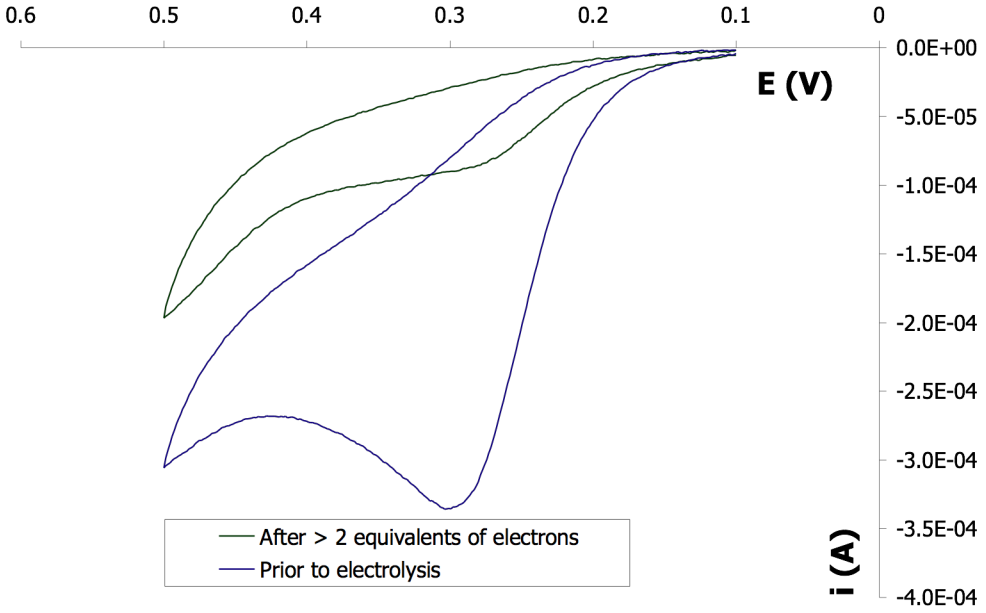

Figure 2.18. Experiments with 3.04 mM *N,N*-dimethyl-*p*-toludine and 48.01 mM phenyl acetate exhibit an oxidation at the peak potential characteristic of *N,N*-dimethyl-p-toludine after passage of 2+ equivalents of electrons. Conditions: 0.5 M H_2O, 0.5 M n-Bu_4NClO_4, CH_3CN at 600 mV/s.

To further investigate the electrochemical behavior of this system a smaller excess factor (2) was used and similar experiments were performed. The voltammogram from these experiments (**Figure 2.19**) does exhibit a quasi-reversible voltammogram characteristic of *N,N*-dimethyl-*p*-toludine's oxidation after the solution consumed nearly two equivalents of electrons. These two results provide qualitative

evidence for the catalytic regeneration of the neutral amine and the likelihood of an electron transfer mechanism in the reaction under study.

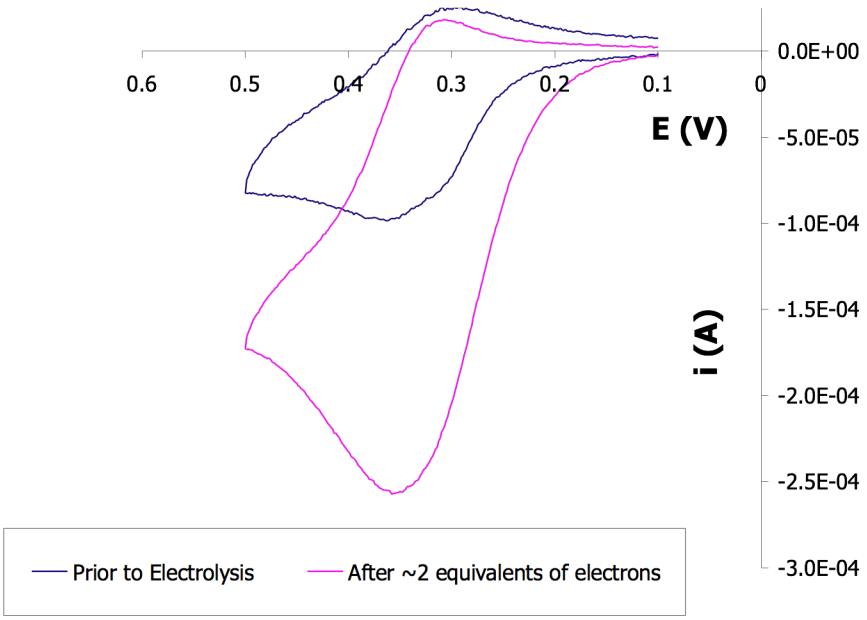

Figure 2.19. Experiments with 3.04 mM *N,N*-dimethyl-*p*-toludine and 4.80 mM phenyl acetate exhibit quasi-reversible voltammograms characteristic of *N,N*-dimethylanilines after passage of 1.7 equivalents of electrons. Conditions: 3.0 mM n-$Bu_4NPhOAc$ in 0.5 M H_2O, 0.5 M n-Bu_4NClO_4, CH_3CN at 600 mV/s.

Quantitative evidence for the electron transfer mechanism was found by measuring the degree of conservation of amine after consumption of enough electrons to irreversibly convert all of the amine to product via a deprotonation mechanism. In the electron transfer mechanism the amine is regenerated in each reaction with carboxylate. After consumption of two moles of electrons per mole of amine, in our experiments with a 10 fold excess of carboxylate, a notable quantity of amine could still be detected in our electrochemical studies. In order to verify the identity of the catalytic amine we sought to isolate and characterize the products of our reaction. Several methods of isolation of the *N,N*-dimethyl-*p*-toludine were attempted (liquid-liquid

extraction, HPLC and solid phase extraction) but were unsuccessful due to complications introduced by the large quantities of the organic salt (supporting electrolyte) present in electrolyzed solutions and the low molecular weight of *N,N*-dimethyl-*p*-toludine. Column chromatography was not attempted as literature reports of decomposition of the proposed deprotonation products on both silica and alumina would preclude unbiased use of this method for product studies. Gratifyingly, supercritical fluid chromatography afforded efficient separation of the starting amine and other products detected by UV-Vis. Supercritical fluid chromatography separated *N,N*-dimethyl-*p*-toludine from other amine based products that may exhibit similar absorbances before spectroscopic quantitation. Supercritical fluid chromatography of *N,N*-dimethy-*p*-toludine standards allowed us to confirm the peak associated with *N,N*-dimethyl-*p*-toludine was correctly identified in the chromatogram. These same standards facilitated generation of a calibration curve by which the concentration of *N,N*-dimethyl-*p*-toludine was determined via UV-vis of the post-reaction mixtures. **(Table 2.10).**

Table 2.10. Percent of moles of *N,N*-dimethyl-*p*-toludine measured in post-reaction mixtures relative to the initial number of moles of *N,N*-dimethyl-*p*-toludine.

Carboxylate	% Moles *N,N*-dimethyl-*p*-toludine Conserved
Acetate	25.7 (±6.2)%
Phenyl Acetate	17.6 (±1.0)%

The concentrations of *N,N*-dimethyl-*p*-toludine detected suggest that the amine is quasi-catalytic in these reactions; likely a result of a dominate electron transfer mechanism combined with a small amount of competing irreversible deprotonation. Contributions from other reactions occurring may also be significant. The authors suspect that some likely candidates are reaction of the decarboxylation products

(radicals) with the radical cation (possibly via α-carbon deprotonation of the amine by the radical generated by the decarboxylation). We have no evidence to support this particular contributing pathway, rather it is put forth to highlight that there is a likelihood that the decarboxylation products are reactive toward the amine or amine radical cation. Interestingly, a notable quantitity of one other products which exhibit absorption maxima in a similar region of the visible spectrum was noted in the chromatograms reaction mixtures of acetate but not phenyl acetate (**Figure 2.20**).

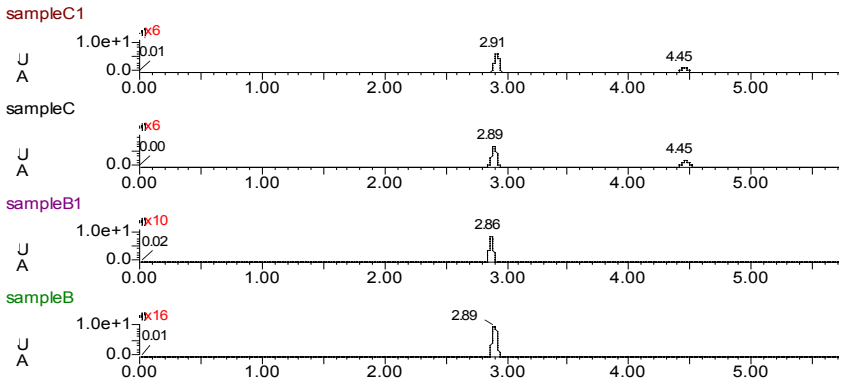

Figure 2.20. Chromatograms for post reaction mixtures of reactions of acetate (C, C1) and phenyl acetate (B, B1) with *N,N*-dimethyl-*p*-toludine. Peak at 2.9 corresponds to *N,N*-dimethyl-*p*-toludine.

The location of the absorption maxima in the spectra of this second product suggests incorporation of the aniline in this product (**Table 2.11).**

Table 2.11. Supercritical fluid chromatography retention times and UV absorption maxima for peaks observed after constant potential electrolysis compared to standard *N,N*-dimethyl-*p*-toludine.

Post Reaction Mixture Or Authentic Standard	Retention Time (minutes)		
	2.7-2.9	4.4-4.5	6.1-6.3
	λ_{max} (nm)		
N,N-dimethyl-p-toludine Standard	247	None	None
Phenylacetate/*N,N*-dimethyl-*p*-toludine	247	239	236
Phenylacetate/*N,N*-dimethyl-*p*-toludine	247	239	236
Acetate/*N,N*-dimethyl-*p*-toludine	247	239	236
Acetate/*N,N*-dimethyl-*p*-toludine	247	239	236

Although not apparent in the chromatogram shown, trace quantities of this slower eluting (presumably larger) product was observed in both reaction mixtures. Additionally, trace quantities of another amine based product was also observed in both mixtures at a later retention time. Identification of these products in future work by performing the reactions on larger scale and isolating or comparing to authentic standards or LCMS for these assumedly higher molecular weight products may indeed provide additional insight into the mechanism of the reaction.

Generally, we conclude from these studies that these reactions are consuming carboxylate at a significantly more rapid rate than they are consuming amine. This phenomena has been observed in both kinetic studies (at the surface of the electrode) and in product studies (homogeneous solutions). At the present, we expect that these results suggest electron transfer is occurring and the amine is being catalytically regenerated by this process and that some competing process is responsible for the irreversible conversion of some portion of the amine to other, yet unknown, products. Further analysis of the nature of the products and identification of the pathways by which they are formed is integral to fully understanding the significance of the results obtained in this product study.

2.3 Conclusions

Using multiple sweep cyclic voltammetry and laser flash photolysis k_{Total} for the reactions of a series of para-substituted *N,N*-dimethylanilines were measured and shown to span a range of 3 orders of magnitude from 10^4 to 10^7 1/Ms; indicating a significant role of the electron withdrawing or donating nature of the para-substituent on radical cation stability. Through use of multiple sweep cyclic voltammetry we have

shown that the major reaction pathway is electron transfer not deprotonation. Further supporting this supposition, we determined that *N,N*-dimethyl-*p*-toludine was at least partially regenerated in the reaction under study by constant potential coulometry product studies. This observation is indicative of the occurrence of an electron transfer and not a deprotonation mechanism being the primary reaction pathway. Moreover, we have studied these reactions in both aqueous and anhydrous acetonitrile showing only a small effect on rate constant and no evidence of a change in mechanism judging from the voltammogram behavior and the magnitude of the observed kinetic isotope effects. The isotope effects observed in our study are in accord with those reported by previous investigators of these systems. Furthermore, the magnitude of the isotope effects reported herein are also consistent with the magnitude expected for a secondary effect associated with electron transfer involving aryl radical cations. Finally, the diffusion coefficients for the reacting species have been investigated and are all on the order of normal diffusion coefficients suggesting that neither solvation nor a surprisingly low diffusion of acetate are responsible for the voltammogram behavior observed in our studies. On the basis of these results we are satisfied to report the identification of a previously unreported mechanism for the reaction of *N,N*-dimethylanilines with acetate anion. This reaction prefers to proceed via electron transfer rather than deprotonation.

Our studies with phenyl acetate using similar methods show that a) the prepeak is observed in studies utilizing an excess of amine to carboxylate and b) product studies show the amine to be catalytic suggesting a similar mechanism is likely occurring in these systems. Further kinetic analysis of this system is required to gain insight as to the relative propensity for this system to undergo deprotonation or electron transfer.

Additional analyses of all systems studied are required to identify the products observed and the reason (competing reaction pathways) that make the amine only quasi-catalytic.

REFERENCES:

[1] aM. Wainwright, *Dyes and Pigments* **2008**, *76*, 582-589; bE. Rosa, A. Guerrero, M. P. Bosch, L. Julia, *Magnetic Resonance in Chemistry* **2010**, *48*, 198-204; cA. A. Yassin, N. A. Pizk, *Journal of Polymer Science: Polymer Chemistry Edition* **1978**, *16*, 1475-1485.

[2] N.S.Scrutton, A. W. Munro, D.Leys, M.J.Sutcliffe, A. v. Theil, H. Toogood, A. W. Mohsen, J. P. Combe, J. Basran, S. E. Rigby, *Biochemical Society Transaction* **2005**, *33*, 754-757.

[3] aI. G. Denisov, T. M. Makris, S. G. Sligar, I. Schlichting, *Chemical Reviews* **2005**, *105*, 2253-2277; bB. Meunier, S. P. d. Visser, S. Shaik, *Chemical Reviews* **2004**, *104*, 3947-3980.

[4] R. P. Hanzlik, M. A. Cerny, *Journal of the American Chemical Society* **2/15/06 web**.

[5] R. B. Silverman, *Accounts of Chemical Research* **1995**, *28*, 335-342.

[6] aG. W. Dombrowski, J. P. Dinnocenzo, *Journal of Organic Chemistry* **2004**, *70*, 3791-3800; bV. D. Parker, M. Tilset, *Journal of the American Chemical Society* **1991**, *113*, 8778-8781; cX. Zhang, S.-R. Yeh, S. Hong, M. Freccero, A. Albini, D. E. Falvey, P. S. Mariano, *Journal of the American Chemical Society* **1994**, *116*, 4211-4220.

[7] aP. F. A. Buijsen, N. P. Hacker, *Tetrahedron Letters* **1993**, *34*, 1557-1560; bY. Ito, *Tetraheron* **2007**, *63*, 3108-3114.

[8] aO. Markovitch, N. Agmon *Journal of Physical Chemistry A* **2007**, *111*, 2253-2256. bT. M. Alligrant, J. C. Hackett, J. C. Alvarez, *Electrochimica Acta* **2010**, *55*, 6507-6516.

[9] H. Sun, W. Chen, A. E. Kaifer, *Organometallics* **2006**, *25*, 1828-1830.

[10] D. Britz, *Digital Simulations in Electrochemistry, Vol. 23*, 1st ed., Springer, Heidelberg New York, **2005**.

[11] B. Abel, J. Assmann, M. Buback, C. Grimm, M. Kling, S. Schmatz, J. Schroder, T. Witte, *Journal of Physical Chemistry A* **2003**, *107*, 9499-9510.

[12] B. S. Jensen, V. D. Parker, *Electrochimica Acta* **1973**, *18*, 665-670.

[13] aS. Farid, I. R. Gould, R. H. Young, R. E. Moody, *Journal of Physical Chemistry* **1991**, *95*, 2068-2080; bT. Guarr, *Journal of the American Chemical Society* **1983**, *105*, 3763-3767; cJ. W. Verhoeven, T. J. d. Boer, F. M. Martens, *Tetrahedron Letters* **1979**, *31*, 2919-2920.

Contributions:

The following chapter comprises original work toward the Ph.D. of Amber Hancock. Acknowledgement and thanks to the others who contributed toward the synthesis and kinetic characterization presented is given here. Professor Carl Schiesser and Professor Jim Tanko contributed significantly to the intellectual merit of this work as well as the conceptual and experimental education of the student performing the work. Dr. Sofie Lobachevsky performed integral synthetic methodology development as well as contributed to the experimental design of kinetic studies.

ABSTRACT

The design and synthesis of selenium containing heterocycles has received considerable attention resultant from their utility as antioxidants, anti-virals, anti-inflammatories, and immunomodulators. To establish the synthetic utility of homolytic substitution at selenium, for preparation of selenium containing heterocycles, kinetic analysis has been performed determining both rate constants and Arrhenius parameters. A series of photochemically labile Barton and Kim esters have been employed as radical precursors and the effect of leaving radical stability on kinetics have been investigated. Notable leaving group effects on measured kinetic parameters have been observed; more facile cyclization occurs with radicals which cyclize to form stable leaving radicals. Formation of 5-membered rings, for all leaving radicals studied, exhibited rate constants an order of magnitude greater than their 6-membered counterparts. This work constitutes the first report of a comprehensive leaving group study on kinetics of intramolecular homolytic substitution of at a higher order

chalcogenides and is the first example of a tertiary substituted selenides synthesized in the Schiesser group. On a whole, our results suggest that intramolecular homolytic substitution at selenium is a convenient means of synthesizing selenocycles under mild conditions.

3.1 Introduction

The element selenium, discovered in 1818, was long held to be extremely toxic due to the adverse health effects in those exposed to excessive quantities of the element.[1] While the first organoselenide, diethylselenide, was first synthesized and isolated in 1836, investigation of selenides was unpopular due to their toxicity, instability and challenging purification.[1b, 2] Further antagonizing progress in selenium chemistry was the notoriously intense and persistent fetid odors encountered with even the most miniscule concentrations of selenides. [1b]

In 1957, the first indication of selenium as an essential nutrient was noted when Foltz and coworkers showed that selenium prevented liver necrosis in rats, mice and chicks.[3] Two more decades passed before it was realized that selenium was essential to bacterial enzyme function in both glycine reductase and formate dehydrogenase.[4] The key finding that popularized the study of organoselenides was the 1973 discovery of its incorporation into the active site of the mammalian enzyme glutathione peroxidase (GPx).[5],[6] Compounding these breakthroughs was Sharpless' concurrent finding that reduced phenylselenide could efficiently induce ring opening in epoxides to give alcohols in high yields.[7] Consequently, selenides quickly became attractive target molecules in both synthesis and biology.

3.1.1 Biology of Selenocycles

Today we know selenium is not only an essential trace nutrient but that it is incorporated into the 21st amino acid, selenocysteine. At least 25 selenoproteins exist in humans, including important antioxidant enzymes that integrate selenocysteine into their active sites because of its enhanced reducing power (relative to cysteine).[8] Arguably, the most well-known antioxidant selenoenzyme is GPx. Glutathione peroxidases protect mammalian cells from peroxide induced oxidative damage by reducing peroxides to water or alcohols as shown in the catalytic cycle below in **Scheme 3.1**.

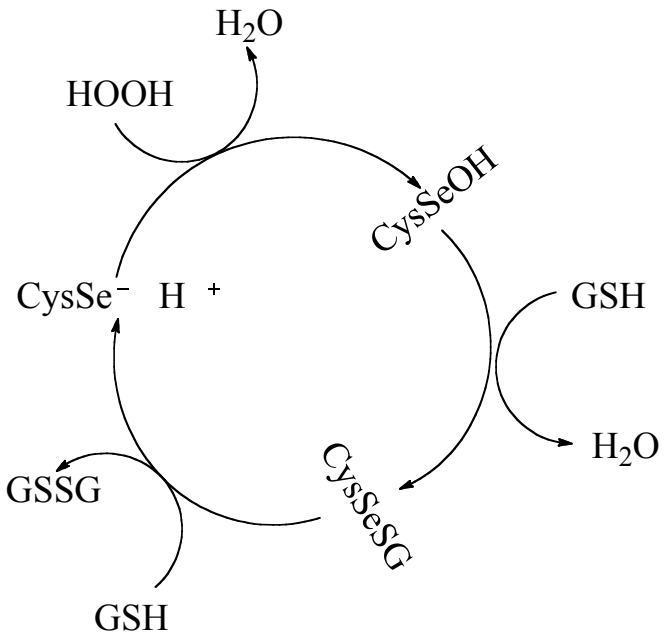

Scheme 3.1. Glutathione Peroxidase Catalytic Cycle. The reduced form of the enzyme reduces peroxide to give a molecule of H_2O and a selenol in the enzyme active site. The active site is partially reduced reacting with a first glutathione to give a second H_2O molecule and a selenosulfide in the active site. Reaction with a second glutathione molecule regenerates the fully reduced active site Se and yields dimeric glutathione.

In mutagenic studies of glutathione peroxidase replacing the selenium with sulfur shows a marked decrease in enzymatic activity.[8] Analogous results have been observed with other selenoproteins and selenoprotein mimics. Glutathione peroxidase is unique from other selenoenzymes in that it is a tetrameric protein with four identical subunits. While most selenoenzymes readily dimerize; glutathione peroxidase does not because the selenium is buried in the active site of each monomeric subunit where it is inaccessible to adjacent protein subunits.[9] This novel feature has led to interest in design of selenide mimics that utilize steric hindrance in preventing dimerization. Selenides of this type are expected to be significantly more stable than others and therefore present viable candidates for synthetic and pharmaceutical applications.

Synthetic organoselenium compounds have a variety of biological functions, in addition to the aforementioned antioxidant function, showing promise as anti-inflammatories, anti-virals, anti-bacterials, anti-fungals, enzymatic inhibitors, cytokine inducers, immunomodulators and antihypertensives.[10] The intrinsic antioxidant properties of many selenides enhances their pharmaceutical appeal as these molecules have the potential to serve as both antioxidants and function as therapeutics for an auxiliary purpose.

One class of these dual acting selenium-based drugs are selenosartans. Sartans (selective angiotensin one receptor antagonists) are inhibitors to the Angiotensin II receptors and are a well-tolerated class of antihypertensive drugs. The interaction of Angiotensin II with type 1 receptors triggers an array of physiological responses that ultimately lead to increased blood pressure.[11] Like selenosartans, many selenocycles are synthesized to mimic a sulfur-containing compound predicated on the idea that

incorporation of selenium will lead to a more effective reductant (**Figure 3.1**).

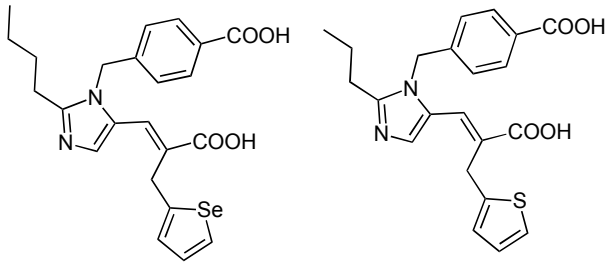

Figure 3.1. Selenoeprosartan and it sulfur containing parent compound eprosartan.

Schiesser, *et.* al has synthesized three selenofonsartans, one selenomilfonsartan and two selenoeprosartans (**Figure 3.2)**.[11-12] Selenofonsartans have been shown to antagonize Angiotensin II in hamster ovary cells; both selenofonsartans in **Figure 3.2** are effective inhibitors at nM concentrations.[12]

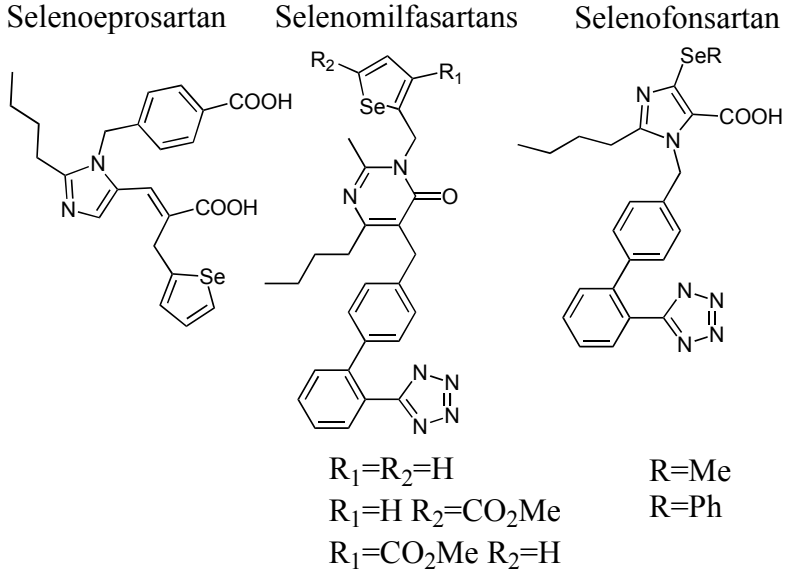

Figure 3.2. Antihypertensive selenocycles

Furthermore, predicted pK_Bs for selenium containing milfonsartans are slightly higher than those predicted for the sulfur containing analog implying that these compounds are likely to be more effective at suppressing the renin-angiotensin cascade than the

equivalent sulfides.[11]

Selenocycle anti-tumor agents are still in their infancy, having not yet entered clinical evaluation although several 5-membered selenocyclic compounds show promise in cell and animal models.[13] Anti-tumor activity of selenocycles (**Figure 3.3)** is currently believed to result from disruption of mitosis wherein these compounds disrupt the ability of the cells to divide properly by some mechanism which impacts the microtubules of the dividing cell.[14] In *vitro* studies of **1** decreases proliferation of mouse lymphocyte leukemia cells (L1210 cell line).[15] Moreover, in *vivo* studies of **2** and **3** in the P388 mouse leukemia model significantly down regulated tumor growth with no toxicity effects at therapeutic concentrations.[14, 16]

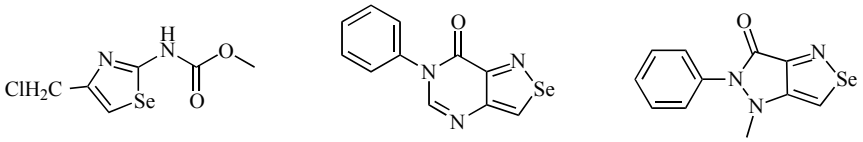

1 **2** **3**

Figure 3.3. Selenocycles exhibiting anti-tumor activity.

The antiviral properties of selenocycles often result from these compounds being guanine biosynthesis inhibitors. Unfortunately, some of these compounds have proven to be extremely toxic at therapeutic doses impeding their use. However, **4-8** (**Figure 3.4)** exhibit promising in *vitro* results toward the HIV virus.[17]

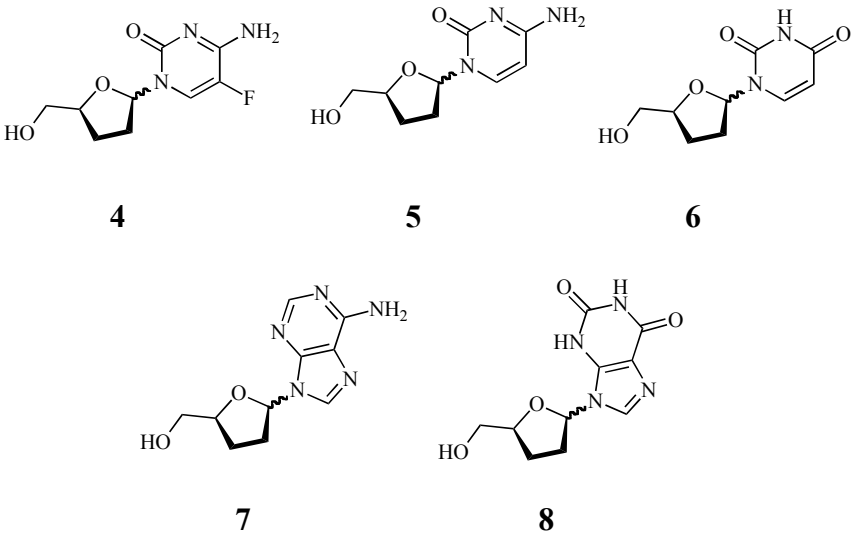

Figure 3.4. Anti-viral selenides active against HIV without toxicity at therapeutic dosages.

In fact, selenium based anti-virals targeted toward type 1 herpes simplex, encephalomyocarditis and type 3 influenza, among many other viruses, present themselves as promising candidates for therapeutics in low concentrations and exhibit minimal toxicity. What is more, anti-infective agents have been reported to inhibit growth of bacteria and fungi.

Ebselen (**Figure 3.5)** and its derivatives are some of the most well studied and motivating selenocycles. Ebselen is a GPx mimic that has been through phase III clinical trials which protects against lipid peroxidation by scavenging peroxynitrite.[18] Ebselen's primary mode of oxidative protection results from peroxide reduction via a catalytic mechanism analogous to GPx. [19]

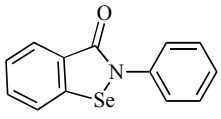

Figure 3.5. Ebselen a potent GPx mimic.

Inflammation causing cyclooxygenases and lipoxygenases rely upon hydroperoxides for their activity; thus, Ebselen acts as an anti-inflammatory by down regulating their activity through decreasing cellular quantities of these peroxides. Importantly, the low toxicity that makes Ebselen so attractive as a therapeutic is postulated to be a result of it being stored in a selenylsulfide form because it is primarily protein bound in cells.[20] It is effective at low concentration and may be applicable for other purposes; for example, Ebselen shows antibacterial properties against *Staphylococcus aureus* by reacting with thiols in in *vitro* studies. [17b, 21] Although Ebselen is not water-soluble pursuit of water-soluble analogs could potentially increase the value and number of Ebselenlike compounds. Because of its potential therapeutic value the synthesis of Ebselen and its derivatives, some of which also possess analogous or improved pharmacological activities are of immense interest. Unfortunately, Ebselen's difficult synthesis has been a mitigating factor in its utility as a therapeutic. Some of the more promising routes to Ebselen have involved intramolecular homolytic substitution and a reaction where selenium is inserted at the ortho position of benzanilide and undergoes an oxidative cyclization.[19, 22]

3.1.2 Methods for Synthesis of Selenocycles

As evidenced above, many biologically relevant compounds contain heterocycles, particularly selenocycles. Accordingly, finding an efficient means to synthesize them under mild conditions and at low cost is critical for the development of new pharmaceuticals. Knowledge of cyclization kinetic trends is key to the development of reactions of synthetic value. Several ionic routes to heterocycles have been developed.[17b, 22b, 23] In spite of this radical routes to cyclization are increasingly popular

because they afford regio and stereoselective products under mild conditions.[24] Stereoselective synthesis is often desirable because enantiomers of many drugs will interact with the body differently. Moreover, radical methods afford these products in high yields and exhibit impressive functional group tolerance.

Intramolecular homoloytic addition is a useful way to form cyclized compounds. Cyclization onto a carbon on the preferred end of a double bond (*see* ***Chapter 1.3.1****)* typically occurs where a radical initiator generates a sterically hindered organotin radical. This radical then abstracts an atom from the radical precursor.[25] The radical formed from this process can then cyclized onto itself. Unfortunately, tin is highly toxic and is notoriously difficult to separate. If the kinetics of cyclization are not rapid enough, side reactions will occur and some percentage of the radical will be further reduced by tin-hydrides decreasing reaction efficiency toward the desired product. These hurdles can be overcome with the useful reagent tris(trimethylsily)silane as it is less reactive toward carbon centered radicals and do not require involving toxic stannanes.[26]

Another method of radical generation, and the one used in this work, is the use of thiohydroximate esters. These radical precursors are attractive from a synthetic perspective because they can be used to form a variety of radicals under mild conditions by exploiting the weak N-O bond, which readily undergoes homolytic scission by both thermolysis and photolysis. The corresponding acetoxyl radical then undergoes rapid decarboxylation yielding the synthetically useful radical **(Scheme 3.2)**.

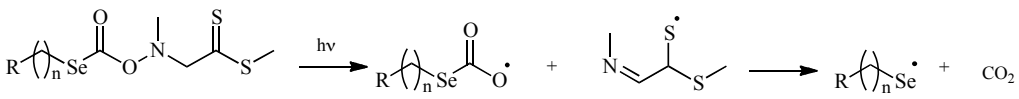

Scheme 3.2. Generation of selenoradical can be achieved by photolysis of a thiohydroximate ester.

Since the Barton method was devised over 25 years ago,[27] Barton esters and their Kim ester analogs have proven to be to be useful precursors for generating N, O, P, Si, B, S and Se radicals, creating significant interesting in exploiting this method for a host of applications ranging from precursors for indirect kinetic studies to acting as grafting agents in polymerization reactions.[28] In synthesis, these radicals are often either judiciously trapped or undergo intramolecular cyclizations to give interesting heteroatom-containing compounds. Barton ester reactions yield the desired product as well as pyridine-2-thiyl radicals, which conveniently undergo self-trapping reactions (**Scheme 3.3**). Pyridine-2-thiyl radicals are also resonance stabilized, thus providing little threat of interference with the reaction of interest.

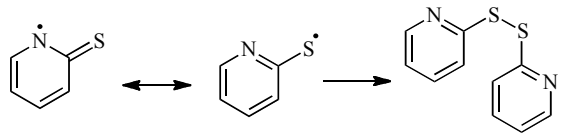

Scheme 3.3. Self deactivation of pyridine-2-thiyl radical

A similar approach to generation of nitrogen radicals can also be applied by substituting a different thiohydroximate group that undergoes less facile self-deactivation. Kim and coworkers developed their own class of thiohydroximate esters that are not afforded the same stabilization by self-trapping.[29] These compounds are more versatile for synthetic applications, as self deactivation of the nitrogen radical yielded upon decomposition of the ester is significantly retarded relative to their pyridine-2-thione containing cousins. This structural difference affords additional practical advantage, as Kim esters are less labile making them easier to purify and handle in laboratory experiments. The Barton method in general provides particular

advantage relative to hydride methods; affording heterocycles under mild conditions without the undesired generation of toxic and difficult to purify byproducts.

Use of the Barton method over the past two decades has adumbrated the scope of application of intramolecular homolytic substitution for formation of heterocycles, particularly those containing chalcogens. Homolytic substitution reactions at acyl radicals may become as prevalent and synthetically useful as nucleophillic substitution, but their use in synthetic methodologies are currently limited by the paucity of fundamental kinetic and thermodynamic data in the chemical literature. The Schiesser group has presented several elegant examples of the use of intramolecular homolytic substitution at selenium, but the properties of precursors that affect reaction efficiency is still not fully understood. The purpose of this work is to investigate some of the factors likely to influence efficiency these reactions.

Homolytic substitution has commonality to nucleophillic substitution as both processes involve the same orbitals. However, it is postulated that the radical process is solvent insensitive, as with most neutral radical reactions, because the transition state is not charged.[30] Homolytic substitution reactions typically proceed through one of two mechanisms, depending on the nature of the reacting species(s). A concerted process involving simultaneous, instantaneous bond cleavage and formation or a stepwise reaction proceeding through a hypervalent intermediate **(Scheme 3.4)** .[30]

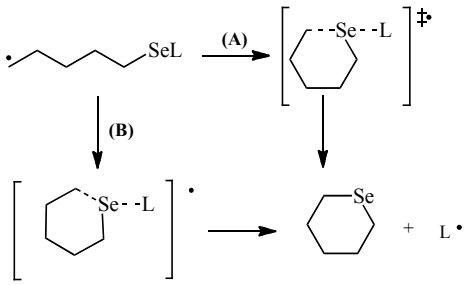

Scheme 3.4. Intramolecular homolytic substitution can proceed through a stepwise pathway (B) involving a hypervalent intermediate or a concerted pathway (A) involving a transition state where the leaving and attacking radical are collinear.

Reported success utilizing homolytic substitution reactions for substitution at carbon is limited to- at best- moderately yielding reactions for a small number of product types.[30-31] Aside from the halogen atom substitution induced ring opening of cyclopropanes and a very few other confirmed cases of homolytic substitution at strained carbons in ring systems; oxygen is the only other first period element reported to undergo favorable homolytic substitution. [31] These reactions of oxygen are specific to peroxides whose weak, non-polarized bonds make substitution possible.[31] The limited applicability to period one atoms is attributed to these elements forming strong, polarizable bonds, which favor heterolytic cleavage. [30]

Harnessing these reactions for synthesis requires attention to stereochemical outcomes of these processes. The familiar idea of S_N2 reactions occurring via backside attack, forming substitution products with inversion of configuration also extends to the homolytic process. Homolytic substitution at sp^3 hybridized atoms are reported to occur through a transition state with a trigonal pyramidal geometry suggesting a similar stereochemical outcome can be expected.[30] In most cases of homolytic substitution at heteroatoms a concerted process is favored. For the process to be stepwise, the

transition state will either deviate from the energetically favored collinear arrangement of the attacking and leaving radical, or the atom undergoing substitution must be stabilized by electron donating substitutent (or itself possess intrinsic internal stabilization). The latter case is exemplified by the preference for tellurium substitutions to proceed through hypervalent intermediates, unlike sulfur and selenium which prefer concerted substitution.[8] This can be rationalized on the basis of stabilization imparted to row five tellurium by low-lying d orbitals.[32]

One might expect that selenium behaves similarly in homolytic substitution to its more studied relative sulfur, and in cases where available data facilitates comparison this is generally true. Because it is not appropriate nor wise to develop synthetic methodologies based merely on assumptions of similarity, we undertook an analysis to provide a more quantitative argument to explain intramolecular homolytic substitution at selenium by determining activation parameters and rate constants relevant to these cyclizations. The chain length of the cyclizing radical and leaving group stability were varied. Additionally, the experimental design was intended to provide a preliminary foray into the role (if any) of solvent in these reactions. The work presented herein permits a more detailed and complete comparison of the substitution trends at the two heteroatoms than is currently available in the literature; which is integral to establishing a basis for demarcating the suitability of these reactions for synthesis of commercially valuable selenocycles.

3.2 Results

3.2.1 Experimental Rationale and Complications

Rate constants and activation parameters were determined via competition kinetics (***see 4.1.3***). The radical was partitioned between two competing pathways; hydrogen atom transfer (at a known rate constant from the radical trap) and intramolecular homolytic substitution.

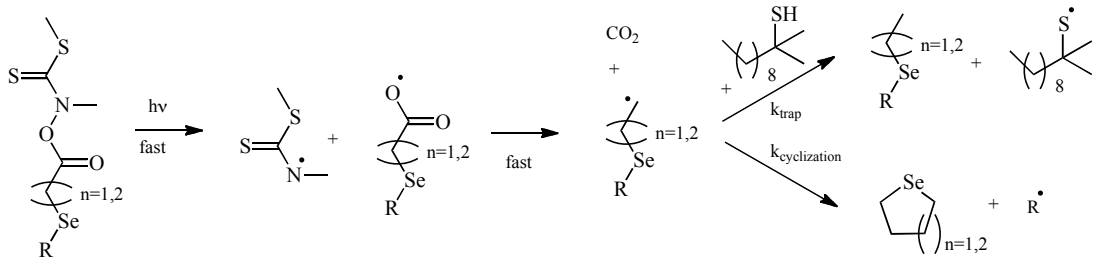

Scheme 3.5. Competition between two competing pathways was used to determine the rate constant for formation of the cyclized product by employing a hydrogen atom donor that reacts with a carbon centered radical at a known rate. Kinetics were characterized by monitoring the ratio of product concentrations.

Utilizing the photolability of Barton esters, radicals were generated for study by irradiating with a 250 W broad-spectrum medium pressure Hg lamp. Reactions were temperature controlled, and relative activation parameters were determined using a series of temperatures between 0 and 85 ^{o}C. The trapping agents utilized were *t*-dodecanethiol and tributyltin hydride.[i] In order to facilitate the use of *t*-dodecanethiol as a trap, the critical assumption that the rate constant for hydrogen abstraction for a primary carbon centered radical from *t*-dodecanethiol was not appreciably different from the rate constant for hydrogen abstraction from the structurally similar and well-studied trap, *t*-butylthiol, had to be made. This assumption was confirmed via comparison of

the reaction for the octylselenobutane radical with tributyltin hydride, whose rate constant for trapping via hydrogen transfer to a primary alkyl radical is reported.[33] Measured $k_{cyclization}$ are reported in **Table 3.1** and are in good agreement for experiments utilizing both tributyltin hydride and *t*-dodecane thiol.

Table 3.1. Cyclization rate constants for formation of selenobutane with an octyl leaving radical with different traps are in good agreement.

Radical Trap	***k*** **(1/s)**
t-dodecanethiol[32]	5.58 (+.29) x 10^4
t-dodecanethiol	6.23 (+.19) x 10^4
Bu_3SnH	5.31 ($\pm$.16) x 10^4

The *t*-butylthiol and tributyltin hydride traps have been used extensively for kinetic studies involving 5-hexenyl radical type cyclizations by similar competition means. In these studies it was shown that the rate constant for hydrogen abstraction from these traps were not subject to appreciable solvent effects.[34] Likewise, it was anticipated that no notable solvent effect on the kinetics of the competing cyclization pathway would be observed because the cyclizing radical is neutral. However, to more thoroughly investigate this aspect, the reaction was studied in both polar (CH_3CN) and non-polar (benzene) solvents. At 21 ^oC the rate constants reported for hydrogen transfer to a primary carbon-centered radical from t-butyl thiol and tributyltin hydride are 7.6 x 10^6 1/Ms and 1.4 X10^6 1/Ms. In the case of less facile competing cyclization reactions tributyltin was used as a radical trap. As discussed in Chapter 4, in competition kinetics experiments it is undesirable to have a large difference in the rate constant for the trapping and experimental process. As demonstrated in **Figures 3.6-3.8,** consideration

[i] *It should be pointed out that the use of tributyltin hydride as a radical trap does not affect the toxicity of product formed if these reactions are used for synthesis because these competition experiments are meant to be a means of determining reaction efficiency. Tributyltin hydride would not be used when these reactions were applied to practical syntheses.*

of the rate constant for the experimental process was especially necessary for reactions involving formation of 6-membered rings.

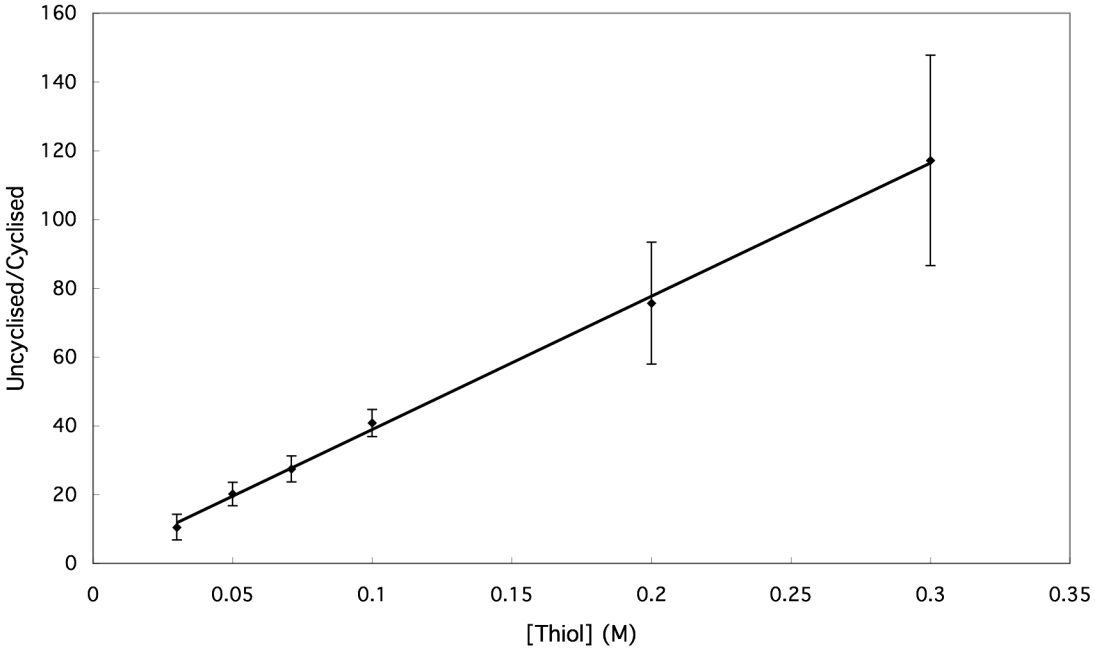

Figure 3.6. Ratio of concentrations of products for competition experiments involving formation of tetrahydro-*2H*-selenopyran and elimination of a sec-octyl leaving radical. Tributyltin hydride was necessary to calibrate significantly slower cyclization. Notably data collected at higher trap concentrations exhibited significantly larger error bars than low concentrations a consequence of the increased propensity for formation of the trapped product.

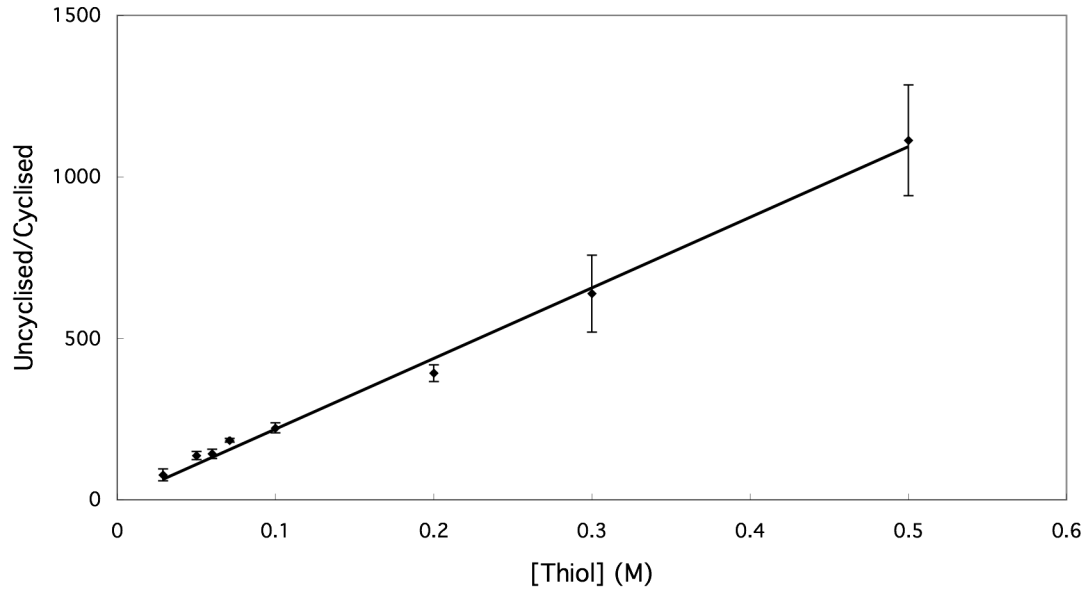

Figure 3.7. The significantly slower cyclization of tetrahydro-2H-selenopyran and release of the primary octyl radical even with the slower (tributyltin hydride trap) is almost too slow to be studied . What is more, the range on concentrations able to be studied with precision is severely limited.

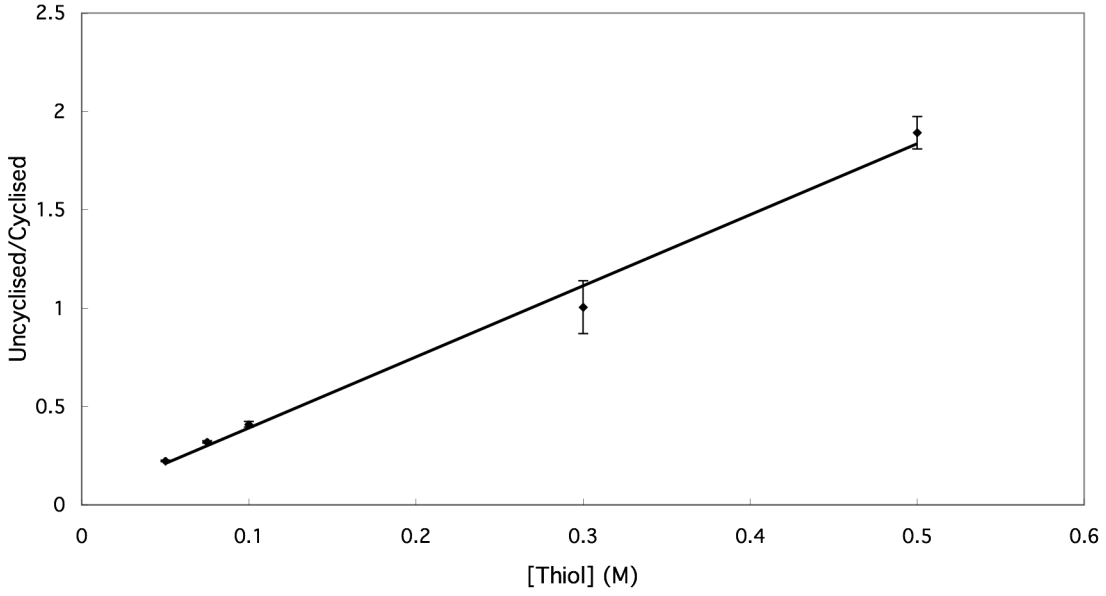

Figure 3.8. Tert-dodecanethiol was used when cyclizing to form tetrahydroselenophene and release of the tert-butyl leaving radical as this was a significantly faster reaction. The faster trap was appropriate as illustrated by the nearly equal ratio of cyclized to uncyclized product.

The use of a silyl traps such as those shown in **Table 3.2** may have increased the ease with which the experiments were performed for the slower cyclizing selenopentanes**.**

Table 3.2. Rate constants for hydrogen abstraction from each radical trap by a primary carbon centered radical.[33]

Radical Trap	k_{21oC} (1/Ms)
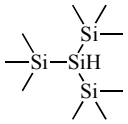	3.8×10^5
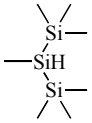	3.2×10^4
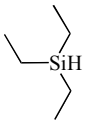	7.0×10^2

Utilizing the traps that were available meant a) trap concentrations had to be sufficiently low to afford a notable quantity of the cyclized product. Because it is desirable to span an entire order of magnitude in trap concentration (to confirm there is not a change in mechanism at high concentrations), it was necessary to replicate high concentration experiments a large number of times. Even still, the magnitude of error associated with using high concentrations of radical traps was enormous compared to their low concentration equivalent experiments.

Kim ester radical precursors were used for all radicals studied by indirect means (this includes all radicals studied with alkyl leaving groups). Kim esters were chosen due to their enhanced stability under laboratory conditions. Moreover, indirect studies were preferred because these methods provided not only rate constants and activation parameters, but also afforded confirmation of product identity, in a single experiment, by

comparison of post reaction mixtures to authentic products. The benzyl-substituted compound was studied by laser flash photolysis because it contained an appropriate chromaphore for detection and reacted on the laser flash time regime. It was not studied through indirect means as previous attempts, in the Schiesser group, were met with complications. In these experiments, significant quantities of a number of byproducts were observed; some products were able to be identified and others were not.[32] To circumvent these complicating factor direct kinetic measurements by laser flash photolysis using pyridine-2-thione containing esters were performed. Monitoring the formation of the benzyl radical at 310 nm was employed to determine kinetic parameters. The laser flash studies were subject to bleaching effects due to competing absorption of the reactant and the product leaving radical. Wild and Schiesser had attempted to study this same system some years earlier and were met with the same issues and abandoned these experiments. While competing absorption may have affected the exact precision of these measurements, results were satisfactorily obtained. In fact, reported theoretical results for intramolecular homolytic substitution of benzylselenobutane are in good agreement with the experimental results reported here, in spite of the bleaching effect observed. Rate constants of 1.6×10^7 1/s and $1.51(\pm.29) \times 10^7$ 1/s were reported and determined (from theoretical methods and experimental methods), respectively.[35] By performing kinetic measurements at several temperatures reasonably accurate values for the reaction barrier can be determined. A good fit of rate constants to the Arrhenius equation **(Figure 3.9)** was observed.

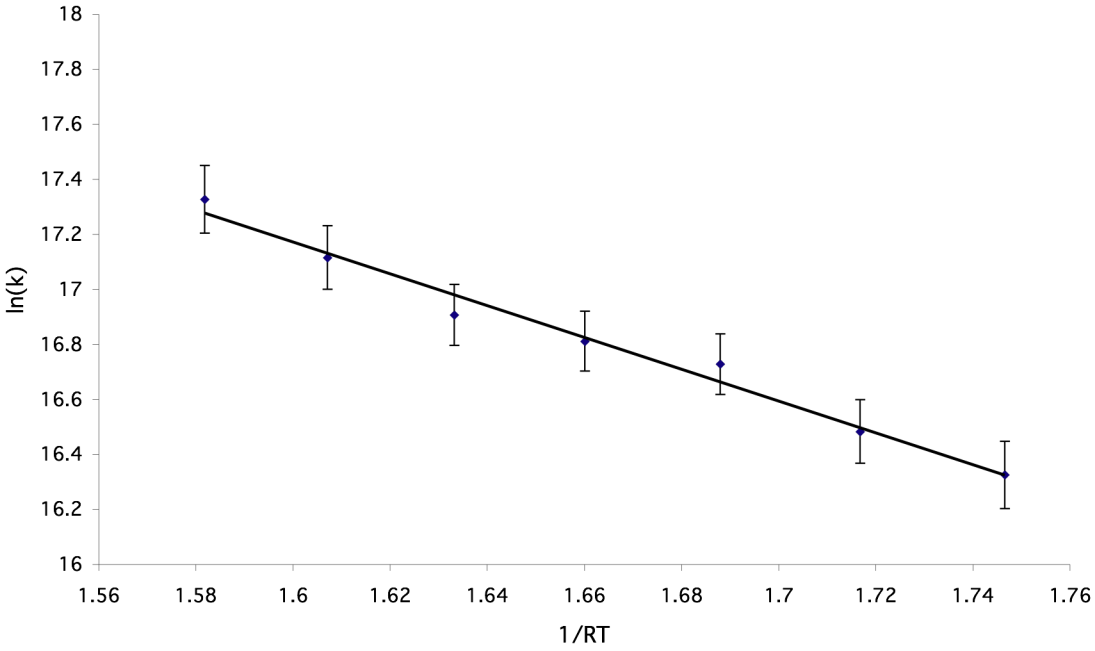

Figure 3.9. Arrhenius analysis for benzylselenobutyl radical.

A log(A) of 11.8 was determined in this study for the cyclization of benzylselenobutane. This value supports the assumption of an erroneous pre-exponential factor; typical values for substitution at primary carbon fall between 9 and 10. If error due to bleaching was observed in rate constant data, this error would manifest itself in an offset in the intercept of the Arrhenius plot (log(A)). Consequently, no strong conclusion regarding the validity of the measured value of log(A) for the benzylselenobutane radical can be put forth on the basis of this comparison.

Radical precursors were synthesized according to **Scheme 3.6**.

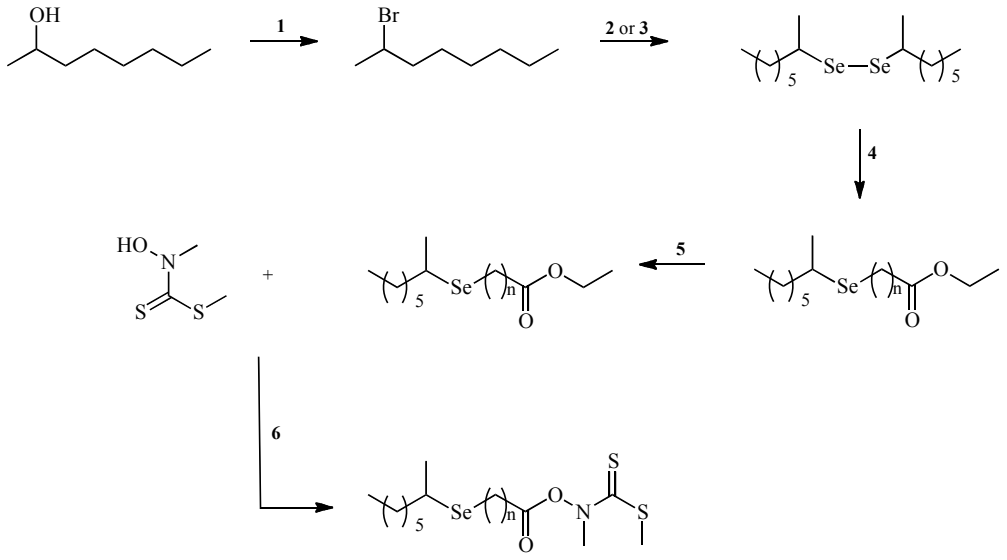

1: PBr_3, Et_2O, 0 °C, 24 hr. **2:** $NaBH_4$, EtOH, reflux **3:** Mg, Et_2O, Se **4:** $NaBH_4$, $Br(CH_2)nCOOEt$, EtOH
5: NaOH, EtOH, reflux/CH_3NOH_2, CS_2, CH_3I, Et_3N, CH_2Cl_2, 0 °C **6:** DCC/DMAP, CH_2Cl_2

Scheme 3.6. Synthesis of Kim and Barton Ester radical precursors

These methodologies are commonly used in the Schiesser lab and thus are not the focus of this report. The desired selenides were afforded in moderate to excellent yields and were used with or without purification (as needed) in subsequent steps toward formation of the final radical precursors. Care was taken to purify all Kim ester radical precursors utilized in this work, although it should be noted that for given studies this was not necessary for accurate determination of rate constants as the Kim ester is used in extremely low concentrations and the concentration of contaminates would presumably be negligible. Moreover, the types of molecules that precede the synthesis of the radical precursors do not participate in competing reactions as shown in previous work in the Schiesser group. As no other report from the Schiesser group of intramolecular homolytic substitution at a tertiary leaving radical from a selenide exists because S_N2 reaction at a tertiary center is disfavored, the literature methodology shown in (**Scheme 3.6 (Step 3))** was used. This method was met with success and

yielded moderate quantities of the ditertbutyldiselenide that could then be used as conveniently as any of the other diselenides in subsequent steps of the synthesis.

3.2.2 Ring Size

It is well established for radical cyclizations that 5-membered rings are the preferred ring size (***see 1.3.1***). Longer chains sample too many conformations on their path to cyclized products due to the high number of rotational degrees of freedom (that increasing with increasing chain length) notably slowing cyclization. Slower cyclization for smaller rings is well precedented, and results from increases in ring strain for 4-member and smaller rings. In intramolecular homolytic substitution at selenopentane the *endo* product is postulated to form exclusively because a) homolytic substitution onto carbon is not favorable and in this case it has no lone pairs available to form bonds with the radical center, b) selenium is an electron rich element and an excellent candidate for homolytic substitution and c) the carbon α to selenium does not have the thermodynamic driving force of stability imparted by displacement of a good leaving radical. Notably, Zhen confirmed the supposition of a preference for endo cyclization in analogous 6-membered selenocycles. SmI_2 mediated intramolecular homolytic substitution reactions at selenium to form selenosugars exclusively gave the 6-membered ring product.[36]

Reported kinetic parameters for sulfur cyclizations trend in agreement with trends observed in this work; Beckwith and Duggan demonstrate that the 5-membered ring will form at least one order of magnitude faster than the 6-membered analog.[37] Wild and Schiesser previously performed intramolecular homolytic substitution onto selenium with a diphenylmethyl leaving radical affording results cogent with those described here. This is the only other known example of an experimental study demonstrating ring size

effects for intramolecular homolytic substitution at selenium and these results are shown, in comparison to the ring size effects observed in the current work, in **Table 3.3**.

Table 3.3. Ring size effects for cyclizations forming selenobutanes in benzene.[1]

Ring Size Effects (Carbon Chain Length)		K (1/s)
Octyl	(4)	$5.31(\pm.16) \times 10^4$
	(5)	$1.10(\pm.03) \times 10^3$
Sec-Octyl	(4) [35]	$2.96(\pm.04) \times 10^5$
	(5)	$3.61(\pm.006) \times 10^3$
Diphenylmethyl	(4) [38]	1.0×10^7
	(5) [38]	1.8×10^6

Activation parameters were also determined and are shown in **Table 3.4.** A 7 to 10 kJ/mol increase in activation energy results from cyclization to form a 6-memebered selenocycle relative to a 5-membered selenocycle. Log(A) values for both ring sizes with primary leaving radicals are the same within the limits of experimental error.

Table 3.4. Ring size effects for cyclizations forming tetrahydroselenophene(4) and tetrahydro-*2H*-selenopyran in benzene.

Ring Size Effects (Carbon Chain Length)		Ea (kJ/mol)	Log(A)
Octyl	(4)[32]	27.9(±4.0)	9.5 (±.6)
	(5)	34.9(±1.5)	9.2 (±.2)
Sec-Octyl	(4) [32]	22.1(±3.2)	9.3 (±.6)
	(5)	34.8(±2.9)	9.8 (±.7)

In light of what is known about radical cyclization, it is unsurprising that a preference was observed for formation of 5-membered rings. Because no other heteroatoms were incorporated into the chain, nor were any of the chain carbons substituted, no conclusions regarding how these factors might affect cyclization can be drawn. It may be interesting to investigate these factors as regioselectivity resultant

[1] Notably the six membered ring product was unable to be sufficient purified. Rate constants for the 5 carbon system use response ratios from the 4 carbon system assuming a negligible difference as both the cyclized and uncylized product would differ in a single additional combustible CH_2.

from steric restrictions and electronic changes to the substituted atoms have been demonstrated with intramolecular homolytic addition across double bonds in 5-hexenyl type radical cyclizations. What is more, geminal disubstitution has been reported to induce favorable bond compression allowing for formation of smaller rings in the case of 5-hexenyl radicals.

3.2.3 Leaving Radical Effects

The stability of the leaving radical displaced during intramolecular homolytic substitution has proven to be a mitigating factor in cyclizations onto selenium as demonstrated by the rate constant trends shown for intramolecular homolytic substitution at systematically substituted selenobutane radicals in **Table 3.5.**

Table 3.5. Leaving radical effects for cyclizations forming tetrahydroselenophene in Benzene.

Leaving Radical	$k_{21}{}^{\circ}_{C}$ (1/s)
Octyl	5.31 (±.16) x 10^4
Sec-Octyl	2.96(±.03) x 10^5
Tert-butyl	2.11(±.002) x 10^6
Benzoyl[35]	1.6 x 10^6
Diphenylmethyl[38]	1.0 x 10^7

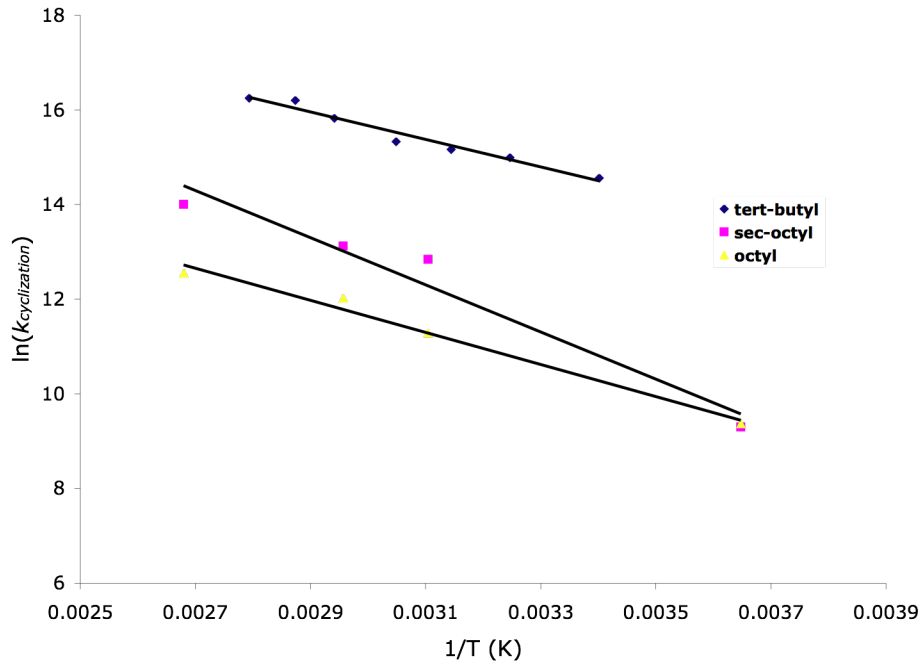

Figure 3.10. Arrhenius data for different leaving radicals and formation of tetrahydroselenophene. Octyl and sec-octyl data are from the work of a previous student.[32]

The trend in activation energy (**Figure 3.10**) is as expected; the activation energy increases as leaving radical stability decreases. Notably, the log(A) for the tertiary substituted compounds is 10.6 $\pm$ .7, which is larger than the value for primary and secondary radicals in the formation of both 5 and 6-membered rings, although within experimental error the values are the same. It is predicted by reported computational work that log(A) are all similar for all leaving radicals forming 5-membered rings.[35] Generally, results for the 5-membered rings parallel the trends **(Table 3.6)** observed for intramolecular homolytic substitution at sulfur.

Table 3.6. Leaving radical effects for intramolecular homolytic substitution to form cyclizations forming tetrahydrothiophene in Benzene.[39]

Leaving Radical	$k_{25}{}^{o}{}_{C}$ (1/s)	Ea (kJ/mol)
Propyl	1.8×10^{1}	12.16
Tert-butyl	2.7×10^{2}	11.36
Benzyl	3.9×10^{3}	8.63

Similarly, bimolecular homolytic substitution by stannyl radicals at selenium show order of magnitude increases in rate constants going from a primary to a tertiary leaving radical.[40]

In 6-membered ring systems, notable leaving radical effects, manifested as a three order of magnitude change in the rate constant, for intramolecular homolytic substitution at selenium was observed. These results for a primary leaving radical along with the reported rate constant for the highly stabilized diphenylmethyl radical are shown in **Table 3.7**.

Table 3.7. Leaving radical effects for cyclizations forming selenopentanes in benzene.

Leaving Radical	k (1/s)
Octyl	$1.10(\pm.03) \times 10^{3}$
Sec-Octyl	$3.61(\pm.006) \times 10^{3}$
Diphenylmethyl[38]	1.8×10^{6}

Arrhenius data for formation of tetrahydro-2*H*-selenopyran are displayed in **Figure 3.11.** Importantly the slopes (activation energies) for intramolecular homolytic substitution at selenium to form a 6-membered ring are not as sensitive to leaving group effects as their 5-membered counterparts. Leaving radical effects going from a primary radical to secondary radical result in measured activation energies of 34.8 $\pm$ 2.9 kJ/mol and 35.2

± 1.5 kJ/mol, illustrating that the activation energies for these two reactions are the same within experimental error (**Figure 3.11)**.

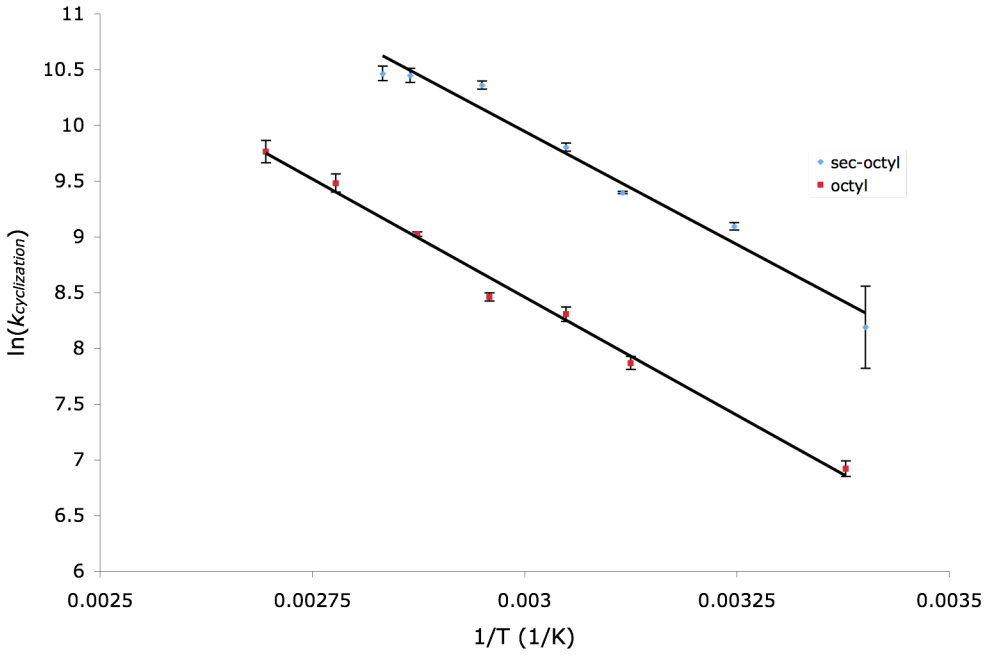

Figure 3.11. Arrhenius plots for formation of tetrahydro-*2H*-selenopyran in benzene for octyl and sec-octyl leaving radicals.

Figure 3.12 shows the relationship between radical stabilization energies and the activation energies for the cyclizations to form tetrahydroselenophene studied herein.

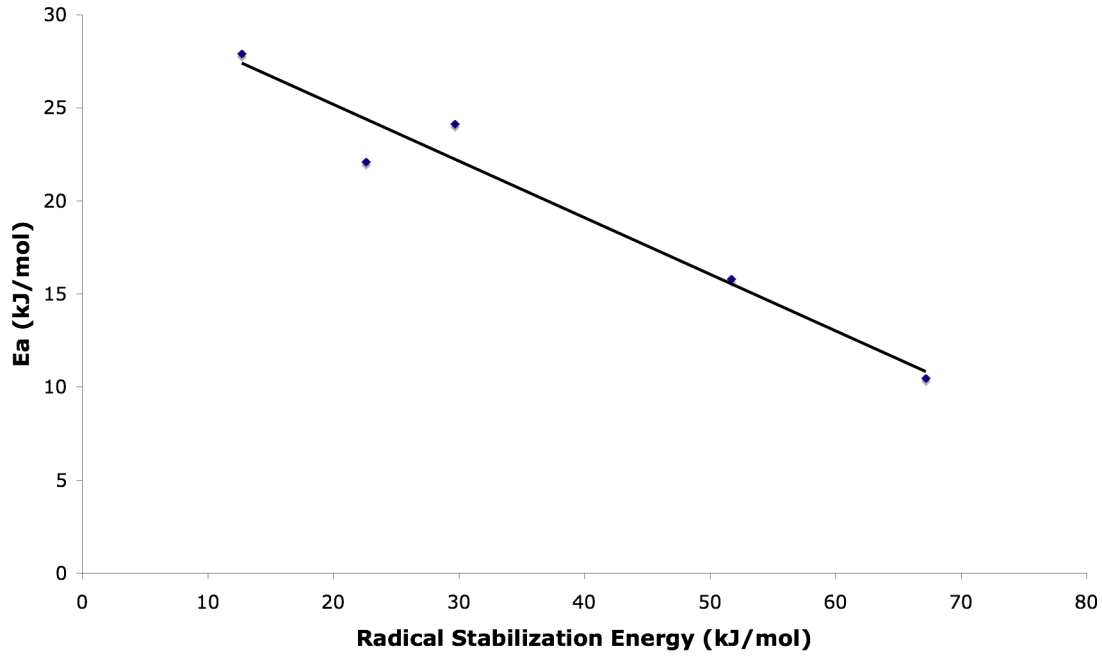

Figure 3.12. Activation barrier as a function of reported computed radical stabilization energies[35] shows a linear correlation

The radical stabilization energies for octyl and *sec*-octyl compounds were approximated to be similar to the radical stabilization energies for butyl and *sec*-butyl radicals because values for the octyl compounds were not available for the analysis. A slope of -.304 was observed for this plot suggesting that the transition state of this reaction is more reactant than product like. The data demonstrates that for intramolecular homolytic substitution, an activation driving force relationship exists and it is largely dependent on the nature of the leaving radical. An R^2 value of .95 was observed for the correlation of kinetic data to the thermodynamic stability of the leaving radicals used in this study. This clearly demonstrates that increased leaving radical stability lends an increased propensity to undergo cyclization because the reaction barrier also decreases; suggesting that it is one of the primary factors governing these reactions. It can be

gleaned from these results that thiohydroximate ester radical precursors containing highly stabilized leaving radicals are attractive for use in synthetic methodologies.

The more facile kinetics for stabilized leaving radicals suggests that the rate-determining step of the reaction involves cleavage of the bond between selenium and the leaving radical. A concerted mechanism for substitution at selenium is proposed by the theoretical work of Schiesser and Lobachevsky, which combined with these results, suggests that these reactions are likely to be primarily influenced by the stability of this leaving radical.[32, 35] Moreover, intramolecular homolytic substitution at sulfur has been reported to occur through a concerted pathway by both experimental and theoretical work.[28c, 41] To clearly determine if a sequential mechanism is possible for intramolecular homolytic substitution at selenium substitution of the attacking carbon with groups which may modulate the rate of attack on selenium may provide key insight into whether the nature of the attacking radical can be considered equally important in determining reaction barrier or if such substitutions might be significant enough to cause a change in mechanism.

3.2.4 Solvent Effects

Comparable leaving radical effects were observed in the study of substituted selenobutane cyclizations in acetonitrile as shown in **Table 3.8.** The magnitude of these effects is equivalent to those observed for the non-polar solvent, suggesting a similarly important role of the leaving radical in acetonitrile. This result suggests a similar mechanism in this solvent as the reaction is governed by analogous factors and to an equivalent degree.

Table 3.8 Leaving radical effects for cyclizations forming selenobutanes in Acetonitrile.

Leaving Radical	$k_{21}^{o}{}_{C}$ (1/s)
Octyl	$3.81(\pm.1) \times 10^{4}$
Sec-Octyl	$1.85(\pm.1) \times 10^{5}$
Benzyl	$1.51(\pm.29) \times 10^{7}$

Several practical considerations preclude the study of selenopentanes in acetonitrile. First, the retention time of tetrahydro-*2H*-selenopyran fell within the cluster of peaks associated with the t-dodecane thiol isomers. Second, the quantity of cyclized product formed was not enough, even at low trap concentrations, to allow resolution of the cycled product peak from the dominate trap peaks. It is suspected that a similar effect to that observed for selenobutane would be observed for selenopentanes. Because tributyltin hydride was insoluble in acetonitrile, this slower trap (which exhibits a G.C. peak at a different retention time from the product), could not be utilized. It is suspected that use of the slowly reacting silyl traps (*vide supra*) are candidates to facilitate study of the selenopentanes in acetonitrile (excluding any similar solubility issues or competing peaks in the chromatogram). While tris(timethylsilyl)silane is known to be insoluble in acetonitrile it is likely that the less bulky cousin triethylsilane is soluble.

Comparing the rate constants and activation energies for polar and non-polar solvents a slight retardation in rate constant is noted as shown in **Table 3.9.**

Table 3.9. Ring Size effects for cyclizations forming tetrahydroselenophene in Benzene.

Solvent Effect		Ea (kJ/mol)	$k_{21}{}^{o}{}_{C}$ (1/s)
Octyl	C_6H_6	27.9(±4.0)	5.31 (±.16) x 10^4
	CH_3CN	28.0(±3.0)	3.81 (±.10) x 10^4
Sec-Octyl	C_6H_6	22.1(±3.2)	2.96 (±.03) x 10^5
	CH_3CN	27.3(±4.3)	1.85 (±.10) x 10^5

It is odd that the rate is decreased in polar solvent as 1) this is a neutral radical reaction and thus a polar effect is not expected and 2) if there were polarization in the transition state the trend would be expected to be reversed as acetonitrile would impart stabilization and likely induce a more facile reaction. Caution should be taken to ascribe high significance to this solvent effect, as the activation energies in the two solvents are relatively close. We have shown that the cleavage of the bond to the leaving radical is extremely important in determining kinetics. If the reaction occurs by a stepwise mechanism, attack of the carbon-centered radical must occur first to form the hypervalent intermediate. If a polar solvent favors this reaction mechanism the rate limiting step would be homolytic scission of the bond from selenium to the leaving radical. The observed solvent effect indicates that acetonitrile either a) stabilizes the hypervalent intermediate favoring this pathway or b) interacts with the starting selenobutyl radical in such a way as to prevent a collinear orientation of the leaving and attacking radical, thus prohibiting reaction via the concerted pathway. As mentioned previously, to validate this result other leaving radicals must be employed. It would be desirable to study selenobutanes with substituents that would destabilize the starting radical so the effect of solvent stabilization on the starting material or a collinear arrangement during cyclization would be more or less favored.

3.3 Conclusions

Kim ester and Barton ester radical precursors have been successfully synthesized and utilized in kinetic studies via competition methods. These compounds have been previously reported to have a variety of applications and easily form useful radicals by irradiating the synthesized radical precursors with UV light. Selective substitution of these esters with primary, secondary, tertiary and highly stabilized benzyl groups demonstrates that in intramolecular substitution at selenium, the stability of the leaving radical has a significant effect on reaction kinetics. Changing from a primary to a tertiary leaving radical when forming selenopentanes results in a three order of magnitude increase in rate constant and a nearly two-fold decrease the reaction barrier. Likewise, significant effects have been reported for bimolecular homolytic substitution at phenylselenide by alkyl radicals. Furthermore, varying chain length for the cyclizing radical introduced significant kinetic effects, showing a preference for formation of a 5-membered ring. This result is quite reasonable considering the enhanced ring strain for smaller rings and the slower cyclization longer chain radicals. This is also in accord with the well-studied and previously reported preference for intramolecular radical addition for 5-hexeny type radicals. The regioselectivity of cyclization is again, in accordance with what would be predicted considering the electronic nature of selenium and its neighboring carbon. *Endo* cyclized products were also reported in studies of 6-membered selenosugars, further affirming the observed regiochemical preference. While these trends follow conventional logic regarding the reactivity of these reactions, quantifying the magnitude of these ring size and leaving group effects in terms of rate constant and activation parameter changes lends valuable insight for application of

intramolecular homolytic substitution at selenium to practical synthetic methods. The one unexpected result observed in this work is the possibility of a slight kinetic solvent effect on these reactions. Because these radicals are neutral it is surprising that there would be polarization in the transition state. Additional work is needed to confirm and explore the scope of this phenomenon.

On a whole our results agree with the reported theoretical data for intramolecular homolytic substitution at selenium, and experimental and theoretical results for related sulfur substitutions. Endo cyclization occurs with both ring sizes, a notable kinetic effect of ring size indicated preference for the 5-membered heterocycles and leaving radical stability are paramount in determining activation barrier and rate constant for reactions. To fully understand our unexpected results regards solvent polarity further analysis is required. Our current opinion is solvent effects of this magnitude are likely insignificant.

REFERENCES:

[1] aJ. J. Berzelius, *Afh. Fys. Kemi Mineralogi* **1818**, *6*, 42; bG. Mugesh, W.-W. d. Mont, H. Sies, *Chemical Reviews* **2001**, *101*, 2125-2179.
[2] C. J. Lowig, *Pogg. Ann.* **1836**, *37*, 552.
[3] K. Swatz, C. M. Foltz, *Journal of the American Chemical Society* **1957**, *79*, 3292-3293.
[4] aJ. R. Andreesen, L. G. Ljungdahl, *Journal of Bacteriology* **1973**, *116*, 867-873; bD. C. Turner, T. C. Stadtman, *Archives of Biochemistry and Biophysics,* **1973**, *154*, 366-381.
[5] L. Flohe, W. A. Günzler, H. H. Schock, *FEBS LETTERS* **1973**, *32*, 132-134.
[6] J. T. Rotruck, A. L. Pope, H. E. Ganther, A. B. Swanson, D. G. Hafeman, W. G. Hoekstra, *Science* **1973**, *179*, 588-590.
[7] K. B. Sharpless, R. F. Lauer, *Journal of the American Chemical Society* **1973**, *95*, 2697-2699.
[8] C. H. Schiesser, *Chemical Communications* **2006**, 4055-4065.
[9] G. Mugesh, W.-W. d. Mont, *Journal of Eurpoean Chemistry* **2001**, *7*, 1365-1369.
[10] L. Zeng, T. Kaoudi, C. H. Schiesser, *Tetrahedron Letters* **2006**, *47*, 7911-7914.
[11] R. L. Grange, J. Ziogas, J. A. Angus, C. H. Schiesser, *Tetrahedron Letters* **2007**, *48*, 6301-6303.
[12] M. K. Staples, R. L. Grange, J. A. Angus, J. Ziogas, N. P. H. Tan, M. K. Taylor, C. H. Schiesser, *Organic Biomolecular Chemistry* **2011**, *9*, 473-479.

[13] J. Mlochowski, K. Kloc, R. Lisiak, P. Potaczek, H. Wojtowicz, *ARAKAT USA* **2007**, *vi*, 14-46.
[14] Y. Kumar, R. Green, K. Z. Borysko, D. S. Wise, L. L. Wotring, L. B. Townsend, *Journal of Medicinal Chemistry* **1993**, *36*, 3843-3848.
[15] H. Ito, J. Z. Wang, K. Shimura, J. Sakakibara, T. Ueda, *Anticancer Research* **1990**, *10*, 891-895.
[16] Y. Kumar, R. Green, K. Z. Borysko, D. S. Wise, L. L. Wotring, L. B. Townsend, *Journal of Medicinal Chemistry* **1993**, *36*, 3849-3852.
[17] aC. K. Chu, L. Ma, S. Olgen, C. Pierra, J. Du, G. Gumina, E. Gullen, Y.-C. Cheng, R. F. Schinazi, *Journal of Medicinal Chemistry* **2000**, *43*, 3906-3912; bJ. Du, S. Surzhykov, J. S. Lin, M. G. Newton, Y.-C. Cheng, R. F. Schinazi, C. K. Chu, *Journal of Medicinal Chemistry* **1997**, *40*, 2991-2993.
[18] aH. Sies, H. Masumoto, *Adv. Pharmacol.* **1997**, *38*, 2229-2246; bA. Muller, E. Cadenas, P. Graf, *Biochem. Pharmacol.* **1984**, *33*, 3235-3239; cV. Narayanaswami, H. Sies, *Free Radical Research Communication* **1991**, *42*, 237-244.
[19] A. Wendel, M. Fausel, H. Safayhi, G. Tiegs, R. Otter, *Biochem. Pharmacol.* **1984**, *33*, 3241-3245.
[20] H. Sies, *Free Radical Biology and Medicine* **1993**, *14*, 313-323.
[21] aR. Nozawa, T. Yokota, R. Fujimoto, *Antimicrobial Agents and Chemotherapy* **1989**, *33*, 1388-1398; bM. J. Parnham, E. Graf, *Progress In Drug Research* **1991**, *36*, 9-47.
[22] aM. C. Fong, C. H. Schiesser, *Tetrahedron Letter* **1995**, *36*, 7329-7332; bM. C. Fong, C. H. Schiesser, *Journal of Organic Chemistry* **1997**, *62*, 3103-3108.
[23] aG. A. Brown, K. M. Anderson, M. Murray, T. Gallagher, N. J. Hales, *Tetrahedron* **2000**, *56*, 5579-5586; bZ.-i. Yoshida, H. Hirai, S. Miki, S. Yoneda, *Tetrahedron* **1989**, *45*, 3217-3231; cM. Wrestling, T. Livinghouse, *Journal of the American Chemical Society* **1987**, *109*, 590-592.
[24] P. Renaud, M. P. Sibi*, Vol. 1-2*, Wiley-VCH, Weinheim, **2001**.
[25] W. P. Neumann, *Synthesis* **1987**, 665-683.
[26] aC. Chatgilialoglu, *Accounts of Chemical Research* **1992**, 188-194; bC. Ferreri, T. Gimisis*, Vol. 2*, WILEY-VCH Verlag, Bologna, **1999**.
[27] D. H. R. Barton, D. Crich, W. B. Motherwell, *Journal of the Chemical Society, Chemical Communications* **1983**, 939-941.
[28] aB. J. Maillard, D. Colombani, *Journal of Organic Chemistry* **1994**, *59*, 4765-4772; bE. Montaudon, X. Lubeigt, B. Mallard, *Journal of the Chemical Society Perkins Transactions 1* **1991**, 1531-1538; cJ. Coulomb, V. Certal, M.-H. Larraufie, C. Ollivier, J.-P. Corbet, G. Mignani, L. Fensterbank, E. Lacôte, M. Malacria, *Chemistry-A European Journal* **2009**, *15*, 10225-10232; dR. A. Batey, D. V. Smil, *Angewandte Chemie* **1999**, *38*, 1798-1800; eM. R. Ashraft, A. Buny, C. J. Cooksey, A. G. Davies, B. D. Gupta, M. D. Johnson, H. Morris, *Journal of Organometallic Chemistry* **1980**, 89-104; fM. F. Saraiva, M. R. C. Couri, M. L. Hyaric, V. V. d. Almeida, *Tetrahedron* **2009**, *65*, 3563-3572.
[29] S. Kim, C. J. Lim, S.-E. Song, H.-Y. Kang, *Journal of the Chemical Society, Chemical Communications* **2001**, 1410-1411.
[30] J. C. Walton, *Accounts of Chemical Research* **1998**, *31*, 99-107.

[31] C. H. Schiesser, L. M. Wild, *Tetrahedron* **1996**, *52*, 13256-13314.
[32] S. Lobachevsky, University of Melbourne (Melbourne), **2008**.
[33] M. Newcomb, *Tetrahedron* **1993**, *49*, 1151-1176.
[34] M. Newcomb, A. G. Glenn, M. B. Manek, *Journal of Organic Chemistry* **1989**, *54*, 4603-4606.
[35] S. Lobachevsky, C. H. Schiesser, C. Y. Lin, M. L. Coote, *Journal of Physical Chemistry A* **2008**, *112*, 13622-13627.
[36] S.-L. Zheng, C. H. Schiesser, O. T. K. Nyugen, M. A. Lucas, *Tetrahedron* **2000**, *56*, 3995-4000.
[37] A. L. J. Beckwith, S. A. M. Duggan, *Journal of the Chemical Society Perkins Transactions 2* **1994**, 1509-1518.
[38] L. M. Wild, University of Melbourne (Melbourne), **1998**.
[39] J. A. Franz, D. H. Roberts, K. F. Ferris, *Journal of Organic Chemistry* **1987**, *52*, 2256-2262.
[40] J. C. Scaiano, P. Schmid, K. U. Ingold, *Journal of Organometallic Chemistry*, *121*, c4-c6.
[41] S. H. Kyne, H. K. Aitken, C. H. Schiesser, E. Lacote, M. Malacria, C. Olliver, L. Fensterbank, *Organic and Biomolecular Chemistry* **2011**, *9*, 3331-3337.

ABSTRACT

For the work presented in previous chapters a variety of approaches were required to solve the problems posed in this dissertation. Physical organic chemistry, particularly ultrafast radical kinetics techniques, are commonly regarded as niche chemistry. While some of the approaches used in this work are commonplace and extensively covered by undergraduate texts on physical and organic chemistry; others are not. It is the intent of the proceeding pages to present a primer on the techniques and methods used in this work so that the chemistry covered herein could be understood and continued by an undergraduate. As with any experimental chapter detailed procedures for the experiments used to answer the questions posed in Chapters 2 and 3 are given. More common techniques will also be discussed but in a more superficial manner as it is assumed that the reader has a sufficient understanding of these topics.

4.1. Technique Primers: Chemical Kinetics

4.1.1 Introduction

For the physical organic chemist, who seeks to optimize a synthetic process or elucidate the mechanism of an important biological pathway, a thorough understanding of chemical kinetics is a critically important tool. The kineticist may design experiments that allow her to deduce the rates of individual elementary steps, trap suspected reactive intermediates or detect the presence of a unique reaction product as evidence for a particular mechanism. None of these tests can unambiguously ascribe a

mechanism to a particular reaction. However, by judicious experimental design coupled with careful consideration of the likely mechanisms these types of experiments able to provide convincing evidence for or against a particular mechanism.

In radical chemistry, many reactions occur at extremely rapid rates because radicals are short-lived species. Today, in principle, there is no reaction whose kinetics are too rapid to measure. Both real-time and *post facto* methods are available for reactions in every conceivable time regime. The following pages describe standard approaches to real-time kinetics as well as provide an introduction the use of radical clocks in competition kinetics experiments as both have been used in this dissertation work.

4.1.2 Real Time Kinetics

Chemical kinetics is the study of reaction rates. For a simple first order reaction where a single molecule of reactant undergoes a unimolecular transformation **(equation 4.1)** to product; the rate can be expressed by the differential equation shown in **equation 4.2.** The rate of the reaction will depend on the concentration of the reactant and a proportionality constant, *k*.

$$A \xrightarrow{k} P \tag{4.1}$$

$$-\frac{d[A]}{dt} = k[A] \tag{4.2}$$

This constant, *k*, is system specific and may be influenced by temperature and pressure for gas phase. For reactions in solution, molecular level stabilizing or destabilizing effects of solvent-solute interaction may also affect the rate constant for a given reaction. For a simple first order reaction, rearrangement and integration of

equation 4.2 yields a linear expression, **equation 4.3**, which expresses concentration as function of time.

$$\ln[A] = -kt + \ln[A]_o \qquad (4.3)$$

Fitting experimental data to this equation and comparing the fit to the analogous higher order linearized rate laws allows the investigator to determine the order of reaction. Moreover, if the reaction is known to be first order this equation will yield an absolute rate constant for the reaction from the plot of the ln([A]) as a function of time.

For a mixed second order reaction the differential form of the rate law exhibits dependence on concentration of both reactants **(equation 4.4 and 4.5)**.

$$A + B \xrightarrow{k} P \qquad (4.4)$$

$$-\frac{d[A]}{dt} = k[A][B] \qquad (4.5)$$

The rate constant can be determined from an integrated form of the rate law if one of the reactants is present in slight excess. Instead, the clever kineticist will approximate to a pseudo first order reaction by flooding with a high concentration of one reactant. In pseudo-first order kinetics, the experimentalist makes the concentration of one reactant so large that it remains effectively constant over the course of the reaction. This approach effectively eliminates the concentration dependence on one species significantly decreasing the experimental rigor required to measure the rate constant by simplifying the expression **(equation 4.6)** that represents the reaction.

$$[B]_o >> [A]_o$$

$$-\frac{d[A]}{dt} = k_{obs}[A]$$

$$k_{obs} = k[B]_o \qquad (4.6)$$

The observed rate constant for this reaction represents a concentration dependent rate. Exploitation of the linear proportionality between k_{obs} and concentration of the species in excess allows the experimentalist to determine the absolute rate constant for a second order reaction with relative ease. This technique was applied in both Chapter 2 and Chapter 3 to determine kinetic parameters.

The preceding discussion assumes reaction kinetics are monitored in real-time. In such an experiment concentration must be monitored either at set intervals or continuously over the course of the entire reaction. When dealing with short-lived radicals ultra-fast technique like pulse radiolysis or flash photolysis (*vide infra*) are often required. These techniques, while invaluable to the radical chemists, suffer from some limitations that may not make them suitable for every reaction in a particular time regime. For instance, using our laser flash system requires a molecule that can be excited to form the reactive intermediate using one of only 4 wavelengths accessible by our laser. Additionally, the excited species must have an appropriate chromophore to facilitate monitoring absorbance associated with formation of the product or decay of the intermediate. Moreover, this absorbance should not be coincident with the excitation wavelength or an absorption maxima for the radical precursor. Finally, the reaction must occur with a rate constant between 10^6 and 10^9 1/s. Aside from experimental limitations laser flash photolysis instrumentation are costly and require significant

expertise to operate and maintain. A less costly and more versatile approach to these studies is through the use of radical clocks and competition experiments.

4.1.3 Competition Kinetics

Competition experiments partition a particular reactant between two pathways **(Figure 4.1)**. A key feature of a successful use of competition experiments to determine kinetic parameters is that the kinetics of one of the competing pathways is known.

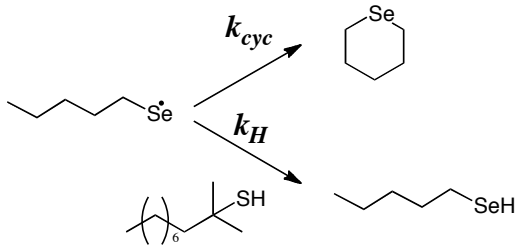

Figure 4.1. Competition between hydrogen abstraction from a thiol radical clock and cyclization for a seleno-radical.

Typically, a kineticist will employ some unimolecular or bimolecular reaction of known rate constant as a "molecular level stopwatch" by which to gauge the kinetics of a competing process of unknown rate constant. It is generally desired for the stopwatch process to be irreversible and exhibit a rate constant similar to that of the unknown process.[1-3] Espenson suggests that a rate constant ratio of no greater than 5 should be allowed for accurate determination of rate constants.[3] Larger difference in rate will lead to insensitivity to changes in the rate constant being measured and an irreversible clock process will complicate data analysis.

The rate law for any given chemical reaction can be written in terms of consumption of the reactant or formation of product. Expressing the relationship between the rate constants for the two competing processes yields the rate quotient in **equation 4.7** from this equation one can very simply determine the unknown rate

constant knowing one rate constant and measuring the relative quantities of the two products formed **(equation 4.8)**.

$$\frac{\frac{d[RSeH]}{dt}}{\frac{d[Cyc]}{dt}} = \frac{k_T[R'H][RSe\bullet]}{k_{cyc}[RSe\bullet]} \quad (4.7)$$

$$k_{cyc} = k_T \frac{[R'H][Cyc]}{[RSeH]} \quad (4.8)$$

In competition experiments the reaction is run to completion then products are identified and quantities from the competing pathways are used to determine the unknown rate constant. Products of competition experiments are most often characterized by the use of standards and an common analytical technique like HPLC or GC.[1]

Radical clocks have been developed and used to calibrate and characterize the kinetics of numerous classes of chemical reactions. Only the most pervasive radical clocks will be discussed here. One commonly used class is nitroxyl radical spin traps. Nitroxyl radicals are known to traps carbon centered radicals at rapid rates facilitating their use in kinetic analysis and detection of reaction intermediates in mechanistic studies. Nitroxyl radicals are most often generated by thermolysis of a peroxide initiator that will abstract a hydrogen producing the desired nitroxyl radical, **Scheme 4.1**.[2]

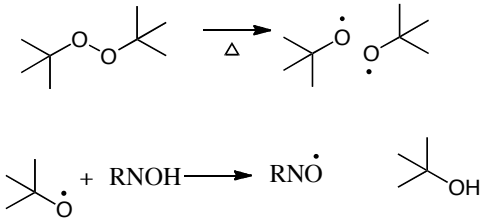

Scheme 4.1. Thermal initiation is a common method for generation of nitroxyl radical spin traps.

Nitroxyls are relatively unselective in their reactivity toward C-centered radical making them widely applicable. Limiting their use is their steric bulk; the persistence of nitroxyl radicals is partially attributable to being bulky and their couplings have proven to be sensitive to steric effects.[2] Additionally, ESR has limited sensitivity as a kinetics technique. In recent years its use has been largely superseded by methods allowing more precise determination of kinetic constants.

Probably the most well known class of radical clocks are tin-hydrides. The tin-hydride method involves halogen abstraction from alkyl halide precursors to generate the radical **(Scheme 4.2).**[2]

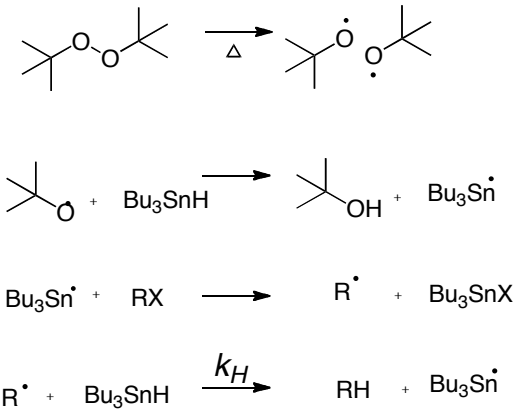

Scheme 4.2. Initiation for a tin-hydride initiated radical generation method.

This method can be used to characterize rate constants for competing unimolecular processes between 10^4 1/s to 10^8 1/s using hydrogen abstraction by tin hydrides (k_H) as a competing process.[2] Another extremely useful class of precursors for radical clocks are pyridine-2-thione-*N*-oxycarbonyl (PTOC) esters **(Figure 4.2)**. PTOC ester radical precursors were developed toward expanding the accessible range of *k* by permitting use of radical clocks with rate constants between 10^5 1/s and 10^{11} 1/s.[2]

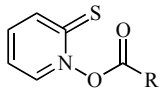

Figure 4.2. General structure of thermally and photochemically labile pyridine-thione esters.

These photolabile compounds were employed in this work in **Chapter 3** as radical precursors to seleno radicals. Tin hydride and *t*-dodecanethiol were used in this work to trap radical. These radical traps exhibit solvent rate constants of on the order of 10^6 1/s for hydrogen abstraction from alkyl radicals. The assumption that seleno radicals generated from a PTOC precursor would exhibit similar rate constants for hydrogen abstraction was made to facilitate their use in this study. PTOC esters undergo thermal or photo-initiated bond homolysis at the labile N-O bond generating carboxylate radical with UV irradiation. Subsequent, rapid decarboxylation yields the radical to be studied, **Scheme 4.3.**

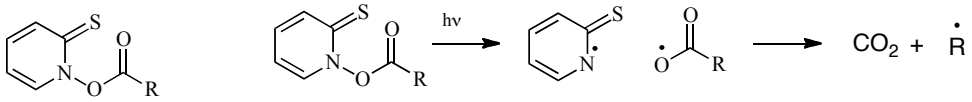

Scheme 4.3. Photochemically initiated bond cleavage and decarbonylation of a PTOC ester is often used to generate radicals for competition experiments.

In all three methods; nitroxyl spin trapping, tin-hydride and PTOC-thiol method pre-calibrated radical clocks are used to determine the rate constant for a previously unreported process. The rate of a radical clock reaction must be calibrated before use as a clock; typically this is done by a direct technique like laser flash photolysis. Radical clocks are comprehensively characterized so that the rate constant for reaction with a particular types of radicals can be known to facilitate widespread applicability.[1] Therefore, while radical traps are a fantastic tool one cannot discount the essential nature of direct kinetics techniques for ultrafast processes. Without direct kinetics

techniques, like laser flash photolysis, radical clocks cannot be calibrated and therefore would not exist.

4.2 Instrumental Techniques

4.2.1 Laser Flash Photolysis

In Chapter 2 the use of direct methods to study radical kinetics is explored. Both photochemical and electrochemical techniques are useful for generating and monitoring short lived radical cations. Unfortunately, these reactive molecules often cannot be monitored by conventional spectroscopic methods. Instead, fast kinetic techniques such as stopped flow systems, pulse radiolysis and flash photolysis are needed.[4]

Laser flash photolysis is an analytical tool utilizing two perpendicular beams of light to simultaneously generate and monitor the decay of a radical species or other reactive intermediate. Flash photolysis has proven useful for monitoring the kinetics of reactions occurring as fast as the femtosecond time regime. Solid state or dye lasers are commonly utilized as excitation sources in laser flash instrumentation. The laser emits high-energy photons that are absorbed by molecules in solution causing excitation and electron transfer or excitation. Electron transfer occurs in the case described in this work. A radical or radical ion containing an appropriate chromophore is then monitored using a xenon arc lamp; which shines an analyzing beam through the sample at a 90^{O} angle from the excitation beam. A monochromator is used to select the wavelength for analysis and a photomultiplier tube is used to amplify the current output associated with the light transmitted through the sample. Alternatively some systems employ diode arrays or ccds (charge coupled devices) as detectors.[5]

For any flash photolysis type experiment (ultrafast or conventional timescale) to be a viable method for kinetic analysis two requirements must be met 1) (as alluded to above) the compound must be able to be generated by photoexcitation and 2) the generation of the reactive intermediate must take place on a time scales that appears instantaneous relative to the timescale of the experiment. In the instrumentation employed in this laboratory the generation occurs during a 4-6 nm pulse of light from the laser and reactions are monitored on a time scale of tens of nanoseconds up to microseconds. Rate constants attained by LFP often are composite rate constants; radical cations are highly reactive and often able to decay via several routes, in addition some simple reactions such as HAT involve sequential mechanisms that may complicate kinetics and analysis.[5] In order to enable use of LFP as a kinetic tool a reasonable signal must be able to be attained at low concentrations of reactants.[5] This requirement is necessary because in a highly concentrated solution the excitation beam may be absorbed strongly by the dense wall of molecules first encountered by the beam preventing light from passing to the center of the solution and exciting molecules in the path of the monitoring beam. Additionally, at high concentrations, there will be an increase in the incidence of collision between two excited species resulting in self deactivation.[5] For example, dimethylaniline radical cations as they are known to dimerize in the absence of base further complicating analysis of their reactivity.

Dimethylaniline radical cations have also been studied by electrochemical techniques. These techniques most obviously differ in that, techniques such as linear sweep and cyclic voltammetry are not subject to spectroscopic limitations, electron transfer occurs on the surface of an electrode rather than from being initiated by

absorption of a photon and laser flash techniques are suitable for significantly faster processes. In light of both methods requirements for use not all reactions in Chapter 2 were able to be studied electrochemically and photochemically.

4.2.2 Cyclic Voltammetry

Cyclic voltammetry is a technique well suited to study chemical kinetics reactions of electrochemically oxidized or reduced species with rate constants between 10^2 and 10^6 1/s. This is a particularly advantageous tool for radical chemists wishing to generate and monitor electronically excited species that do not contain an appropriate chromophore for detection or generation by photochemical methods. In cyclic voltammetry the current response is measured as a function of applied potential. The potential is varied, at a constant rate, from initial to maximum potential, and then reversed.

A reversible system, such as ferrocene **(Figure 4.3),** shows equal magnitude oxidative and reductive waves. Therefore the ratio of the cathodic (i_{pc}) and anodic (i_{pa}) peak currents will equal 1.

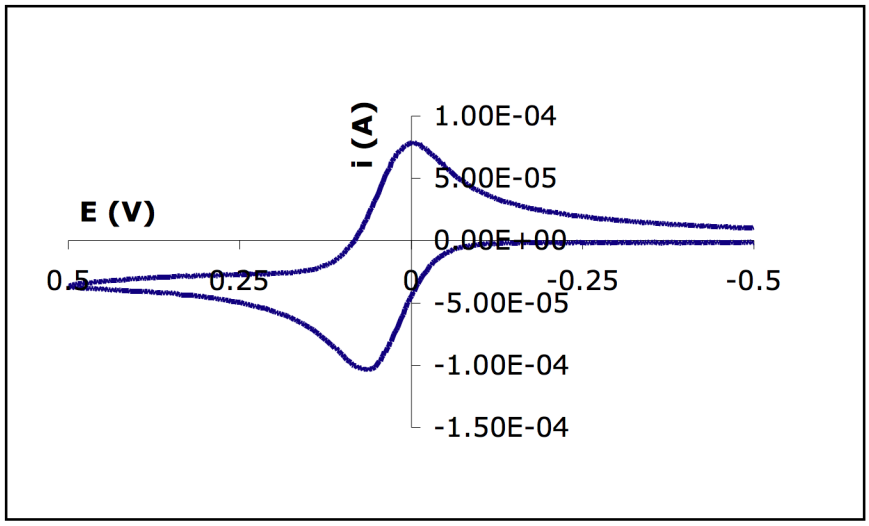

Figure 4.3. Reversible voltammograms are observed when the electroactive species does not undergo a follow up chemical reaction.

Characteristic to reversible systems is the observation of peak widths of 57-60 mV; where peak width is measured as the difference in the E_p and $E_{p/2}$ (where $E_{p/2}$ is the peak current at half height). For reversible systems it is just as convenient to use the difference between E_{pc} and E_{pa} to identify the system as reversible; where the difference is 60 – 63 mV. Cyclic voltammetry cannot be used to yield kinetic information because either the reaction does not undergo a follow up chemical step or the rate of the follow up chemical step is too slow to demonstrate an observable effect on concentration of the reduced or oxidized species in the time frame of the cyclic voltammetry experiment. However, the thermodynamic equilibria between the oxidized and reduced form at the surface of the electrode for a reversible reaction is described by the Nernst equation (**equation 4.9)**, which demonstrates the relationship between concentration and applied potential (E) for a reversible oxidation reaction.

$$E = E_o + \frac{RT}{nF}\ln\frac{O}{R} \qquad (4.9)$$

E_o, the standard electrode potential is related to standard Gibbs free energy change by **equation 4.10**. In practice substitution of formal potential for standard potential accounts for activity in non-ideally behaving systems.[6]

$$\Delta G_o = -nFE_o \qquad (4.10)$$

In contrast to a reversible system; a quasi or irreversible system can provide kinetic information about follow up chemical reactions involving species generated at the electrode surface in an electrolytic cell. In an irreversible system no reverse wave will be observed. In these cases it is unknown wfhether the follow up reaction or heterogeneous electron transfer occurring at the electrode is rate limiting. In the project utilizing electrochemical kinetics in Chapter 2 the system under study has been previously identified as one in which the chemical step is rate limiting. The diagnostic features of the voltammogram used to differentiate between chemical step and electron transfer rate limiting for a first order reaction are shown in **Table 4.1**.[7]

Table 4.1. Characteristics observed for different type of rate control in cyclic voltammetry.

Rate Limiting Step	E_p-$E_{p/2}$	ΔE_p*
Heterogeneous Electron Transfer	95 mV	59 mV
Chemical Step	48 mV	30 mV
Mixed Kinetic Control	>48 mV , < 95 mV	>30 mV , < 59 mV

* denotes slope of plot E_p as a function of log(scan rate) over a one order of magnitude change in scan rate

The reactions studied herein exhibited quasireversible voltammograms. The quasireversible voltammogram, in **Figure 4.4** below, displays observed behavior for uncatalyzed oxidation of *N,N*-dimethylanilines. Notably the magnitude of the peak current is not equal for the oxidative and reductive wave. Furthermore, the relative

magnitude of the reverse (reductive) wave increases with scan rate. These features are inherent to an E.C. (electron transfer followed by chemical step) type mechanism.

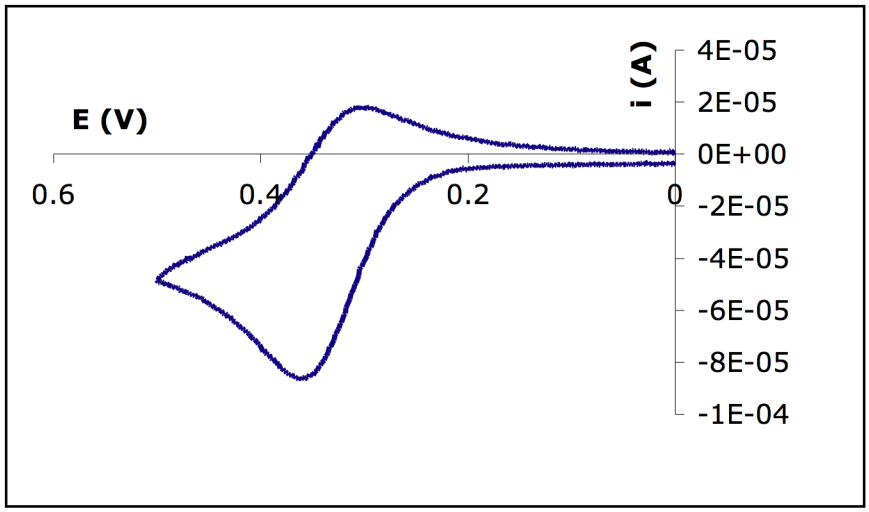

Figure 4.4. Quasireversible or irreversible voltammograms are observed when a follow up chemical reaction consumes the electroactive species. In this case the oxidized compound reacts before it can be reduced again.

For *N,N*-dimethylanilines, electron transfer at the electrode surface generates the radical cation. The radical cation is reported to then undergo an irreversible chemical transformation via dimerization **(Scheme 4.4)**.

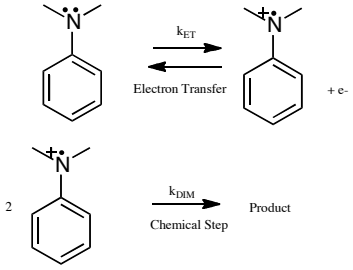

Scheme 4.4. Dimerization mechanism for N,N-dimethylaniline radical cations. The quasireversible voltammogram in Figure 4.4 exhibits the effect of this irreversible chemical step on the observed voltammogram.

At high scan rates the follow up chemical reaction is slower relative to the rate at which the potential is varied; therefore in the timeframe of the experiment little change in the magnitude of the reverse wave (relative to the initial oxidative wave) is observed. At slower scan rates more time is allowed for the *N,N*-dimethylaniline radical cation to

dimerize before the scan reaches the potential at which the radical cation is reduced back to the neutral parent compound. This additional time leads to additional time for the reaction to occur therefore a larger portion of the electroactive species is consumed in the chemical step so less reverse electron transfer can occur producing less of the initial species, consequently drawing less current on the reverse scan. The astute reader may note that this behavior is what makes this system suited for kinetic analysis using cyclic voltammetry.

A relationship between peak current and concentration and the ability to make time based measurements of changes in peak current are essential to determination of kinetic parameters. Delineating relationships between the many factors that govern electrochemical kinetics and rate constant is abstruse when one considers all of the processes occurring in the system. Dimensionless parameters that group these variables allow the investigator to achieve generalized solutions that can be broadly applied for similar reactions. Extracting useful kinetic data from cyclic voltammetry in this way requires knowledge of the reaction mechanism. For an EC mechanism the kinetics of the chemical step can be determined from the dimensionless parameter λ **(equation 4.11)**.[8]

$$\lambda = \frac{RT}{nF}\left(\frac{k}{\nu}\right) \tag{4.11}$$

The value of λ indicates whether a reaction rate is limited by the chemical step or by diffusion as shown in Table 4.2. [8]

Table 4.2. Dimensionless rate constants characteristic of kinetic zones for first order reactions.

Kinetic Zone	Λ
Kinetic Control (KP)	>5
Fast Kinetics in Competition with Diffusion (KI)	$.01 \leq \Lambda \geq 5$
Diffusion Control (DP)	< .1

For reactions under kinetic control determination of the rate constant requires collecting voltammograms at a variety of scan rates. The kinetic analysis is done one of two ways for a reaction of known mechanism. One way is by fitting the ratio of i_{pa}/i_{pc} over a range of scan rates to working curves generated by simulations by plotting both the experimental and theoretical results together in the form of **equation 4.12**.[8] The offset between the experimental curve and the working curve (Δx) will yield a value for *k*.

$$\frac{i_{pa}}{i_{pc}} = \left(\frac{k}{F\nu RT} \right) \qquad (4.12)$$

Similarly fitting data directly to linear **equation 4.13** can yield the same kinetic information.[7]

$$E_p - E_{\frac{p}{2}} = \frac{RT}{2nF}\left(\ln(\lambda) - 1.56\right) \qquad (4.13)$$

In this work, we are also interested in challenging the mechanistic precedent for the reaction under study. Consequently, we chose to use simulations that can assist us in identifying likely mechanisms for the reaction. Our approach is most similar to the working curve method. Rather than constructing working curves, direct fitting of experimental voltammograms to simulated voltammograms based on the proposed mechanism of reaction using rate constants determined by laser flash photolysis were

used as proof of mechanism. Subsequent, varying the rate constant to give a better fit was used to refine the kinetic parameter.

4.3 Electrochemical Simulations

4.3.1 Utility of simulations

The advent of digital electrochemical simulations has revolutionized the way chemists use electrochemistry. The ability to determine kinetic parameters from electrochemical data has existed as long as the associated mathematical methods have; although, electrochemical kinetics measurements have only become commonplace because of modern simulations programs. Electrochemical simulations are predominately used to afford a convenient means to model the concentration of an electroactive species as a function of transport of mass (convection, diffusion and migration), chemical transformations (both the electrode initiated oxidation or reduction of a substrate and its follow up reactions) and other complicating factors (such as electrode adsorption) occurring in an electrochemical reaction.

Simulations are a convenient way to determine mechanistic and kinetic information for cyclic voltammetry experiments. While one can easily describe most electrochemical systems through coupled partial differential equations it is difficult to get analytical solutions for the resultant function when cast in a continuous form for a real system. There are two common approaches to electrochemical simulations the point and the box model. Herein a discussion of the box model is presented as the author believes this approach is more easily conceptualized; although either approach will afford equivalent results.

Digsim BAS is a cyclic voltammetry simulator that does several things to make this task less daunting. Firstly, the use of dimensionless parameters allows the program to generate generalized solutions to the equations; thereby reducing the computational cost and increasing the ease with which a given solution can be applied to different system. These equations, cast in a dimensionless form, can then be discretized by making the model variables correspond to finite increments. The finite difference approximation is used to make the step size for discretized parameters very small and recursively solving equations refines, with each iteration, the accuracy of the model variables input for the next iteration. Ultimately, a high number of iterations and a sufficiently small model parameter increment the discrete model will be needed to give solutions that are comparable to those determined from the continuous model. Once the appropriate equations have been manipulated into the appropriate form and the appropriate boundary conditions for the model have been specified it is simply a matter of programming suitable algorithms. The work performed herein utilized Digisim BAS a windows based program written in C++ that was developed by Bioanalytical Systems, Inc.[9]

Like Digisim BAS the majority of modern commercially available simulations programs have user friendly interfaces.[9] They are so easy to use that very little actual understanding of the simulations is needed for their use. That said, a black box approach to any simulation or computational program is ill advised as there are specific assumptions and variable parameters dependencies that can afford misleading results for a superficial user. As the work discussed in this dissertation was not intended to develop or improve simulations programs, but rather effectively utilize them, the focus of

this will not be a rigorous mathematical explanation of the workings of the different programs available. Rather a general overview of the components incorporated into electrochemical simulations is given. An explanation of numerical methods employed by Digisim BAS will only be invoked where it is necessary to educate the reader on potential pitfalls related to the project at hand. For a detailed comparison of the available programs and the suitability of different numerical methods for solving transport problems the reader is referred to influential authors in this field such as Feldberg, Britz, Reiger, Rudolph.[9-15]

4.3.2 Approximation of mass transport to a discrete function

Digisim is designed for cyclic voltammetry simulations, specifically. In cyclic voltammetry the mass transport term is dominated by diffusion. Solutions are not stirred thus convection is minimized. Electrical migration is abated by the addition of high concentrations of inert ionic compounds (supporting electrolyte). Therefore, the mass transport term is described using Fick's laws of diffusion.[9] Flux of mass through space is proportional to some material specific constant (D_o) multiplied by the rate of change in concentration of the species as a function of distance as shown in **equation 4.14**.

$$J_i(x,t) = -D_i \frac{\partial C_i(x,t)}{\partial x} \qquad (4.14)$$

Because this is a continuous function of the space domain it is desirable to discretize the distance variable. This is achieved by breaking the distance traveled by the molecule (within the timeframe of the experiment) into slices of space such that Δx is very small. This treatment is known as a finite difference approximation and yields the following expression (**equation 4.15**).[16]

$$J_i(x,t) = -D_i \frac{C_i(x+\Delta x,t) - C(x,t)}{\Delta x} \tag{4.15}$$

It is worth noting that the former two equations are written in one dimension implying that the diffusion in all space dimensions will occur similarly. There are, however, special cases where diffusion in a given dimension may be restricted.[9] The system described in this dissertation is not one of those cases.

Fick's second law of diffusion describes the flux of the molecules in solution over a given area in a time increment (**equation 4.16**).

$$-\frac{\partial C_i}{\partial t} = D_i \frac{\partial J_i}{\partial x} \tag{4.16}$$

Substitution of the finite difference form of **equation 4.14** into the finite difference form of **equation 4.16** leads to the expression in **equation 4.17**. This equation will allow accurate description of the concentration gradient when there is not species generated at the electrode and no follow up chemical reaction is occurring.

$$C(x,t+\Delta t) = C(x,t) + \frac{D\Delta t}{\Delta x}[C(x+\Delta x) - 2C(x,t) + C(x-\Delta x,t) \tag{4.17}$$

In terms of dimensionless parameters we arrive at dimensionless **equation 4.18** where f indicates a scaled fractional concentration, D_M (**equation 4.19**) is the dimensionless diffusion coefficient and j and k are parameters representing position in time and space.[16]

$$f(j,k+10 = f(j,k) + \mathbf{D}_M[f(j+10,k) - 2f(j,k) + f(j-1,k)] \tag{4.18}$$

$$D_M = \frac{D\Delta t}{\Delta x^2} \tag{4.19}$$

The purpose of the electrochemical simulation is to provide a representation of current changes over time and with concentration assuming a planar electrode, fast electron transfer and a reduced species that is present prior to electrolysis for a particular mechanism for a cyclic voltammetry experiment where potential is varied regularly between some predefined limit. One important and commonly made assumption in simulations is that the electroactive species and its precursor have identical diffusion coefficients. As it is intuitive to believe that there is a solvation cost to transport of radicals and ions this assumption is tested in Chapter 2.

A dimensionless parameter is simply a representation of a model variable that is not system specific. In cyclic voltammetry simulations, relationships between experimental variables and dimensionless parameters for the variables of time, space, diffusion layer thickness, current and concentration are defined.[16] In all cases these can be determined by dividing a dimensioned variable by some variable(s) that are intrinsic to the specific system. The output of this operation is a dimension free model parameter that can be converted to an experimental variable for a specific system by multiplying by the innate variable for a given system. Moreover, dimensionless parameters can couple variables relating to distinctly different physical variable and in some cases this can afford the investigator unique insight to how a system behaves. Most importantly, dimensionless parameters allow function solutions to be generalized similar to working curves. For example the dimensionless time can provide information for a real system by multiplying by the duration of the experiment. If this operation has been carried out prior to simulation then the solution would be system specific instead of widely applicable to processes varying in an analogous manner. This minimizes

computational effort as the solution to a non-dimensioned equation can be applied not only to several systems that are modeling the same type of phenomena for molecules that have different intrinsic properties (lifetime, concentration, diffusion coefficient, etc.) but it can also be applied to different phenomena with intrinsic parameters with different physical significance varies in a similar manner. For example a dimensionless equation for a first order dimerization reaction will be generally applicable to any number of reactions proceed via a similar mechanism. What is more, a clever user may apply these same dimensionless functions to unrelated system where the dimensionless parameter has a different physical significance if a similar dependence of the function on the dimensionless parameter(s) exists.[8]

4.3.3 Diffusion layer thickness and reaction layer thickness

To effectively model a chemical reaction involving a species generated at the electrode surface the number of slices of both time and space must be defined. In practice the reaction layer is very small compared to the diffusion layer so the increment size used to generate a concentration profile for diffusion is far too large to be sensitive enough to accurately predict the gradient due to reactions of the electroactive species. The thickness of the reaction layer is defined by **equation 4.20** where k is the rate constant for the chemical reaction and D_o is the diffusion coefficient for the species generated at the electrode surface.

$$\mu = \sqrt{\frac{D_a}{k}} \tag{4.20}$$

The rate constant for the reaction must be greater than one or this equation will give a nonsensical result with a reaction layer thicker than the diffusion layer. The

upper limit for k is bounded by diffusion control giving a maximum reaction later thickness of 10^{-5} relative to a diffusion layer thickness of unity.[9] A typical reaction layer thickness for the systems studied in this work would be on the order of 10^{-5} or 10^{-6}. The dimensioned form of the associated flux equation for the reaction layer is shown below **equation 4.21.**[8]

$$J \approx 6\sqrt{\frac{D_a}{dx}} + 1 \qquad (4.21)$$

Obviously the large difference in the diffusion and reaction layer thickness complicates the selection of a finite difference element to describe the space variable. With homogenous chemical reactions involving the electroactive species when solving the flux equation it is desirable to solve the diffusion component of the flux equation before dealing with the components that account for the kinetics of electron transfer or the homogenous chemical process. By using different intervals for the two processes a significantly smaller distance step can be used when solving the portion of the equation relating to the chemical transformations thus providing a more accurate picture of its effect on the concentration gradient.[9] Unequal intervals and dynamic grids are two ways that are commonly used to deal with this when explicitly solving the equations.[9] Dynamic grids decrease the time interval closer to the electrode so that the reaction layer can be accurately modeled. As mentioned previously the space element must also be smaller to characterize the reaction layer than the diffusion layer. This can be practically achieved by solving the matrix element associated with the kinetic portion of the equation on every time increment and the diffusion portion of every other time increment. In this way unequal intervals allows modification of the space element

effectively creating a smaller space element for the kinetic term by sampling at more frequent intervals.

4.3.4 Homogeneous and heterogeneous kinetics

Thus far it appears that programming algorithms to recursively solve a dimensionless finite difference form of Fick's second law to account for diffusion alone is an unnecessarily difficult approach to such a problem. Clearly, simulations have not been studied and refined for the sole purpose of describing simple diffusion problems.[8] Instead, digital simulations are most highly valued by the chemist who intends to study the mechanism and kinetics of electron transfer at the electrode and/or the kinetics of follow up chemical transformations involving the species generated at the electrode surface. For real systems the differential equation accounting for all these processes becomes extremely onerous and is difficult to solve as a closed form expression.

If electron transfer is not extremely rapid it becomes necessary to describe the transport of the electroactive species, and its corresponding concentration gradient, in terms of the kinetics of electron transfer. In the system at hand the chemical step is rate limiting and electron transfer is extremely rapid. A unimolecular reaction involving a molecule oxidized at the electrode surface (**equation 4.22)** can be described in terms of the concentration of the oxidized species (**equation 4.23).**

$$A - e^- \rightarrow A.^+ \qquad (4.22)$$

$$A^+ \rightarrow P$$

$$-\frac{\partial A^{\bullet+}(x,t)}{\partial t} = kA^{\bullet+}(x,t) + D_A \frac{\partial^2 A^{\bullet+}(x,t)}{\partial x^2} \qquad (4.23)$$

In finite difference form with a dimensionless diffusion coefficient it can be expressed as **equation 4.24.**

$$A^{\bullet+}(x,t-\Delta t)-A^{\bullet+}(x,t)=-k\times\Delta t\times A^{\bullet+}(x,t)+D_{MA}\left[A^{\bullet+}(x+\Delta x,t)-2A^{\bullet+}(x,t)+A^{\bullet+}(x-\Delta x,t)\right] \quad (4.24)$$

Dividing by the dimensioned starting concentration of species A gives **equation 4.25.**

$$f_a(j,k+1)-f_a(j,k)=-\frac{k_1 t_k}{\ell}\times\Delta t\times f_a(j,k)+D_{MA}\left[f_a(j+1,k)-2f_a(j,k)-2f_a(j-1,k)\right] \quad (4.25)$$

Typically the diffusion and kinetic term are separated rather than coupling the diffusion and kinetic term. With the diffusion term being solved first then the kinetic portion being solved in a second step.[8] The sequential approach makes it easier to differentiate the effects of the two processes on the concentration profile. The advantage is that the user may explicitly see the effect of manipulating mechanistic and kinetic input to see how the concentration profile depends on mechanism. Another practical advantage of sequential rather than synchronous equations is that the function does not go negative at high rate constant because the reactant can not be fully consumed by diffusion alone.[8] The change in concentration can be related to current by **equation 4.26**. This data can be used to approximate to the experimentally determined parameters.

$$i=nFAD_o\left(\frac{\partial C_i}{\partial x}\right)_{x=0} \quad (4.26)$$

The Gauss Newton least-squares method **(equation 4.27)** is used to determine when the function converges to a minima.[6] The differential equation that represents all of the factors influencing the time and space dependant concentration. C++ uses matrix representation to express the physical variable dependencies of the equations, which describe the kinetics and mass transport. The Jacobian is recalculated after each iteration and the new values are inserted into the matrix; recursively refining the

parameters until convergence on a minimum value. Typically 100 to 1000 iterations are used.[8]

$$\sigma = \sqrt{\frac{\sum \left(i_{sim} - i_{exp\,t} \right)^2}{n}} \qquad (4.27)$$

Generally, there are a variety of ways to characterize the intermediates, products and kinetics of radical reaction mechanisms. In Chapter 2 the kinetics of *N,N*-dimethylaniline radical cation reactions with carboxylate bases is monitored by laser flash and cyclic voltammetry. The cyclic voltammetry simulations provide a key vantage point allowing the investigators to gain important mechanistic insight. In chapter 3 the indirect PTOC-thiol method was used to study the cyclization of alkylselenide radicals. In both chapters systematic substitution of radical precursors afforded significant advantage. The experimental details of the kinetic studies, product analysis and relevant syntheses are discussed in the forthcoming section.

5.1 Experimental Procedures: Chapter 2

5.1.1 Materials

Chemicals and HPLC grade solvents were used as received unless otherwise stated. Tetrabutylammonium acetate was recrystallized from diethyl ether and dried in *vacuo*. Tetrabutylammonium acetate was stored, and its stock solutions were prepared, in an anhydrous, inert atmosphere. For experiments requiring anhydrous conditions CH_3CN was distilled over CaH_2, under dry nitrogen and stored over 4A molecular sieves.[17]. All experiments were performed under argon in oven dried glassware.

5.1.2 Instrumentation

NMR was performed in $CDCl_3$ and chemical shifts were reported in ppm referenced versus an internal standard of 1% tetramethylsilane (TMS). ^{1}H, ^{13}C NMR spectra were recorded on a 400 mHz Varian or 500 mHz JOEL spectrometer; the operating frequency of the NMR used is given along with the chemical shifts at the end of this section. Melting points were determined on a Thomas Hoover Unimelt Capillary Melting Point Apparatus. Gas chromatography was performed using a HP5890A GC (column: Alltech EC-5,S/N: PT 19647, 30m × .025mm, film thickness .025μm). GCMS analysis was carried out on a HP6890 GC with HP 593 Mass Selector (column: J&W Scientific, S/N: US5171516H, 60m × .025mm, film thickness .025 μm) or a (column: J&W Scientific, S/N: USB115513H, 30m × .025mm, film thickness .025 μm). The latter column is a chiral column and was only employed in product studies as it afforded superior separation. UV-Vis spectra were recorded on a HP8452A diode array UV-Vis spectrometer. Instrumentation used in kinetic analysis is described in detail in the corresponding experimental section.

5.1.3 Syntheses

5.1.3.1 *N,N*-dimethylanilines

***N,N*-dimethyl-*p*-anisidine (2-1), *N,N*-dideuteromethyl-*p*-anisidine (2-2), *N,N*-dideuteromethyl-*p*-toludine (2-4), *N,N*-dideuteromethylaniline (2-6) *N,N*-dimethyl-*p*-Cl-aniline (2-7), *N,N*-dideuteromethyl-*p*-Cl-aniline (2-8)**

In a glass bomb 0.05 moles of a *p*-substituted aniline was dissolved in 0.14 moles of CH_3OH. While stirring, 0.12 moles of hydroiodic acid was added.[18] The sealed reaction vessel was heated to 125 ^{o}C under stir for 96 hours. Excess acid in the

cooled reaction mixture was quenched by addition of Na_2SO_4. The product was extracted with hexanes, dried with $MgSO_4$ and evaporated in *vacuo*. The crude oil and 0.09 moles of acetic anhydride were combined under reflux. The amine was neutralized by the addition of NH_4OH. The resulting solution was then washed 3X with 200 mL of 10% HCl to remove excess acetic anhydride. Subsequently, the solution was extracted with hexanes, dried with $MgSO_4$, and evaporated under reduced pressure and recrystallized to afford an oil or solid as specified below.

***N,N*-dimethyl-*p*-anisidine[18] (2-1)**

A rust colored crystalline solid in a 57 % yield. ^{1}H NMR (500 MHz, CHLOROFORM-D) δ 6.93 (d, *J* = 9.1 Hz, 2H), 6.83 (d, *J* = 9.1 Hz, 2H), 3.80 (s, 3H), 2.93 (s, 6H); $C_9H_{13}O$ Molecular weight 151.21 g/mol GC-MS M/Z 151. Spectroscopic data are consistent with published spectra.[19]

***N,N*-dideuteromethyl-*p*-anisidine[18] (2-2)**

A rust colored crystalline solid in a 48 % yield. ^{1}H NMR (500 MHz, CHLOROFORM-D) δ 6.84 (d, *J* = 8.9 Hz, 1H), 6.74 (d, *J* = 9.0 Hz, 1H), 3.76 (s, 2H); $C_9H_7D_6O$ Molecular weight 157.24 g/mol GC-MS M/Z 157. Spectroscopic data are consistent with published spectra.[20]

***N,N*-dimethyl-*p*-toludine (2-3)**

Purchased from Sigma-Aldrich and purified by kügelrohr distillation at 56 ^{o}C and 5 mmHg.

***N,N*-dideuteromethyl-*p*-toludine[18] (2-4)**

A pale yellow oil in a 47% yield. NMR: ^{1}H NMR (500 MHz, CHLOROFORM-D) δ 7.05 (d, *J* = 8.4 Hz, 2H), 6.68 (d, *J* = 8.6 Hz, 2H), 2.25 (s, 3H) $C_9H_7D_6$ Molecular weight

141.24 g/mol GC-MS M/Z 142. Spectroscopic data are consistent with published spectra.[21]

***N,N*-dimethylaniline (2-5)**

Purchased from Sigma-Aldrich and purified by kügelrohr distillation at 48 ^{o}C at 5 mmHg.

***N,N*-dideuteromethylaniline[18] (2-6)**

A pale yellow oil in a 22% yield. ^{1}H NMR (400 MHz, CHLOROFORM-D) δ 7.23 (d, *J* = 9.0 Hz, 2H), 6.74 (d, *J* = 7.9 Hz, 2H), 6.72 (s, 1H); $C_8H_4D_6$ Molecular weight 127.22 g/mol; GC-MS M/Z 127. Spectroscopic data are consistent with previously reported data.[19]

***N,N*-dimethyl-*p*-Cl-aniline[18] (2-7)**

An off white crystalline solid in a 36 % yield. ^{1}H NMR (400 MHz, CHLOROFORM-D) δ 7.16 (d, *J* = 9.1 Hz, 2H), 6.63 (d, *J* = 9.1 Hz, 2H), 2.92 (s, 6H); $C_8H_{10}Cl$ Molecular weight 155.62 g/mol GC-MS M/Z 155. Spectroscopic data are consistent with published spectra.[19]

***N,N*-dideuteromethyl-*p*-Cl-aniline[18] (2-8)**

An off white crystalline solid in a 24 % yield. ^{1}H NMR (500 MHz, CHLOROFORM-D) δ 7.05 (d, *J* = 8.6 Hz, 1H), 6.62 (d, *J* = 8.9 Hz, 1H); $C_8H_{10}Cl$ Molecular weight 161.66 g/mol GC-MS M/Z 161. Spectroscopic data are consistent with published spectra.[22]

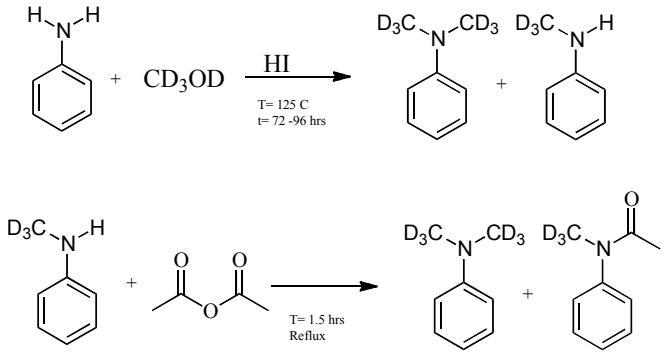

Scheme 5.1. Synthesis of N,N-dimethylanilines was achieved by acid catalyzed nucleophilic substitution at Nitrogen under high pressure. Purification was achieved by acetylation of monosubstitued amines and separation by pH.

5.1.3.2 Tetrabutylammonium perchlorate[23] (2-9)

Tetrabutylammonium perchlorate (Bu_4NClO_4) was prepared by ion exchange between 0.25 moles of tetrabutylammonium bromide and moles of 0.25 moles of 70% perchloric acid in deionized water (DI). The Bu_4NClO_4 was washed to neutral pH with a sufficient quantity of cold DI water to yield a pH neutral eluent. The solid was recrystallized 3-5 times from ethyl acetate/hexane then dried at 80 ^oC in *vacuo* for 8 hours affording a white crystalline solid in 75-85% yield with a melting point of 211-214 ^oC. The melting point falls in within the literature range of 207-214 ^oC.

5.1.3.3 Tetrabutylammonium phenylacetate[24] (2-10)

0.0075 moles of silver oxide was added slowly to 0.01 moles of tetrabutylammonium bromide.[25,26] After stirring the solution for one hour, the supernant solution was tested for bromide according to standard protocol.[27] After achieving a negative bromide test the mixture was filtered over celite on to .01 moles of phenylacetic acid. A hygroscopic, off white solid was afforded in a 98% yield after repeated methanol azeotroping evaporations from hexane under reduced pressure. The melting point was not able to be determined because of the hygroscopic nature of

the compound. Negative bromide test indicates that bromide has been removed and neutral pH washes of compound indicate no acid is present in the final crystalline solid. Spectroscopic data are consistent with literature precedent.

5.1.4 Electrochemical Procedures:

Cyclic voltammetry and constant potential coulometry were carried out on an EG&G Princeton Applied Research Model 273 or 283 Potentiostat/Galvanostat Rate constants were determines from direct fitting of experimentally generated voltammograms to simulated voltammograms using Digisim BAS (version 3.1). All experiments were performed in 0.5 M *n*-Bu_4NClO_4, 0.5 M H_2O in CH_3CN unless noted otherwise.

5.1.4.1 Cyclic Voltammetry (CV)

A typical 3-electrode cell, **Figure 5.1,** consisting of an Ag/AgNO3 (0.56 V vs. NHE) reference electrode, a 3.37 or 2.98 mm diameter glassy carbon working electrode, and a Pt wire counter electrode were used for all cyclic voltammetry experiments. Scan rates of 100 to 1000 mV/s, in increments of 100 mV/s, were employed and rate constants were determined by direct fitting to simultated voltammograms for the proposed reaction mechanism. Simulations were performed using **Digisim BAS**. These experiments utilized both the *N,N*-dimethyl deuterated and undeuteratedanilines, whose preparation is described above, with *p* = OCH_3, CH_3, H, Cl. In the case of *p*-CH_3, experiments were also carried out in anhydrous acetonitrile to probe the effect of solvent on mechanism.

.

A= Auxillary eletrode (Pt Wire)
W=Working electrode (Glassy Carbon)
R=Reference electrode (0.1 M $Ag/AgNO_3$ in CH_3CN)

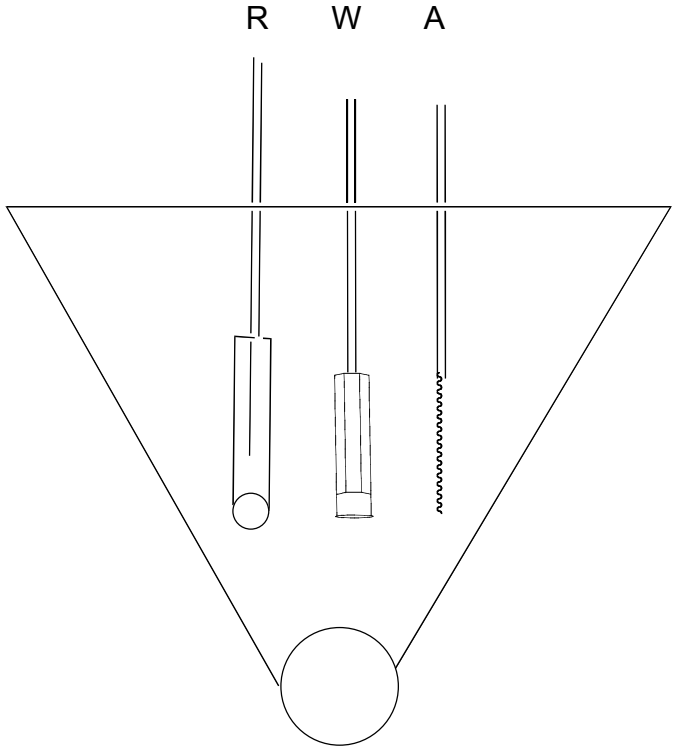

Figure 5.1. Electrochemical cell used in cyclic voltammetry experiments

5.1.4.2 Bulk Electrolysis (BE)

Constant potential coulometry was carried out for the reaction of *p*-CH_3-*N,N*-dimethylaniline and *n*-$Bu_4NPhOAc$ in 0.5 M H_2O 0.5 M *n*-Bu_4NClO_4 to determine the number of molar equivalents of electron passes for the reaction to go to completion. The experiments were performed at 478 mV (+100mV from E_{ox} (*p*-CH_3-*N,N*-dimethylaniline)) until the current decayed to zero for both the reaction mixture and the amine alone. All bulk electrolysis experiments were performed in a glass cell *vide infra.*

5.1.4.3 CV-BE-CV/GC-MS/UV-VIS

A fixed number of electrons were consumed by the solution during constant potential electrolysis experiments and cyclic voltammetry experiments were performed before and after constant potential electrolysis. The number of moles electrons consumed in a given experiment was equal to the number of moles of amine present in solution. These experiments were performed in an effort to provide quantitative (concentration) and qualitative (voltammograms, mass spectra) evidence for the presence or absence of *p*-CH_3-*N,N*-dimethylaniline as a catalytically regenerated reaction product. These experiments were performed at 100 mV more positive than the oxidation potential of the amine and at the prepeak potential. These experiments were performed on neat amine, amine and acetate as well as amine and phenyl acetate. The cell used is shown in **Figure 5.2**; this cell was designed to accommodate the normal bulk electrolysis electrode configuration, with a platinum mesh working electrode, or the electrodes for a cyclic voltammetry experiment (*vide supra)*. Qualitative evidence for the catalytic nature of the amines was derived from the observation of a quasireversible voltammogram at E_{ox} for the amine after passing the number of electrons necessary for amine consumption. The identity and concentration of product materials were respectively determined by GC-MS. Comparison of sample spectra to a calibration curve generated UV-Vis using authentic standards of *p*-toludine afforded concentrations

of amines after reaction.

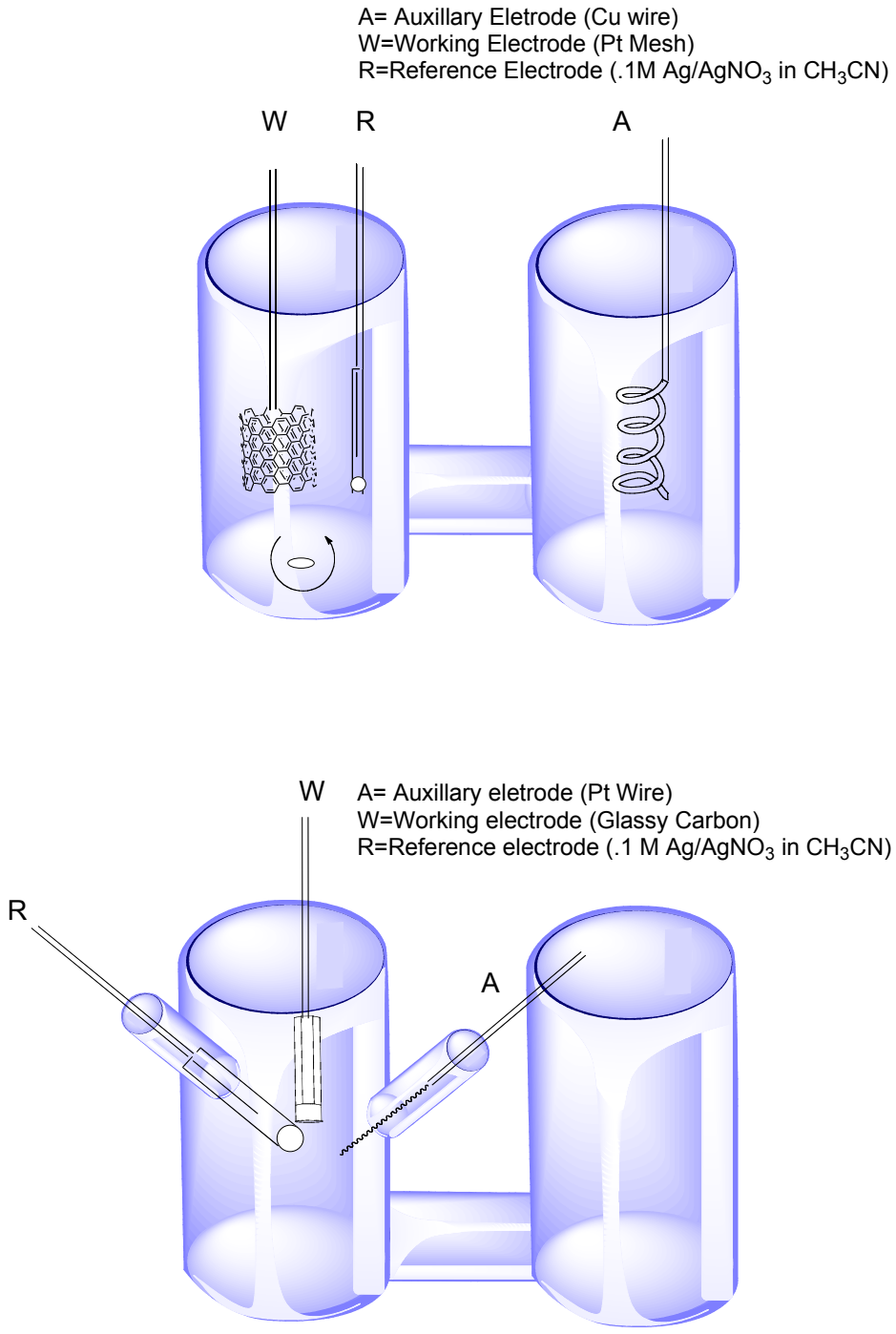

Figure 5.2. Cell used for bulk electrolysis experiments. The cell is designed to accommodate cyclic voltammetry experiments for use in product studies as shown in the latter diagram. The former diagram denotes the electrode configuration for preparative electrolysis.

5.1.5 Photochemical Procedures:

Laser flash photolysis experiments utilized an Applied Photophysics LFP Spectrometer with a Continuum Surelite 1-10 Nd:YAG source. Transient intermediates were generated by direct excitation with a 4 - 6 ns pulse at 266 nm (fourth harmonic) or 355 nm (third harmonic). Signals were monitored using a HP Infinium digital oscilloscope. All experiments were performed in .5 M *n*-Bu_4NClO_4, .5 M H_2O in CH_3CN. For *p*-CH_3-*N,N*-dimethylaniline experiments were also performed under the analogous anhydrous conditions. All experiments were performed at 25 ^oC. Experiments were performed at a variety of carboxylate concentrations and were pseudo first order with respect to amine concentration. Rate constants were determines from regression analysis of concentration dependent rate constants determined by non-linear curve fitting performed by the Applied Photophysics Spectra Kinetic Workstations software (version 4.59).

5.2 General Procedures: Chapter 3

5.2.1 Materials

Chemicals and HPLC grade solvents were used as received unless otherwise stated. All syntheses were performed under dry N_2 and kinetics experiments under dry argon. All products expected to be photo or thermally labile were carefully handled to limit decomposition and stored in brown vials, covered in foil at 0 ^oC. All syntheses of selenides were vented through bleach bubblers to prevent release of noxious H_2Se effluvia. All reactions were performed using oven dried glassware. Dry ethanol was attained by distilling from magnesium ethoxide under dry nitrogen. Dichloromethane,

diethyl ether and tetrahydrofuran were dried using Glass Contour© solvent system under argon. Scharlau silica gel 60 was employed in all purifications performed by flash chromatography. Thin layer chromatography was performed on Merck Kieselgel 60 GF254 silica gel on aluminium-backed plates and stained with 1% potassium permanganate/6.7% potassium carbonate/0.08% sodium hydroxide solution in water. Nuclear magnetic resonance (NMR) spectra were obtained in deuterated chlorofom and chemical shifts were reported in ppm relative to an internal standard of 1% tetramethylsilane.

5.2.2 Instrumentation

^{1}H NMR spectra were collected using a Varian INOVA 400 or 500 mHz NMR. ^{13}C and ^{77}Se NMR spectra were recorded on a Varian INOVA 500 mHz NMR. High resolution mass spectra were collected on a Finnigan LTQ FT by Thermo Electron Corporation. Infrared spectra were obtained using a Perkin Elmer Spectrum One FTIR spectrometer. Melting points were determined using a Stanford Research Systems EZ-Melt melting point apparatus. Gas chromatography analysis was performed using Schimadzu GC-17A gas chromatograph (column: CYDEX-B, 50m × 0.220mm, film thickness 0.25μm). GCMS analysis was carried out on an Agilent 7890A GC system (column: HP- 5MS, 30m × 0.250mm, film thickness 0.25μm).

5.3 Syntheses

5.3.1 1-Bromooctane (3-1) and 2-Bromooctane (3-2)[28]

In a dry reaction vessel 75 mmoles of 1-octanol or 2-octanol was combined with 300 mL of anhydrous Et_2O while stirring, under dry N_2. The mixture was cooled to 0 ^{O}C in an ice bath and 90 mmoles of PBr_3 was added very slowly. Addition of PBr_3 resulted

in formation of an orange yellow solution. The reaction mixture was cooled to room temperature and stirred for 12 hours. The reaction mixture was poured over ice and extracted 3x with 100 mL of Et_2O. The organic fractions were combined and washed successively with water, aqueous 10% $Na_2S_2O_5$, and saturated aqueous NaCl solutions then dried over Na_2SO_4 and evaporated under reduced pressure to afford a pale yellow oil. Distillation of the products at 85 ^oC at a pressure of 4mmHg afforded a sweet smelling, clear oils in excellent yield (95-99%). Comparison of ^1H NMR, ^{13}C NMR, IR, MS collected to reported characterization data identified the obtained oils to be the desired primary[29] and secondary[28] alkyl halides.

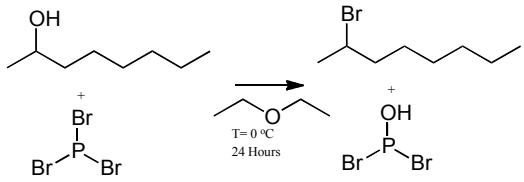

Scheme 5.2. Synthetic pathway for formation of primary and secondary alkyl halides. Displacement of bromine is followed by S_N2 attack on the alkyl group.

5.3.2 Dialkyldiselenides[30,31]

Dioctyldiselenide (3-3) and Di-*sec*-octyldiselenide (3-4)

Dibutyldiselenide (3-5) and Dipentyldiselenide (3-6)

In a 3 neck round bottom flask attached to a condenser vented through a bleach bubbler $NaBH_4$ (25.4 mmol) and selenium black (38 mmol) were combined slowly resulting in evolution of heat and gas. The mixture was cooled to 0 ^oC in an ice bath under stir and argon. Subsequent slow, dropwise addition of 35 mL of ethanol induced rapid evolution of gas in conjunction with the formation of a red-orange solution. Upon the cessation of gas evolution, the mixture was heated to reflux for 2 hours. After

cooling to room temperature (12.7 mmol) of the appropriate alkylselenide was added slowly and the reaction was allowed to proceed overnight. The resultant mixture was bubbled through bleach for 2 hours to remove residual H_2Se then diluted with saturated NaCl solution. The diselenide product was extracted with 50 mL Et_2O 3X. The ethereal phase was washed successively with water and brine then dried with Na_2SO_4 and evaporated under reduced pressure to afford a bright yellow, noisome oils. The crude product was used without purification in the subsequent synthetic steps. Characterization data collected by ^{1}H NMR, ^{13}C NMR, ^{77}Se NMR, IR and MS were consistent with those reported by our group and others.[28,32,33]

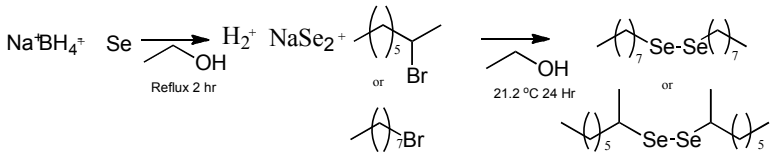

Scheme 5.3. Synthetic pathway to primary and secondary diselenides. Selenium is reduced by the hydride source and subsequent S_N2 attack on the electron deficient carbon bonded to the halide yields the desired product.

5.3.3 Di(*t*-butyl)diselenide (3-7)[34]

Due to steric constraints prohibiting S_N2 at a tertiary carbon center the tertiary diselenide was not successfully synthesized by the above procedure. Alternatively, a grignard reaction was employed.

In a flame dried 3 neck round bottom flask attached to a condenser vented through a bleach bubbler under stir and dry argon 200 mmoles of *t*-butyl bromide was combined with 100 mL of anhydrous THF and 250 moles of oven dried, ground magnesium turnings. To promote initiation a small quantity of I_2 was added. Between 30 minutes and 2 hours the reaction mixtures became cloudy and the evolution heat

and bubbles from the magnesium particles was noted. Slow dropwise addition of an additional .18 moles of *t*-butyl bromide followed and upon cessation of reflux a suspension of 300 mmoles of selenium black in anhydrous THF was added with caution over 1 hour so as to maintain a gentle relux. Evolution of heat and formation of a red solution accompanied addition of the selenium suspension. The sealed mixture was allowed to react under stir for an additional hour before cooling to 0 ^{o}C in an ice bath and adding 100 mL of saturated NH_4Cl. Subsequently, 40 mL of KI_3 solution (preparation described in the reference) was added slowly while still on ice. The mixture was extracted 3X with 200 mL of THF and washed successively with 10 % aqueous $NaHSO_4$, saturated NH_4Cl, dried with Na_2SO_4 and evaporated by bubbling with nitrogen to afford a bright yellow, extremely volatile and mephitic oil which was used in further syntheses without additional purification. Comparison of the crude compounds characterization data (^{1}H NMR, ^{13}C NMR, ^{77}Se NMR, IR and EI-GC-MS data) with literature data for the diselenide suggested successful formation of the intended product.[34 35]

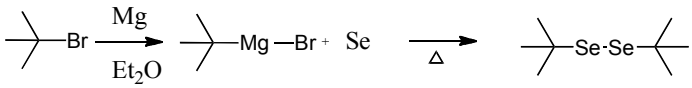

Scheme 5.4. Synthetic scheme for tertiary diselenide. The authors believe it is reasonable that this reaction proceeds via formation of a grignard, followed by nucleophilic addition of elemental selenium to the grignard and elimination of the magnesium halide to form t-butyl seleno radical anions. Interaction of these units in solution results in homologous addition to form the desired diselenide.

5.3.4 Selenovalerates and Selenohexanoates[36]

Ethyl 5-(octylselanyl)valerate (3-8) , Ethyl 5-((2-octyl)selanyl)valerate (3-9), Ethyl 6-(octylselanyl)hexanoate (3-10), Ethyl 6-((2-octyl)selanyl)hexanoate (3-11), Ethyl 5-((*t*-butyl)selanyl)valerate (12), Ethyl 6-((*t*-butyl)selanyl)hexanoate (3-13)

In a dry reaction vessel vented through a bleach bubbler crude diselenide was dissolved in 25 mL of anhydrous ethanol under argon and stir. $NaBH_4$ was added slowly; hydride addition was accompanied by gas evolution, formation of a silvery-white precipitate and a loss of color in solution. Upon the cessation of gas evolution ethyl-5-bromovalerate or ethyl-6-bromohexanoate was added dropwise. The reaction mixture was left to stir overnight at room temperature. The reaction mixture was bubbled through bleach for 2 hours prior to work up to remove any small volatile selenides. Solvent was removed from the resultant solution in *vacuo* and the residue was resuspended in H_2O and extracted 3X with 50 mL of Et_2O. The ethereal phase was dried with Na_2SO_4 and solvent evaporated under reduced pressure. The resultant oil was purified by flash chromatography on silica in 1% ethyl acetate in petroleum spirits (40 – 60 ^oC) to yield 50-85% of pale yellow to bright yellow oils over two steps. Characterization data for compounds **(3-8)** and **(3-9)** are consistent with those reported previously by our (Prof. Schiesser's) group.[28] Characterization data for **(3-10)** – **(3-13)** are reported at the end of this section and are consistent with expectations for the intended products.

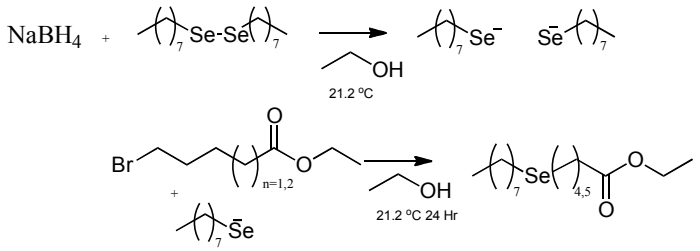

Scheme 5.5. The syntheses of alkylslenoalkanoates proceeds via hydride induced reduction of the diselenide and subsequent S_N2 attack on the alkyl halide.

5.3.5 Methylhydroxy(methyl)carbamodithioate (3-14)[37]

In a round bottom flask 18 mmoles of *N*-methyl hydroxylamine hydrochloride was suspended in 50 mL of anhydrous dichloromethane and cooled to 0 ^{o}C in an ice bath under stir and nitrogen. 20 mmoles of carbon disulfide was added followed by the addition of 20 mmoles of methyl iodide. Subsequently, 27 mmoles of triethylamine was added slowly. After addition of all reaction components the mixture was allowed to warm slowly to room temperature and continue to react under stir for 1 hour. The mixture was diluted with water and extracted 3X with 25 mL of dichloromethane. The combined organic fractions were dried over Na_2SO_4 and evaporated under reduced pressure to yield a gray-brown oil. The crude product was purified by washing through a plug of silica with 40% ethyl acetate/petroleum spirits (40-60°C) affording a gray-green solid in 75% yield with a melting point of 45-47°C. Comparison of the compounds characterization data (^{1}H NMR, ^{13}C NMR, ^{77}Se NMR, IR and MS data) with in literature data for the diselenide suggested successful formation of the intended product.[37]

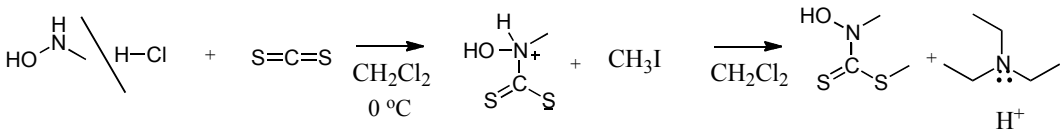

Scheme 5.6. Syntheses of (3-14) proceeds via reduction of CS_2 followed by methylation of the sulfide.

5.3.6 Selenovaleric and Selenohexanoic Acids[38]

5-(octylselanyl)valeric acid (3-15) , 5-((2-octyl)selanyl)valeric acid (3-16), 6-(octylselanyl)hexanoic acid (3-17), 6-((2-octyl)selanyl)hexanoic acid (3-18), 5-((*t*-butyl)selanyl)valeric acid (3-19), 6-((*t*-butyl)selanyl)hexanoic acid (3-20)

In a round bottom flask 10 mmoles of an ester **(3-8)** – **(3-13)** was diluted in 30 mL of ethanol and 10 mmoles of NaOH was added as an aqueous solution. The reaction was done in the presence of air. Under stir and reflux the reaction was allowed to proceed for 1 hour. After cooling the solution to room temperature ethanol was removed in *vacuo* and the residue was dissolved in water and washed with Et_2O to remove any residual starting ester. Acid was added to the aqueous phase until a pH of less than 4 was achieved and the solution was again extracted 3X with 20 mL with Et_2O. The Combined organic phases from the second set of extractions were combined and dried over Na_2SO_4 before reducing in *vacuo* to white to yellow solid in quantitative yields. The solids were slightly amorphous at room temperature therefore melting points could not be determined but are expected to be near room temperature as exposure to colder conditions affords a crystalline solid. Characterization data for compounds **(3-15)** and **(3-16)** are consistent with those reported previously by our (Prof. Schiesser's) group.[28] Characterization data for **(3-17)** – **(3-20)** are reported at the end of this section and are consistent with expectations for the intended products.

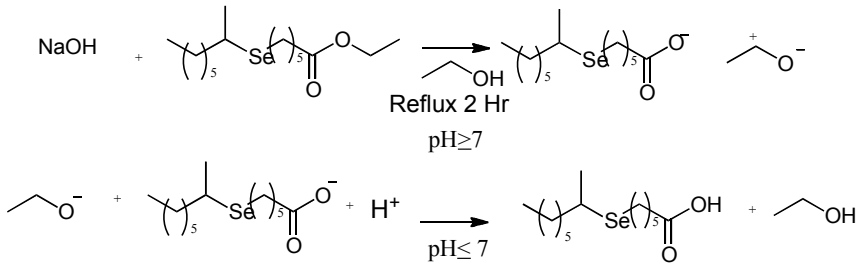

Scheme 5.7. Saponification of esters (3-8) - (3-15) yields the corresponding carboxylic acid.

5.3.7 Syntheses of Kim Esters[36]

5-(octylselanyl)pentanoyloxyl-*N*-*S*-dimethylthiocarbamate (3-21) ,

5-((2-octyl)selanyl)pentanoyloxyl-*N*-*S*-dimethylthiocarbamate (3-22),

6-(octylselanyl)hexanoyloxyl-*N*-*S*-dimethylthiocarbamate (3-23),

6-((2-octyl)selanyl)hexanoyloxyl-*N*-*S*-dimethylthiocarbamate (3-24),

5-((*t*-butyl)selanyl)pentanoyloxyl-*N*-*S*-dimethylthiocarbamate (3-25),

6-((*t*-butyl)selanyl)hexanoyloxyl-*N*-*S*-dimethylthiocarbamate (3-26)

In a dry reaction vessel vented through a bleach bubbler 1 mmole of a selenovaleric or selenohexanoic acid **(3-15)** – **(3-20)** and 1 mmole of *N,N'*-Dicyclohexylcarbodiimide were combined with a catalytic quantity of 4-dimethylaminopyridine in anhydrous CH_2Cl_2 under stir and dry N_2. 1.5 mmoles of N-methylhydroxydithiocarbamate was dissolved in 1 mL of anhydrous CH_2Cl_2 and added in a dropwise manner forming a precipitate. The reaction was allowed to proceed for 12 hours before filtering through celite. The filtrate was washed with saturated aqueous $NaHCO_3$ and saturated aqueous NaCl successively, 3X each. The liquids were then dried with Na_2SO_4 and evaporated to afford grayish-green oils that were purified by flash chromatography in on silica with 2-10% ethyl acetate/petroleum spirits (40-60°C) to afford yellow to pale green oils in 40-60% yield. Characterization data for compounds

(3-21) and **(3-22)** are consistent with those reported previously by our (Prof. Schiesser's) group. Characterization data for **(3-23)** – **(3-26)** are reported at the end of this section and are consistent with expectations for the intended products.

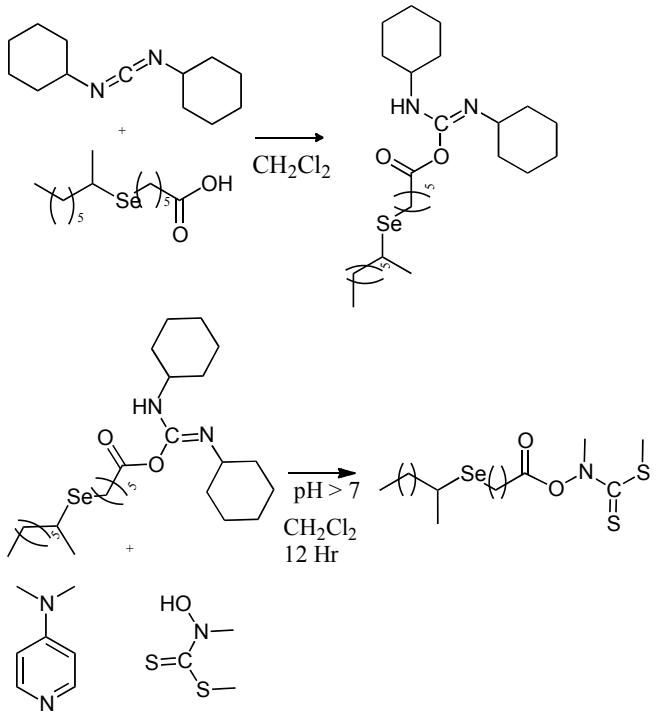

Scheme 5.8. DCC/DMAP Coupling to form Kim Esters. Esterification of dithiocarbamate by selenoalkanoic acid yields the desired product. A similar method is used in synthesis of Barton Esters.

5.3.8 2-thioxopyridin-1(2*H*)-yl 5-(benzylselanyl)pentano-ate (3-27)[36]

In a 3 neck round bottom flask attached to a condenser vented through a bleach bubbler, chilled in a cyclohexane and dry ice slurry at 5 ^{o}C, .05 mmoles of 5-(benzylselanyl)pentanoic acid (synthesized by Sophie Lobachevsky) was combined with a catalytic quantity of 4-dimethylaminopyridine and .05 mmole of *N,N'*-dicyclohexylcarbodiimide were combined in 1 mL **of** anhydrous benzene under stir and argon. The reaction mixture was shielded from light and .15 mmoles of *N*-hydroxy-pyridine-2(1*H*)-thione dissolved in .5 mL of anhydrous benzene was added slowly. After

1.5 hours the reaction was filtered through celite. The filtrate was evaporated in *vacuo* to afford an oil that was purified by prep TLC in on silica in 30% ethyl acetate/hexanes while taking care to limit exposure to ambient light. A brightly colored band corresponding to the desired product was extracted with CH_2Cl_2 and evaporated to dryness affording a yellow oil in 45% yield. Characterization data for compounds **(3-27)** are consistent with those reported previously by our (Prof. Schiesser's) group.

5.3.9 Tributyltin Hydride (3-28)[39]

In a 3 neck round bottom flask attached to a condenser vented through a bleach bubbler 9 mmoles of $NaBH_4$ was added over 5 minutes to a solution of 11.5 mmoles of bis(tributyltin)oxide in 15 mL of dry ethanol under stir and dry N_2. A cloudy solution resulted that was allowed react for 2.5 hours before adding H_2O until H_2 ceased to bubble from solution. Similarly NH_4Cl was then added in a dropwise manner until no additional H_2 bubbles were observed. Ethanol was removed in *vacuo* and the solution was diluted with H_2O until the solid was fully dissolved. The solution was then extracted 3X each with saturated aqueous solutions of $NaHCO_3$ then NaCl before drying with Na_2SO_4. The product was purified by kügelrohr distillation at 87 ^oC at a pressure of .8 mmHg affording a clear oil in 75% yield. Characterization data for the compound are consistent with the known spectra.[39]

5.3.10 Syntheses of Authentic Products:

5.3.10.1 Dialkylselenides[36]

***t*-butylselenopentane (3-29), *t*-butylselenohexane(3-30), *sec*-octylselenopentane(3-31), *sec*-octylselenohexane(3-32), octylselenopentane(3-33), octylselenohexane(3-34)**

In a 3 neck round bottom flask attached to a condenser vented through a bleach bubbler 4.8 mmoles of the appropriate diselenide was added to 20 mL of ethanol under dry N_2 and stir. $NaBH_4$ was added slowly until a colorless solution was achieved. 9.3 mmoles of the appropriate alkyl halide* was added upon cessation of gas evolution in a dropwise manner resulting in the formation of a silvery-white precipitate. The reaction was allowed to proceed in a sealed reaction vessel overnight. The solution was bubbled with N_2 for 2 hours to remove any volatile small selenides and ethanol was evaporated in *vacuo*. The residue was resuspended in H_2O and extracted 3X with 50 mL of Et_2O. The combined organic fractions were washed with brine and dried with Na_2SO_4 before evaporating by bubbling with N_2 to afford clear to orange oils. Most products were sufficiently pure for use as standards although some required further purification via distillations. Products were afforded in 15 to 65% yield. The low yields are suspected to be partially attributable to evaporative loss during solvent removal due to the low molecular weights of the *t*-butyl selenides. Products **(3-31)** and **(3-33)** matched that previously reported by our (Prof. Schiesser's) group. Characterization data for **(3-29), (3-30), (3-32)** and **(3-34)** are reported at the end of this section and are consistent with what is expected for the intended products.[28]

*tert-butylselenoalkanes were synthesized using di-primary-alkyl-diselenides not di-*t*-butyl diselenide.

5.3.10.2 Tetrahydro-2*H*-selenopyran (3-35)[31]

In a 3 neck round bottom flask attached to a condenser vented through a bleach bubbler 27 mmoles of selenium black was suspended in 20 mL H_2O under stir and N_2 in an ice bath at 0 ^{O}C. A separate solution of 60 mmoles of $NaBH_4$ in 10 mL H_2O was cooled to 0 ^{o}C and added with extreme caution. The addition of $NaBH_4$ to the aqueous selenium suspension resulted in rapid evolution of heat and bubbling. Once gas evolution has ceased for 30 minutes 18 mmoles of 1,5-dibromopentane was added in a dropwise fashion. The mixture was warmed slowly to room temperature and left to stir for 12 hours in a sealed reaction vessel. The reaction vessel was attached to a bleach bubbler for the entirety of the reaction to prevent pressure increase due to further evolution of bubbles over the 12 hours. A deep orange sweet smelling solution was produced and was diluted with an additional 10 mL of H_2O before extracting 3X with 25 mL of Et_2O. The combined organic fractions were washed with 25 mL of brine 3X, dried over Na_2SO_4 and solvent was removed by bubbling with dry N_2. The cyclized product was sufficiently pure for use as a standard for GC analysis. Characterization data are shown at the end of this section.

Ethyl 6-(octylselanyl)hexanoate (3-10) ^{77}Se NMR (95 MHz, $CDCl_3$) δ 161.01, M/Z 336.20, M.W. 335.4 g/mol

Ethyl 6-(octylselanyl)hexanoic acid (3-17) ^{77}Se NMR (95 MHz, $CDCl_3$) δ 160.99, M/Z 308.0, M.W. 307.33 g/mol

6-(octylselanyl)hexanoyloxyl-*N*-*S*-dimethylthiocarbamate (3-23)) ^{1}H NMR (500 MHz, $CDCl_3$) δ 3.77 (s, 3H), 2.54 (s, 9H), 1.97 – 1.49 (m, 6H), 1.31 (d, J = 43.4 Hz, 12H), 0.85 (s, 3H); ^{13}C NMR (126 MHz, $CDCl_3$) δ 196.92, 169.98, 104.99, 42.90, 32.04, 31.57, 30.88, 30.31, 30.20, 29.45, 29.41, 29.35, 24.38, 24.21, 23.68, 22.87, 18.88, 14.31; ^{77}Se NMR d 160.6.

Ethyl 6-((2-octyl)selanyl)hexanoate (3-11) ^{77}Se NMR (95 MHz, $CDCl_3$) δ 267.03, M/Z 336.16, M.W. 335.38 g/mol.

Ethyl 6-((2-octyl)selanyl)hexanoic acid (3-18) ^{77}Se NMR (95 MHz, $CDCl_3$) δ 271.34, M/Z 308.13, M.W. 307.33 g/mol.

6-((2-octyl)selanyl)hexanoyloxyl-*N*-*S*-dimethylthiocarbamate (3-25)

^{1}H NMR (500 MHz, $CDCl_3$) δ 3.79 (s, 3H), 2.56 (s, 3H), 1.88 – 1.16 (m, 24H), 0.97 – 0.78 (m, 3H); ^{13}C NMR (126 MHz, $CDCl_3$) δ 196.95, 170.00, 42.91, 38.34, 35.31, 34.50, 31.99, 31.57, 30.48, 29.60, 29.36, 28.03, 24.89, 24.23, 22.85, 22.72, 22.35, 18.89, 14.30; ^{77}Se NMR (95 MHz, $CDCl_3$) δ 266.6.

Ethyl 5-((*t*-butyl)selanyl)valerate (3-12) ^{77}Se NMR (95 MHz, $CDCl_3$) δ 377.61, M/Z 265.11 g/mol, M.W. 265.25 g/mol.

Ethyl 5-((*t*-butyl)selanyl)valeric acid (3-19) ^{77}Se NMR (95 MHz, $CDCl_3$) δ 376.11, M/Z 237.08 M.W. 238.05 g/mol.

Methyl (5-(*t*-butylselanyl)pentanoyl)oxy(methyl)carbamodithioate (3-26) ^{1}H NMR (500 MHz, $CDCl_3$) δ 3.71 (s, 3H), 2.20-2.67 (m, *J* = 5.9 Hz, 4H), 1.94 – 1.56 (m, 4H), 1.41 (s, 9H), 0.89 (t, *J* = 7.3 Hz, 3H); ^{13}C NMR (126 MHz, $CDCl_3$) δ 196.77, 169.60, 42.67, 38.82, 32.52, 30.99, 29.96, 24.93, 21.00, 18.66; ^{77}Se NMR (95 MHz, $CDCl_3$) δ 376.36, M.S. 356.07, M.W. 356.41.

Ethyl 5-((*t*-butyl)selanyl)hexanoate (3-13) ^{77}Se NMR (95 MHz, $CDCl_3$) δ 274.34, GC-MS 280.1 , M.W. 307.33 g/mol.

6-((*t*-butyl)selanyl)hexanoyl)oxy(methyl)carbamodithioate (3-27) ^{1}H NMR (400 MHz, $CDCl_3$) δ 3.72 (s, 3H), 2.63 – 2.33 (m, 6H), 1.67 (ddd, *J* = 21.9, 15.2, 7.6 Hz, 4H), 1.38 (s, 9H), 1.19 (s, 3H); ^{13}C NMR (126 MHz, $CDCl_3$) δ 196.77, 169.60, 42.67, 38.82, 32.52, 30.99, 30.89, 29.96, 24.93, 21.00, 18.66.

Diselenides

Dibutyldiselenide (3-5) ^{1}H NMR (500 MHz, $CDCl_3$) δ 3.34 – 2.77 (m, 4H), 1.89 – 1.69 (m, 4H), 1.53 – 1.38 (m, 4H), 0.96 (t, *J* = 7.9 Hz, 6H); ^{13}C NMR (126 MHz, $CDCl_3$) δ 32.97, 29.80, 22.64, 13.54; ^{77}Se NMR (95 MHz, $CDCl_3$) δ 305.00, GC-MS 274.00 , M.W. 272.97 g/mol.

Dipentyldiselenide (3-6) ^{1}H NMR (500 MHz, $CDCl_3$) δ 2.89 (td, *J* = 7.5, 2.9 Hz, 4H), 1.81 – 1.63 (m, 4H), 1.42 – 1.23 (m, 8H), 0.89 (t, *J* = 6.9 Hz, 6H); ^{13}C NMR (126 MHz,

$CDCl_3$) δ 31.71, 30.70, 30.23, 22.21, 13.97; ^{77}Se NMR (95 MHz, $CDCl_3$) δ 3060.09; GC-MS 302.0; M.W. 300.20 g/mol.

Authentic Products

***t*-Butylselenobutane (3-29**) ^{1}H NMR (400 MHz, $CDCl_3$) δ 2.68 – 2.47 (m, 2H), 1.89 – 1.58 (dt, *J* = 19.7 Hz, 1.8 Hz, 4H), 1.41 (s, 9H), 0.89 (t, *J* = 7.3 Hz, 3H); ^{13}C NMR (126 MHz, $CDCl_3$) δ 32.81, 32.56, 29.77, 23.35, 21.59, 13.71; ^{77}Se NMR (95 MHz, $CDCl_3$) δ 378; M/Z 1950.09, M.W. 193.19 g/mol

***t*-Butylselenopentane (3-30)** NMR (500 MHz, $CDCl_3$) δ 2.74 – 2.45 (m, 2H), 1.78 – 1.47 (m, 15H), 1.00 – 0.92 (t, *J*= 1.5 Hz, 3H); ^{13}C NMR (126 MHz, $CDCl_3$) δ 38.31, 32.81, 32.55, 32.37, 29.70, 23.39, 21.70, 13.64; ^{77}Se NMR (95 MHz, $CDCl_3$) δ 264.06; GC-MS 208.00; 207.22 g/mol

***sec*-Octylselenohexane (3-32)** ^{1}H NMR (500 MHz, $CDCl_3$) δ 2.95 (dd, *J* = 12.7, 5.9 Hz, 1H), 2.58 (t, *J* = 6.9 Hz, 2H), 1.77 – 1.61 (m, 3H), 1.48 – 1.23 (m, 16H), 1.04 – 0.81 (m, 6H); ^{13}C NMR (126 MHz, $CDCl_3$) δ 38.15, 34.82, 32.33, 32.18, 31.78, 30.54, 30.38, 290.14, 27.82, 22.63, 22.49, 22.25, 14.06, 13.97; ^{77}Se NMR (95 MHz, $CDCl_3$) δ 264.17; M/Z 263.17, M.W. 263.32 g/mol.

Octylselenohexane (3-34) ^{1}H NMR (500 MHz, $CDCl_3$) δ 2.60 – 2.48 (m, 4H), 1.73 – 1.59 (m, 4H), 1.44 – 1.20 (m, 14H), 0.89 (dd, *J* = 18.7, 9.6 Hz, 6H); ^{13}C NMR (126 MHz,

$CDCl_3$) 32.40, 32.05, 30.91, 30.60, 30.22, 29.42, 29.36, 24.44, 24.20, 24.15, 22.87, 22.45,14.29, 14.18;^{77}Se NMR (95 MHz, $CDCl_3$) δ 158.85; GC-MS 264.00 M.W. 263.30.

Tetrahydro-2*H*-selenopyran (3-35) ^{1}H NMR (500 MHz, $CDCl_3$) δ 3.42 (t, *J* = 6.7 Hz, 4H), 2.00 – 1.84 (m, 4H), 1.65 – 1.54 (m, 2H); ^{13}C NMR (126 MHz, $CDCl_3$) δ 33.74, 33.46, 32.47, 32.10, 30.33, 29.81, 28.25, 27.03, ^{77}Se NMR (95 MHz, $CDCl_3$) δ 266.60; GC-MS 150 M.W. 1490.09.

5.3.11 Kinetics Procedures:

5.3.11.1 Competition Kinetics (Kim Ester Cyclizations)

Kim esters and radical traps (either tributyltin hydride or *p*-thiocresol) were combined in either benzene or acetonitrile. (In solutions where acetonitrile was solvent miscibility issues were observed and it is suspected that the reactions may exhibit rate constant differences because the reactions were interfacial rather than occurring in homogeneous solution. This point is addressed in more detail in Chapter 3) Trap concentrations were varied over one order of magnitude and were used in concentrations such that the reaction was under pseudo-first order conditions with respect to the Kim ester. The mixtures were degassed with dry argon for 30 seconds before irradiation and were irradiated for 1 to 2 hours with a 250 Watt low pressure broad spectrum mercury lamp. Experiments were performed at temperatures between 15 and 75 ^{o}C to obtain activation parameters for cyclization. Rate constants were determined by linear regression as described in the previous section addressing competition kinetics (***see 4.1.3***). Product ratios for the cyclized and trapped products

were determined by GC analysis and comparison to a calibration curve generated by GC using authentic product standards synthesized in our lab.

5.3.11.2 Laser Flash Photolysis (Barton Ester (25) Kinetics)

Laser flash photolysis experiments utilized an Applied Photophysics LFP Spectrometer with a Continuum Surelite 1-10 Nd:YAG source. Transient intermediates were generated by direct excitation with a 4 ns pulse at 266 nm (fourth harmonic). Signals were monitored using a HP Infinium digital oscilloscope. All experiments were performed under argon in dry acetonitrile. Experiments were performed at temperatures between 0 ^{o}C and 85 ^{o}C. Rate constants were determines from regression analysis of concentration dependent rate constants determined by non-linear curve fitting performed by the Applied Photophysics Spectra Kinetic Workstations software (version 4.59).

5.3.11.3 GC Calibration

Using authentic products synthesized above differing ratios of the cyclized and trapped product were combined and analyzed by GC. Plotting the ratio of peak areas as a function of the ratio of concentrations afforded linear equations used to convert peak area ratios measured for kinetics experiments into their corresponding concentrations affording a convenient means of determining rate constants for the cylizations of interest.

REFERENCES:

(1) Griller, D.; Ingold, K. U. *Accounts of Chemical Research* **1980**, *13*, 317.

(2) Newcomb, M. *Tetrahedron* **1993**, *49*, 1151.

(3) Espenson, J. H. *Chemical Kinetics and Reaction Mechanisms*; 2 ed.; McGraw-Hill: New York, 2002.

(4) Anslyn, E. V.; Dougherty, D. A. In *Modern Physical Organic Chemistry*; Murdzek, J., Ed.; University Science Books: Sausalito, 2006, p 397.

(5) Litwinienko, G.; Ingold, K. U. *Journal of Organic Chemistry* **2005**, *70*, 8982.

(6) Bott, A. W.; Feldberg, S. W.; Rudolph, M. *Current Seperations* **1996**, *15*, 67.

(7) Andrieux, C. P.; Hapoit, P.; Saveant, J.-M. *Chemical Reviews* **1990**, *90*, 723.

(8) *Handbook of Electrochemistry*; 1 ed.; Zoski, C. G., Ed.; Elsevier: Amsterdam, 2007.

(9) Britz, D. *Digital Simulations in Electrochemistry*; 1st ed.; Springer: Heidelberg New York, 2005; Vol. 23.

(10) Reiger, P. H.; Gosser, D. K. *Analytical Chemistry* **1988**, *60*, 1159.

(11) Joslin, T.; Pletcher, D. *Electroanalytical and interfacial electrochemistry* **1974**, *49*, 171.

(12) Rudolph, M. *Journal of Electroanalytical Chemistry* **1994**, *375*, 89.

(13) Rudolph, M. *Journal of Electroanalytical Chemistry* **1991**, *314*, 13.

(14) Rudolph, M. *Journal of Electroanalytical Chemistry* **1992**, *338*, 85.

(15) Feldberg, S. W. *Journal of Electroanalytical Chemistry* **1981**, *127*, 1.

(16) Allen J. Bard, L. R. F. *Electrochemical Methods: Fundamentals and Applications*

(17) *Vogel's Textbook of Practical Organic Chemistry*; 4 ed.; Longman: London, 1978.

(18) Humphreys, R. W. R. *Journal of Organic Chemistry* **1983**, *48*, 1483.

(19) Bertrand, S. H., N.; Humbel; S.; Pete, J.P. *Journal of Organic Chemistry* **2000**, *65*, 8690.

(20) Wang, M. Z. Z., C. Y.; Wong, M. K.; Che; C. M. *Chemistry-A European Journal* **2010**, *16*, 5723.

(21) Selva, M. P., A.; Tundo, P.; Brunelli, D. *Journal of Organic Chemistry* **2006**, *71*, 5770.

(22) Loeppky, R. N. S., S.P.; Elomari; S.; Hastings; R.; Thiess; T.E. *Journal of American Chemical Society* **1998**, *120*, 5193.

(23) House, H. O. F., E.; Peet, N.P. *Journal of Organic Chemistry* **1971**, *56*, 2371.

(24) Eberson, L. L., M.; Finelstein, M.; Hart, S.A.; Moore, W. M.; Ross; S. D. *Acta Chemica Scandinavica* **1988**, *B 42*, 666.

(25) Eberson, L. L., M.; Finelstein, M.; Hart, S.A.; Moore, W. M.; Ross; S. D. *Acta Chemica Scandinavica* **1988**, *B42*, 666.

(26) Barry, J. E. F., M.; Moore, W.M.; Ross, S. D.; Eberson, L.; Jonsson, L. *Journal of Organic Chemistry* **1982**, *47*, 1292.

(27) http://www.chemguide.co.uk/inorganic/group7/testing.html; 5/11/2011.

(28) Lobachevsky, S., University of Melbourne, 2009.

(29) http://riodb01.ibase.aist.go.jp/sdbs/ National Institute of Advanced Industrial Science and Technology, 9/9/09 SDBS # 1740 CAS Registry # 111-83-1; 1/11/2009.

(30) Thompson, D. P.; Boudjouk, P. *Journal of Organic Chemistry* **1988**, *53*, 2109.

(31) Klayman, D. L.; Griffin, T. S. *Journal of American Chemical Society* **1973**, *95*, 197.

(32) Krief, A.; Delmotte, C.; Dumont, W. *Tetrahedron* **1997**, *53*, 12147.

(33) Ruan, M.-D.; Zhao, H.-R.; Fan, W.-Q.; Zhou, X.-J. *Journal of Organometallic Chemistry* **1995**, *485*, 19.

(34) Block, E.; Birringer, M.; Jiang, W.; Nakahodo, T.; Thompson, H. J.; Tuscanp, P. J.; Uzar, H.; Zhang, X.; Zhu, Z. *Journal of Agricultural Food Chemistry* **2001**, *49*, 458.

(35) Anderson, J. A.; Odom, J. D.; Zozulin, A. J. *Organometallics* **1984**, *3*, 1458.

(36) Schiesser, C. H.; Benjamin, L. J.; Sutej, K. *Tetrahedron* **1993**, *49*, 2557.

(37) Kim, S.; LIm, C. J.; Song, S.-E.; Kang, H.-Y. *Synthetic Letters* **2001**, 688.

(38) Du, J.; Surzhykov, S.; Lin, J. S.; Newton, M. G.; Cheng, Y.-C.; Schanazi, R. F.; Chu, C. K. *Journal of Medicinal Chemistry* **1997**, *40*, 2991.

(39) Maillard, B.; Gadrat, C.; Burgeois, J. M. *Journal of Organometallic Chemistry* **1982**, *236*, 61.